From Institute for Signal Processing

Director:
Prof. Dr. -Ing. Alfred Mertins

Applications of textile based capacitive ECG recordings

Dissertation

for Fulfillment of Requirements for

Doctoral Degree of the University of Luebeck

- from the Dept. of Informatics/Technology

Submitted by Bhavin Chamadiya

Born in Porbandar, India

Luebeck, May 2012.

1. Berichterstatter : Prof. Dr. Ulrich G. Hofmann

2. Berichterstatter : Prof. Dr. Hartmut Gehring

Tag der mündlichen Prüfung: 24.09.2012

Zum druck genehmigt. Lübeck, den 28.09.2012

Bhavin Chamadiya

Doctoral Student
Institute for Signal Processing
University of Luebeck
Ratzeburger Allee 160,
23538, Luebeck
Germany

To

Maa & Bapa

(grandma and grandpa)

Acknowledgement

This doctoral work has been most significant academic challenge for me till now. It would not have finished without the help of some people so I would like to take the opportunity to express my sincere gratitude to some of them here.

First and foremost, I am extremely grateful to Mr. Manfred Wagner for giving me this opportunity and to support me throughout the work. He has incubated me fascination and vision for research work as well as non-technical aspects of it. My most sincere gratitude goes to my academic supervisor Prof. rer. Nat. Ulrich G. Hofmann for his encouragement, support, advising and guidance during my entire PhD work. He taught me academic research methodology and scientific writing, what was absolutely essential doing my thesis in Daimler AG, without these, my PhD work would not have been possible. His feedbacks in all my papers and this thesis were thoroughly important and invaluable.

A very special thanks to my friend Jörg Mahrle for his advices and translation help and to Mr. Martin Spieth for teaching and sharing with me his vast practical laboratory experience. I would like to thank all my colleagues at Research and Development, Daimler AG, Böblingen, specially Dr. Wolfgang Wondrak, Mr. Rolf Kleinheyer, Mathias Baumann and Ms. Minja Gamerdinger. It has been a great privilege, honor and life changing to spend several years with you guys. I also thank my friend Kunal Mankodiya for his assistance and some interesting interactions during this research work.

I owe a lot to my parents and my grandparents, who always encouraged me and supported me unconditionally in every situation of my life. I am very much indebted to my wife, who supported me in every possible manner to see the completion of this work. This moment, I owe great gratitude to Dr. A. P. J. Abdul Kalam and all other heroes who are remarkably inspiring to us in our society and being driven force behind many successes.

Abstract

The average age of the population is continuously on the rise in several developed countries. This aging population increases the in-advance chronic illnesses and therefore raises the need of permanent health monitoring. One of the major chronic illnesses around the world is in this context cardiovascular diseases. Hence monitoring of heart activity in various environments might prove a beneficial tool to keep track of the state of the heart. The usual way of monitoring the heart, like ECG with wet electrodes with wires and Holter monitoring, are not comfortable at times, even they need special preparation and observation. These conventional methods are even impractical in some environments like wheelchairs (in home and hospital) and automobiles. In this case the possibility of measuring the heart activity without any direct contact to the body may be a useful but an nascent tool. These systems can improve patients' life greatly in hospital and home by providing free mobility and comfort while being monitored. Measurement in an automobile supports comfort as well as safety features. It can be used to measure the ECG of the driver and consequently enables the possibility to judge driving fitness of the driver, which may help to improve the safety of the occupants.

The aim of this study is to show the feasibility of a broader monitoring concept by monitoring contactlessly vital signs with sensors embedded in various environments like Home, Hospital and Automotive. A capacitively (non-contact) coupled ECG (CCECG) system is developed with PCB (stiff) electrodes as pilot work. Subsequently, this system is transformed into a flexible and textile form to enable the possibility of incorporating such systems in various setups.

First, the system was implemented by reassembling prior work with a two layer capacitive textile electrode and Starflex PCB structures. A Final version with a three layer capacitive textile electrode and a compact PCB was implemented while trying different capacitive textile electrode designs. Various analog techniques like guarding, shielding, movement compensation were implemented to improve performance of the electronics. Analog and digital signal processing tool was applied to minimize noises and artifacts.

The CCECG system was integrated in setups like a car’s, wheel chairs, a clinical bed and a stretcher to analyze the feasibility study and system performance. Some subjects were tested with the setups to gain short term and long term measurements. Standard ECG analysis like QRS-complex detection and heart rate variability (HRV) were performed to assess the quality of the signals in the experimental setups.

Integration of the system into an automobile was very crucial as the work was part of a German ministry funded “INSITEX” project. Both the system with two layer and three layer structures were tested in our demonstrator seat in the laboratory. Finally real world tests in an Automobile, Mercedes Benz C-class (W204 Series) were performed by integrating the CCECG system into its car seat. Various measurements were carried out by considering real life aspects like driving in highway or city street surfaces. The influence of car seat functions, like seat movements, heating and ventilation, on the measurements was examined. Measurements were also performed by switching on various car systems, like GPS, radio, and hands-free telephony, to observe their influence on the signal. Lastly, measurements with various climatic clothes like rain jackets, winter jackets and sport coats were carried out on the same subject to find out their effect on the measurements.

Contents

1 Introduction

1.1 Motivation

D.Kirk's demographic transition theory is a model to represent demographic changes from high birth rates and death rates to low birth rates and death rates as a nation progresses from a pre-industrialized to an industrialized economic system [1]. Hence it suggests a higher aging society in the developed world than the underdeveloped world. This observation is also evident in present demographic situations in many developed countries, where the aging society is on the rise.

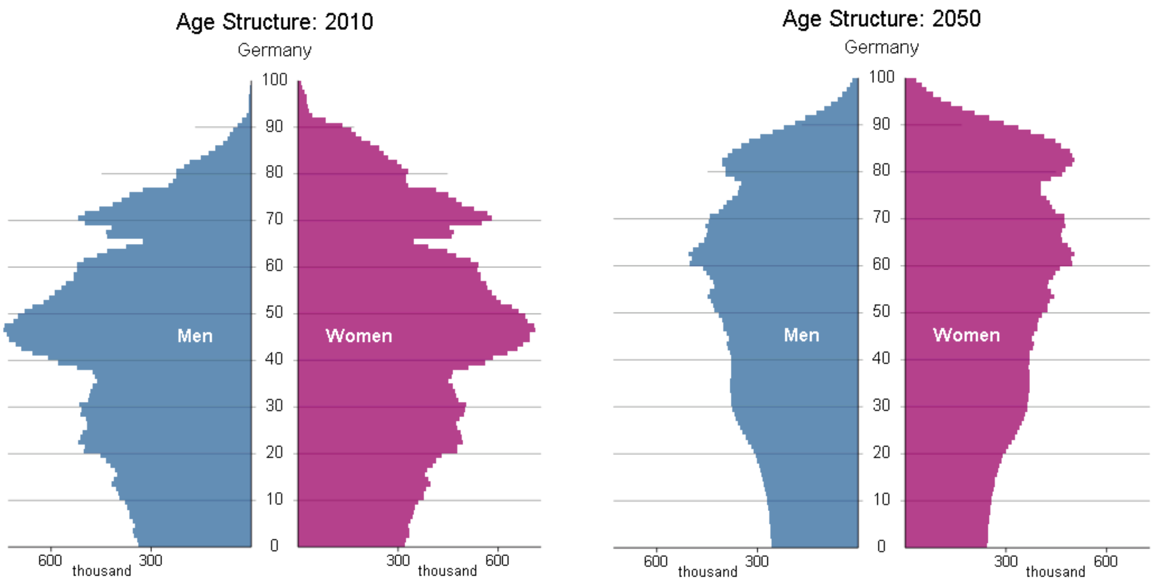

Figure 1.1 Current and Projected population of Germany by 2050 [4].

According to a study, between 2004 and 2050 in Europe, the elderly population, aged 65+, will rise sharply by 58 million (77 %) and the fastest growing segment of the population will be the very old (aged 80+) [2]. The population of Germany alone, will be expected to fall by 12 million by 2050, while those who remain will be old, half of the aged will be over 51 [3]. Figure 1.1 graphs current (2010) and projected populations of Germany by 2050 by federal statistical office of Germany (Statistisches Bundesamt) [4].

The aging population increases the in-advance chronic illnesses and therefore raises the need of permanent health monitoring. One of the major chronic illnesses around the world is cardiovascular disease. As of 2007, cardiovascular disease was the leading cause of death in the United States [5][6] (accounting for 25.4 % of total fatalities) [7]. Hence, monitoring of heart activity in various environments might prove a beneficial tool to keep track of the state of the heart. Since nowadays even older people spend a long time in automotive environments a non-contact measurement of Electrocardiogram will become a handy tool for long-term heart monitoring besides its potential short-term purpose of microsleep detection. At the same time, enabling non-obtrusive monitoring in the difficult car environments would open new paths in other areas of monitoring.

Although traffic safety is continuously improving, transportation causes considerable personal and property damage. There are around 6,000 fatalities and 440,000 injuries occurring every year in Germany [8]. In the United States, the leading cause of death is motor vehicle crashes among persons aged 5-34 years [9]. As per a study conducted by K. Rumar, using British and American crash reports as data, the majority of accidents happen because of human error [10]. One phenomenon known as microsleep resulting from tiredness, alone is responsible for 25% of all traffic accidents in Germany [11]. Driving long distances at night or on monotonous roads is especially dangerous, since full attention is not demanded permanently. In the year 2004, according to a survey, 43% of all asked truck drivers admitted to having dozed off while driving during the last year and 25% in last 4 weeks [12].

According to a UN report on global road safety crisis, the injuries and disability resulting from road traffic crashes put a significant strain on the economy, typically consuming between 1 and 3 percent of a country's gross national product per annum [13]. Globally, estimates suggest that the economic costs of road traffic injuries amount to $518 billion per annum. Thus the potential savings through avoiding accidents caused by one of the major factors, microsleep, can run in billions of dollars in a first approximation. If somehow, the reasons for these accidents can be analyzed and the cases can be reduced, human and economical sufferings can be avoided to a great extent.

A technical system which, within certain, limits can predict imminent microsleep (tiredness) would therefore mark a milestone in the development of passenger safety. From literature, it is known that driver's psychophysiological conditions (e.g. stress) can be recognized quite well through a combination of driving parameters (e.g. steering angle measurement) [14] and physiological parameters such as Heart Rate (HR), Heart Rate Variability (HRV) [15], skin impedance[16][17] and skin temperature [18].

However, the requisition of physiological parameters like Electrocardiogram during driving using conventional methods of wet electrodes is absolutely uncomfortable and impractical. A favorable solution for this application might be found in Intelligent Technical Textiles that can be integrated into the automobile interior and measure physiological parameters without compromising comfort at a low cost. At the same time such Intelligent Technical Textiles could be used for other safety features like reliable seat occupant detection and occupant position detection to trigger the airbag. Additionally such a system has a very good chance of being utilized for health monitoring.

In present day “budget driven hospital environments” only the most needy patients are continuously supervised with alarm monitors. Subsequently, mobile patients are not monitored, even though it might provide useful baseline recordings for further diagnosis and treatment.

Besides budgetary restrictions, obtrusiveness is a stronger hindrance to permanent monitoring: No mobile patient is happy to push a cart with monitors along his way, just to maintain the optimal position of cable bound electrocardiogram (ECG) electrodes. Even when using a portable Holter-type device, electrode-skin contact still forms a delicate interface prone to degradation of conductive gel, motion artifacts, and skin irritations. Metal electrodes in long term recordings might even lead to allergies and skin irritations and may result in pressure necroses [19].

Thus it might be considered as an important step towards non-obtrusiveness capacitive recording of electrical biosignals by devices not in intimate skin contact. The first capacitive recording of an ECG signal without conductive body contact was described by Richardson [20]. The surfaces of these capacitive electrodes are electrically insulated and remain stable for long-term monitoring.

Another important aspect of unobtrusiveness is a possible integration of non-contact sensors in everyday clinical objects or home furniture, thus avoiding any stirrup for "wiring" a patient and still providing monitoring options.

So all in all, the non-contact Electrocardiography with textile capacitive electrodes might be applicable from safety and health monitoring in an automotive environment to a hospital or home environment. Research work for this thesis was conducted under the funding of INSITEX (Aktive **In**sassen**S**icherheit durch **I**ntelligente Technische **Tex**tilien) project.

1.2 The INSITEX Project

INSITEX stands for "Aktive **In**sassen**S**icherheit durch **I**ntelligente Technische **Tex**tilien", which literally means active passenger safety through intelligent technical textiles [21]. This project was funded by BMBF, the German Federal Ministry for Education and Research (funding code: 16SV346) [22].

Within the project, some systems were developed like Textile Capacitive Electrocardiography, Seat Occupant Detection through knitted textile sensor and vital parameter sensors integrated in the steering wheel as depicted in the Figure 1.2(bottom). The work has been published in various forms of print media, indicating a future for intelligent textile trends in a vehicle like healthcare [23] [24] intelligent car interior [25] and drive assisting systems [26].

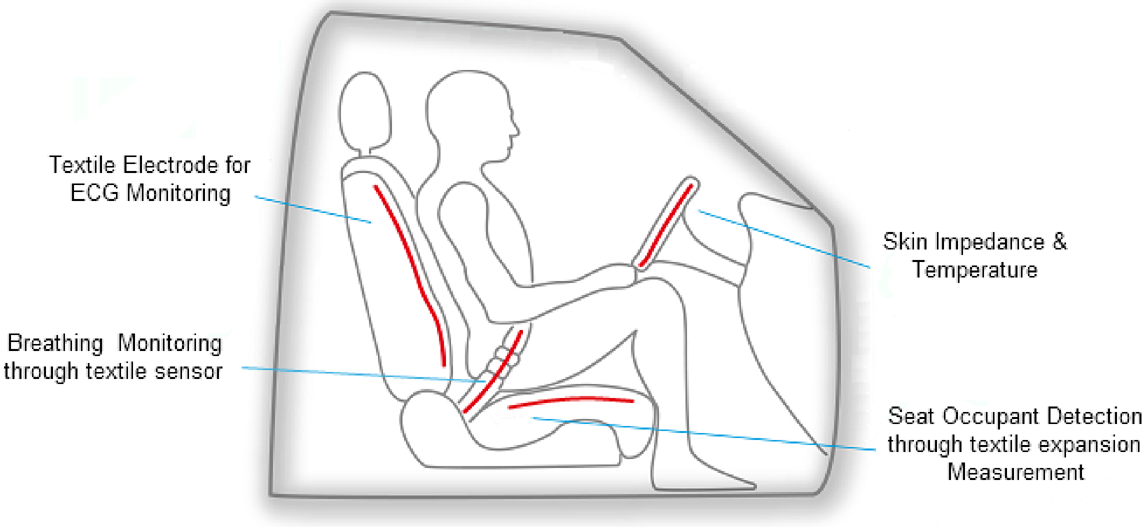

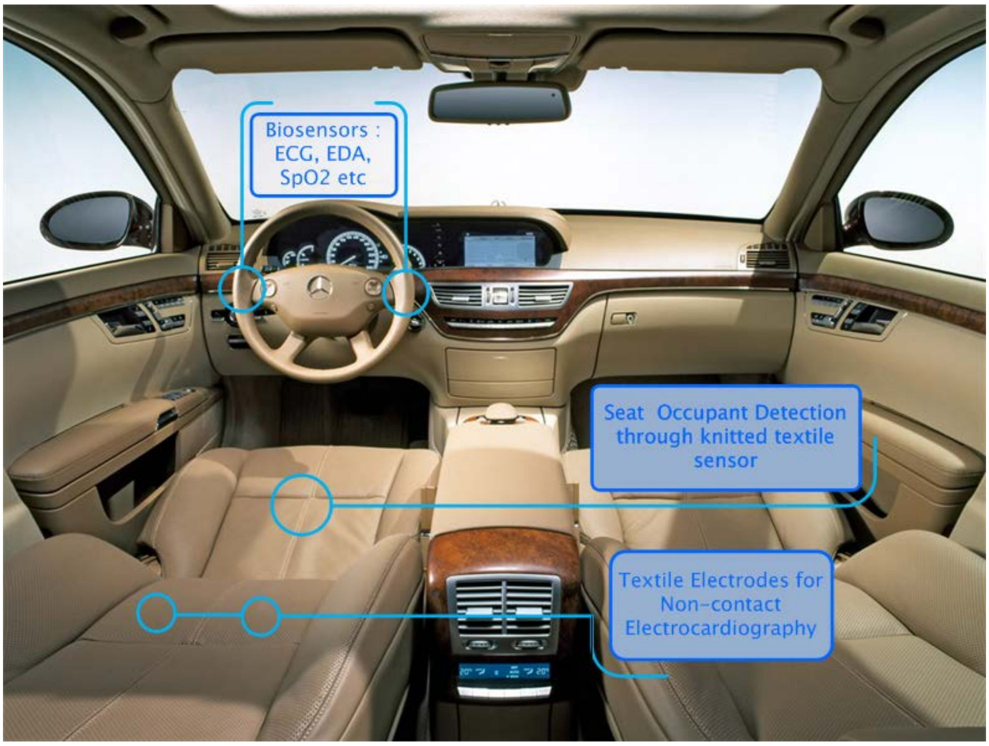

Figure 1.2 Concept of the INSITEX project (top), systems developed within the INSITEX project (bottom).

The trend to utilize smart textile technologies and health monitoring for various applications is growing and the number of products with intelligent textiles is on rise. The following are some of the projects based on technical textile sensors applied to different usages.

BIOTEX : The BIOTEX project aims at developing dedicated biochemical-sensing techniques capable of integration into textiles [27]. This allows, for the first time, the monitoring of body fluids via sensors distributed on a textile substrate and performing biochemical measurements. BIOTEX is addressing the sensing part and its electrical or optical connection to a signal processor. The approach aims at developing sensing patches, adapted to different targeted body fluids and biological species to be monitored, where the textile itself is the sensor. The extension to whole garment and the integration with physiological monitors is part of the roadmap of the consortium.

PROeTEX : The project is an IST Integrated Project which focuses on textile-based Micro-Nano technologies within a communicating framework [28]. The project is developing textile and fiber based integrated smart wearables for emergency disaster intervention personnel with a goal of improving their safety, coordination and efficiency. An additional system, for injured civilians, aims at optimizing their survival management. This focused application area will drive a wide range of key technology developments to create micro-nano-engineered smart textiles - integrated systems (fabrics, wearable garments) using specifically textile-based micro-nano technologies. These developments will feed through to a wide range of other markets from extreme sports, through healthcare to transportation maintenance and construction workers.

MyHeart : The project is an IST Integrated Project whose goal is to gain knowledge on a citizen's actual health status by continuous monitoring of vital signs [29]. It integrates system solutions into functional clothes with integrated textile sensors. The combination of functional clothes and integrated electronics, capable of processing them on-body, can be defined as intelligent biomedical clothing. The processing consists of making diagnoses, detecting trends, and reacting to them. MyHeart comprises feedback devices, able to interact with the user as well as with professional services. This system is suitable for supporting citizens' fight against major CVD (Cardio Vascular Disease) risk factors and helps to avoid heart attack and other acute events, by personalized guidelines; and gives feedback. It provides the necessary motivation to adopt new life styles.

Wealthy : The project is an IST project in which smart materials in fiber and yarn form endowed with a wide range of electro-physical properties (conducting, piezo-resistive, etc.) are being integrated and used as basic elements to implement a wearable system for collecting physiological data [30]. Wealthy system integrates computing techniques, smart sensors, a portable device and telecommunication, together with local intelligence and a decision support system. The proposed system assists patients during rehabilitation or subjects working in extreme stressful environmental conditions, by ensuring continuous intelligent monitoring.

SmartSenior : The project is one of the very big BMBF funded projects, containing funding of 25 million € [31]. The goal of the project is to develop an integrated service platform and the creation of different exemplary services with common user interfaces that consider elderly users. Health services, anomaly detection, personalized recommendations, telemedicine, usability evaluation, and financial models are the central research topics within this project.

1.3 Scope of the thesis

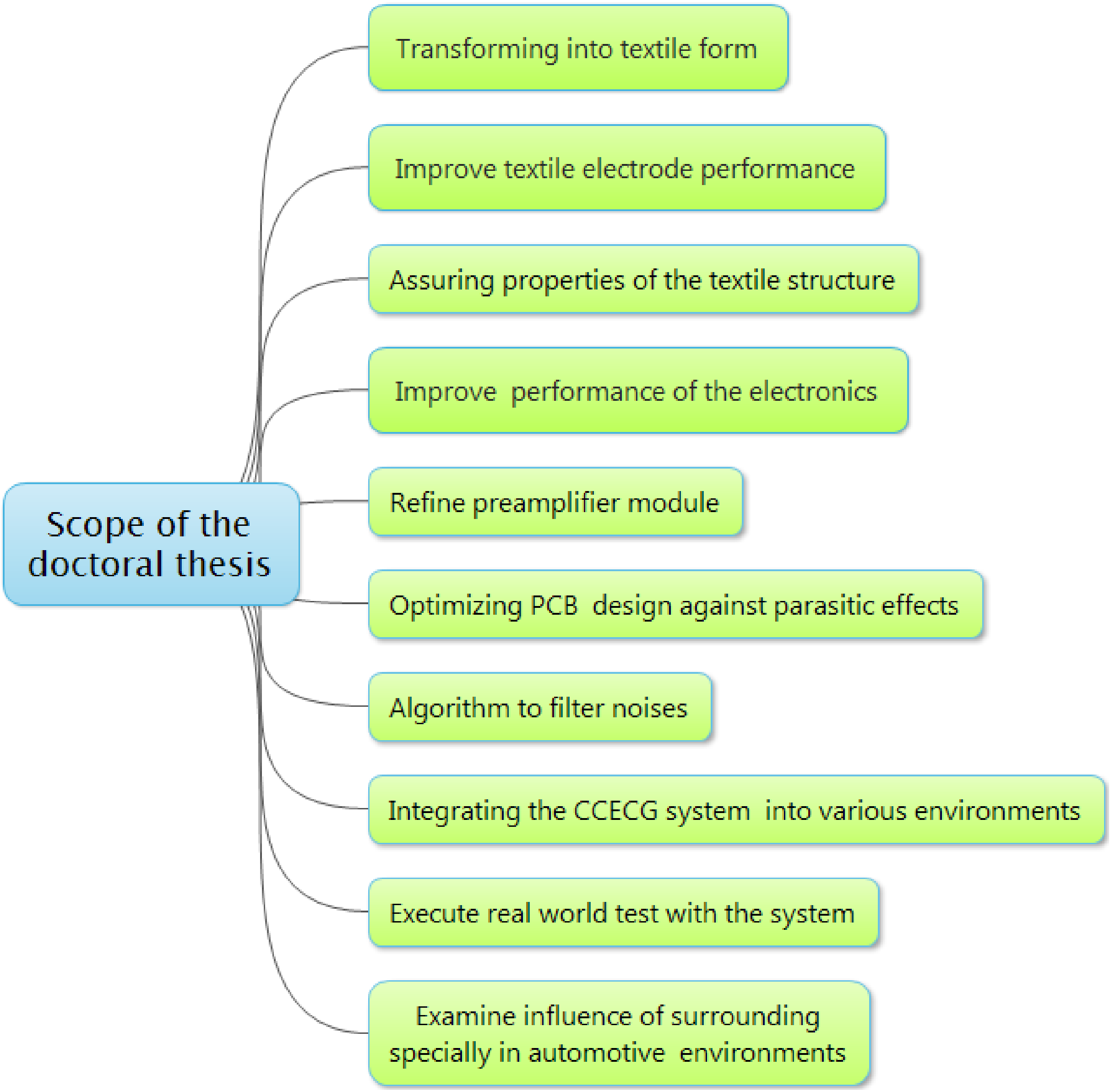

Figure 1.3 Scope of this doctoral study.

The need to acquire Electrocardiograms without any galvanic contact to the skin arose to fulfill the requirement described earlier. Electrocardiography has to be incorporable in various environments like automotive, hospital, home etc. It should adhere to the body contour and hence provide a flexible and comfortable feeling for the subject. Thus a textile non-contact Electrocardiography system is thought to fulfill the entire requirement explained above.

Within the project INSITEX, a capacitive coupled ECG system based on PCB electrodes was developed in previous work as a pilot study. The hard nature of this stiff electrode made it impractical to integrate the system into the automotive environment and discomforting to the subject as well. There was also room to improve the overall electronics of the system. Furthermore, amendment of the analogue and digital signal processing of the capacitive ECG signal was necessitated improvement in signal resolution and signal to noise ration.

Considering the above described requirements, different studies mentioned in Figure 1.3 need to be executed to fulfill the scope of this doctoral work.

Reference

[1] Dudley Kirk, “Demographic Transition theory,” Population studies vol. 50, pp. 361-387, 1996.

[2] G. Carone and D. Costello, “Can Europe afford to grow old ?,” Finance and Development (a quarterly magazine of the IMF) Vol. 43 No. 3, September 2006.

[3] The Aging society-Goethe Institute, ”Fear of aging or fear of old?- call for positive approach to aging,” retrieved on 2 June 2011. Source : www.goethe.de /ges/soz/dos/dos/age/en1275489.htm, last accessed on 10 June 2011.

[4] Federal Statistical office of Germany, ”Population projection of Germany,” retrieved on 2 June 2011. Source : http://www.destatis.de/jetspeed/portal/cms/Sites/destatis/Internet/EN/Navigation/Statistics/Bevoelkerung/VorausberechnungBevoelkerung/VorausberechnungBevoelkerung.psml , last accessed on 10 June 2011.

[5] Arialdi M. Minino et al, ”Deaths: final data for 2004,” National vital statics reports, Vol. 55, No. 19, 21 August 2007.

[6] White house news, “American Heart Month 2007, A Proclamation by the President of the United States of America,” 1 February 2007.

[7] Jiaquan Xu et al., “Deaths: final data for 2007.” National vital statics reports, Vol. 58, No. 19, 20 May 2010.

[8] Federal Health Monitoring of Germany (Gesundheitsberichterstattung des Bundes), “Unfällen kapitel 2.2.4 (Accidents Chapter 2.2.4),” Gesundheit in Deutschland 2006, pp. 1-15, 2006.

[9] Centers for disease control and prevention, “Vital Signs: Nonfatal, Motor Vehicle--Occupant Injuries (2009) and Seat Belt Use (2008) Among Adults -United States,” Morbidity and Mortality Weekly Report, 59 (51), pp. 1681-86, 7 January 2011.

[10] Harry Lum and Jerry A. Reagen, “Interactive highway safety design model: Accident predictive module,” Public roads, Vol. 59, No. 2, winter 1995.

[11] Cynthia Mouchbahani, “Ich schau dir in die Augen, Kleines ,” Technik und Kommunikation, pp. 94-95, February 2005.

[12] ADAC (Allgemeiner Deutscher Automobil-Club e.v.), “Schläfrigkeit am Steuer wirkungsvoll begegnen ,“ Fakten & Argumente kompakt, pp. 1-20, 2010.

[13] United Nations General Assembly, “Global road safety crisis, report of the secretary general,” Fifty-eight session, A/58/228, 7 August 2003.

[14] R. Sayed and A. Eskandarian “Unobtrusive drowsiness detection by neural network learning of driver steering,” Journal of Automobile Engineering, Vo. 125, No. D9, pp. 969-975, 2001.

[15] H. Lee, J. Kim, Y. Kim, H. Baek, M. Ryu, K. Park, “The relationship between HRV parameter and stressful driving situation in the real road,” 6th International Special Topic Conference on ITAB. Tokyo, Japan 2007.

[16] J.A. Healey and R. W. Picard, “Detecting stress during real-world driving tasks using physiological sensors,” Intelligent Transportation Systems, IEEE Transactions on, Vol. 6(2), pp.156-166, June 2005.

[17] M. M. Bundele and R. banerjee, “ Detection of Fatigue of Vehicular Driver using Skin Conductance and Oximetry Pulse: A Neural Network Approach,“ Proceedings of Information Integration and wed based application service 2009, pp. 725-730, 14-16 December 2009.

[18] T. Yamakoshi, K. Yamakoshi, S. Tanaka, M. Nogawa, M. Shibata, Y. Sawada, P. Rolfe, and Y. Hirose, ”A preliminary study on drivers stress index using a new method based on differential skin temperature measurement,” In Proceedings of the 29th Annual International, pp. 722-724, August 23-26, 2007.

[19] A. Aleksandrowicz and S. Leonhardt, “Wireless and Non-contact ECG measurement system – the “Aachen Smartchair”,” Acta Polytechnica, vol. 47, No. 4-5, pp. 68-71, 2007.

[20] Richardson, P. C., “The Insulated Electrode,” In Proceedings of the 20th Annual Conference on Engineering in Medicine and Biology. Boston, MA (USA), p. 157, 1967.

[21] INSITEX Project flyer, Source : http://www.mstonline.de/foerderung/projektliste/printable_pdf?vb_nr=V3TEX028, last accessed on 10 June 2011.

[22] INSITEX Project Briefed by BMBF, Source : http://www.mstonline.de/foerderung/projektliste/detail_html?vb_nr=V3TEX028, 10 June 2011.

[23] Financial Times, Germany, “Medizin in PKW, Wenn das Auto den Arzt ruft (Medicin in car, when car calls the doctor) ”, Webpage : http://www.ftd.de /unternehmen/industrie/:medizin-im-pkw-wenn-das-auto-den-arzt-ruft/60065026.html, last accessed on 15 june 2011.

[24] Daimler, RD Inside, Newspaper for employees in group Research and Mercedes Benz cars Development, “Der Sitz denkt mit (the seat thinks with you),” June 2011 Edition.

[25] I. Hofmann, “Daimler AG is investigating the potential of smart technologies for car interior,” Systex Newsletter Vol.3, p. 5, July 2010.

[26] Thomas Schreiner, “Hallo-wach-Effekt, Müdigkeitswarner und Aufmerksamkeits-Assistenten sagen dem tückischen Sekundenschlaf den kamfen an,” Auto & Reise Magazine pp. 44-45, June 2011.

[27] BIOTEX Project, Webportal : http://www.biotex-eu.com. Last accessed on 10 June 2011.

[28] PROeTEX Project, Webportal : http://www.proetex.org/. Last accessed on 10 June 2011.

[29] MyHeart Project, Website : http://www.hitech-projects.com/euprojects/myheart/. Last accessed on 11 June 2011.

[30] Wealthy Project, Webportal : http://www.wealthy-ist.com/. Last accessed on 11 June 2011.

[31] SmartSenior Project, Webportal : http://www1.smart-senior.de. Last accessed on 11 June 2011.

2 Theoretical Background

Before starting with the description of the technical work, this chapter will give an introduction to certain fields of knowledge that are addressed in this thesis.

2.1 Cardio-vascular system

2.1.1 Anatomy of heart

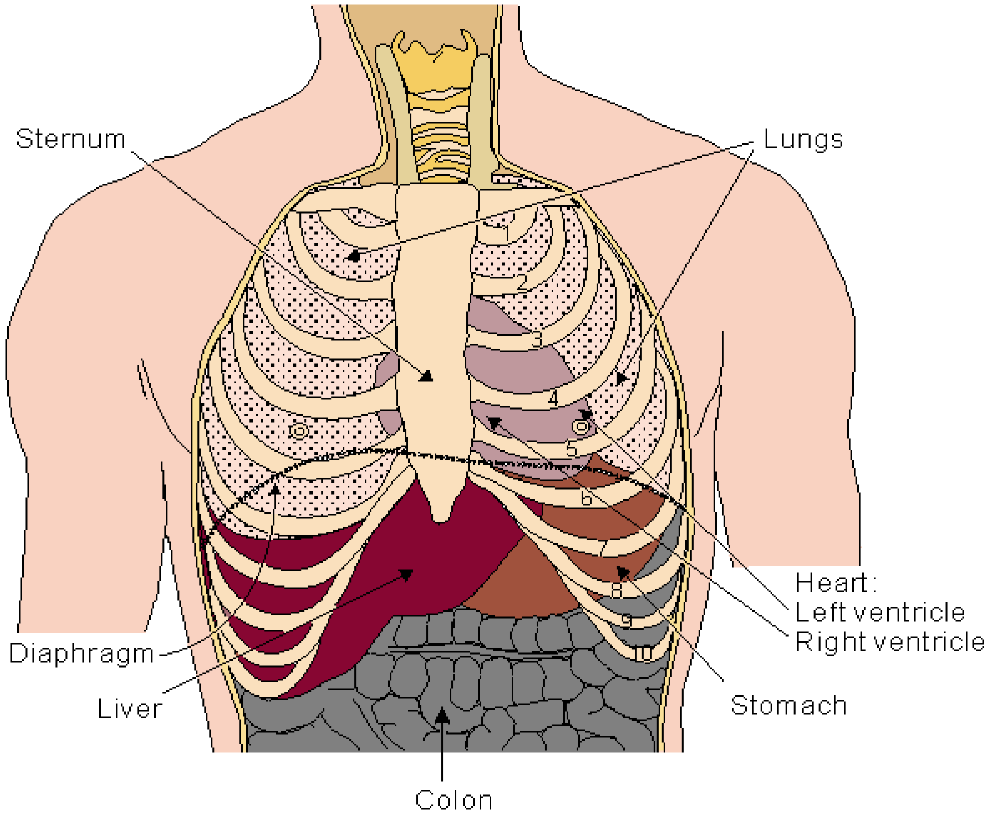

Figure 2.1 Location of heart [1].

The human heart is located between the lungs and the middle of the chest, behind and slightly left to the sternum [2]. A double-layered membrane called the pericardium surrounds the heart like a sac. The outer layer of the pericardium surrounds the roots of heart's major blood vessels and is attached by ligaments to the spinal column, diaphragm, and other parts of the body. The inner layer of the pericardium is attached to the heart muscle. A coating of fluid separates the two layers of membrane, letting the heart move as it beats, yet still be attached to the body.

The heart's wall is made up of cardiac muscle and is called myocardium. It has four chambers- the upper chambers are called right and left atria and the lower chambers are called right and left ventricles [1]. The wall of the left ventricle is thicker than any other chamber as it has to pump the blood to the body with high pressure. The right atrium and ventricle are connected through the tricuspid valve and the left atrium and ventricle through the mitral valve. The flow of blood to the left pulmonary artery from the right ventricle and to the circulatory system from the left ventricle is controlled by the pulmonary valve and aortic valve respectively.

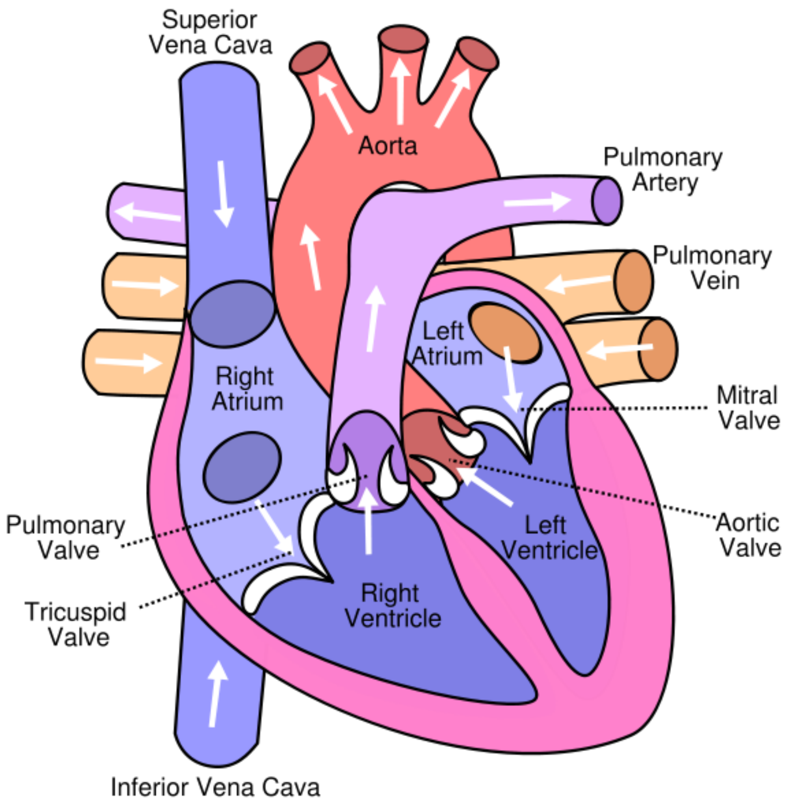

Figure 2.2 The heart [3].

Deoxygenated blood from the veins flows to the right atrium through the inferior and superior vena cava and flows to the right ventricle through the tricuspid valve [1]. Then the right ventricle pumps the blood to the lungs though the pulmonary valve to oxygenate it. The oxygenated blood comes back to the left atrium and flows to the left ventricle though the mitral valve. Finally the left ventricle supplies the blood to the circulation system.

2.1.2 ECG generation from heart

The group of muscle cells located on the top of right atrium at the SA (sinoatrial) Node acts as a pacemaker. These cells are self-excitatory and produce pulses at a rate of 70 beats per minute normally. A complex change in ionic concentration across the cell membranes establishes an extracellular potential field. This excites neighboring cells, and hence cell to cell propagation of electrical events takes place. Because the body acts as an electrolytic medium, these potential fields extend to the body surface and form body surface potentials.

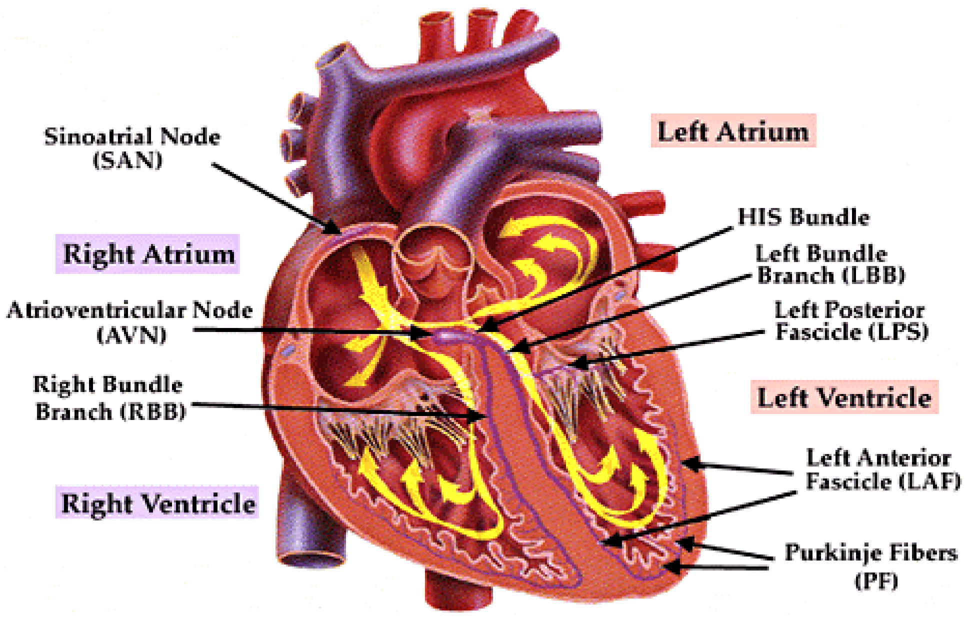

Figure 2.3 Electrical conduction of heart [4].

The character of the body surface waves depends on the amount of tissue activated at one time and the relative speed and direction of the activation wavefront [5]. Therefore, the pacemaker potentials that are generated by a small tissue mass are not seen on the ECG. As the activation wavefront encounters the increased mass of atrial muscle, the initiation of electrical activity is observed on the body surface, and the first ECG wave of the cardiac cycle is seen. This is the P wave as shown in Figure 2.4, and it represents the activation of the atria. Conduction of the cardiac impulse proceeds from the atria through a series of specialized cardiac cells (the A-V node and the His-Purkinje system) which again are too small in total mass to generate a signal large enough to be seen on the standard ECG. There is a short, relatively isoelectric segment following the P wave. Once the large muscle mass of the ventricles is excited, a rapid and large deflection is seen on the body surface. The excitation of the ventricles causes them to contract and provides the main force for circulating blood to the organs of the body. This large wave appears to have several components. The initial downward deflection is the Q wave, the initial upward deflection is the R wave, and the terminal downward deflection is the S wave. The polarity and actual presence of these three components depend on the position of the leads on the body as well as a multitude of abnormalities that may exist.

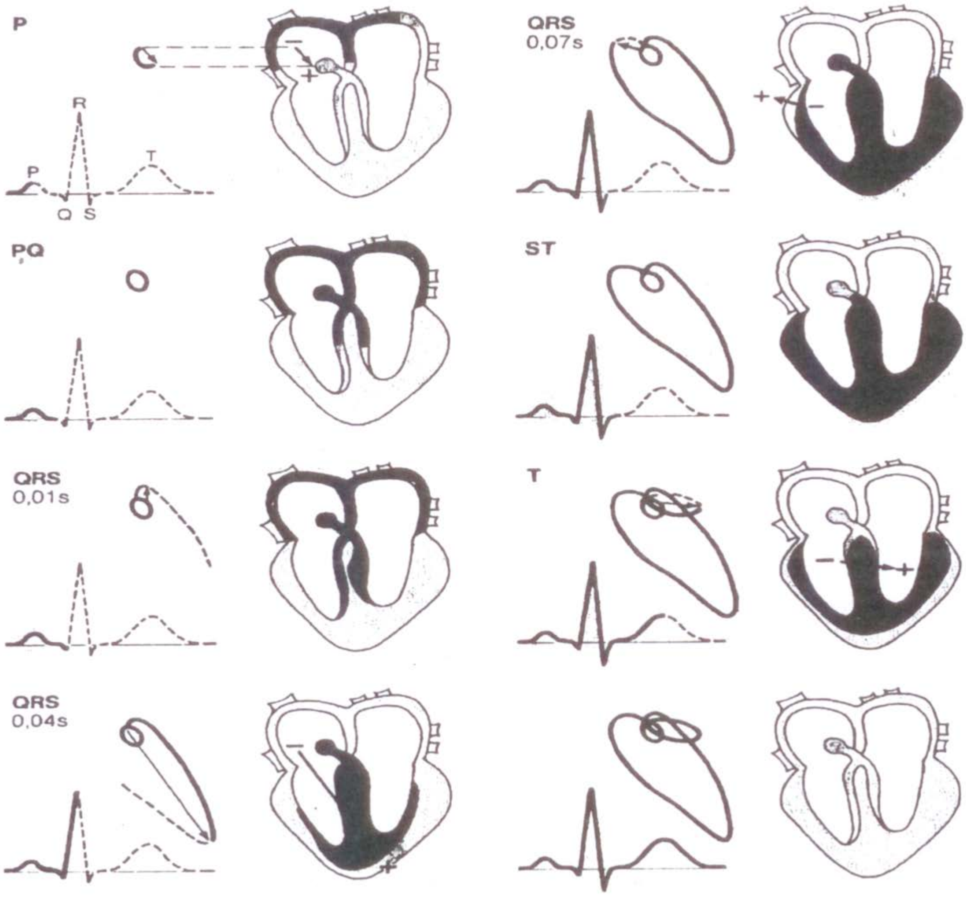

Figure 2.4 Heart cycle for the ECG wave generation [6].

In general, the large ventricular waveform is generically called the QRS complex regardless of its makeup. Following the QRS complex is another short relatively isoelectric segment. After this short segment, the ventricles return to their electrical resting state, and a wave of repolarization is seen as a low-frequency signal known as the T wave. In some individuals, a small peak occurs at the end or after the T wave and is the U wave. Its origin has never been fully established, but it is believed to be a repolarization potential [5]. The latency shown in Figure 2.4 approximates that normally found in the healthy heart [1].

2.1.3 Body surface potential mapping

When the heart beats, it produces, as described above, muscle stimulation and generates a spatial and temporal electric field. The electric stimulation spreads across the conductive body and can be recorded as electrocardiogram with several leads. In 1887, August Waller recorded the electric field distribution on the surface of the human thorax as depicted in Figure 2.5.

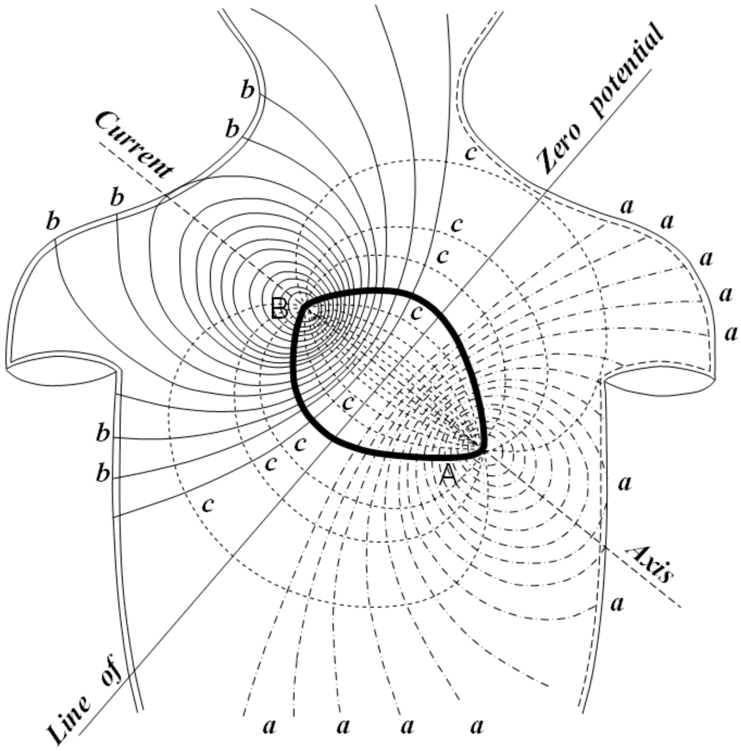

Figure 2.5 Electric field of the heart on the surface of the thorax, recorded by Augustus Waller (1887) [1].

Body surface potential maps show lines joining area of same potentials (isopotential lines) in the normal human body at a specific time instance. Figure 2.6 shows isopotential maps of a normal healthy subject mid-way through the heart’s QRS (ventricular depolarization) period. The map has been superimposed onto the outline of a human torso and is obtained from multiple ECG electrodes located substantially fully around the torso from the anterior to the posterior as shown in Figure 2.6 [7].

The curves (a) and (b) represent the recorded positive and negative isopotential lines, respectively. These indicate that the heart is a dipolar source having the positive and negative poles at (A) and (B), respectively. The curve (c) represents the assumed current flow lines [1].

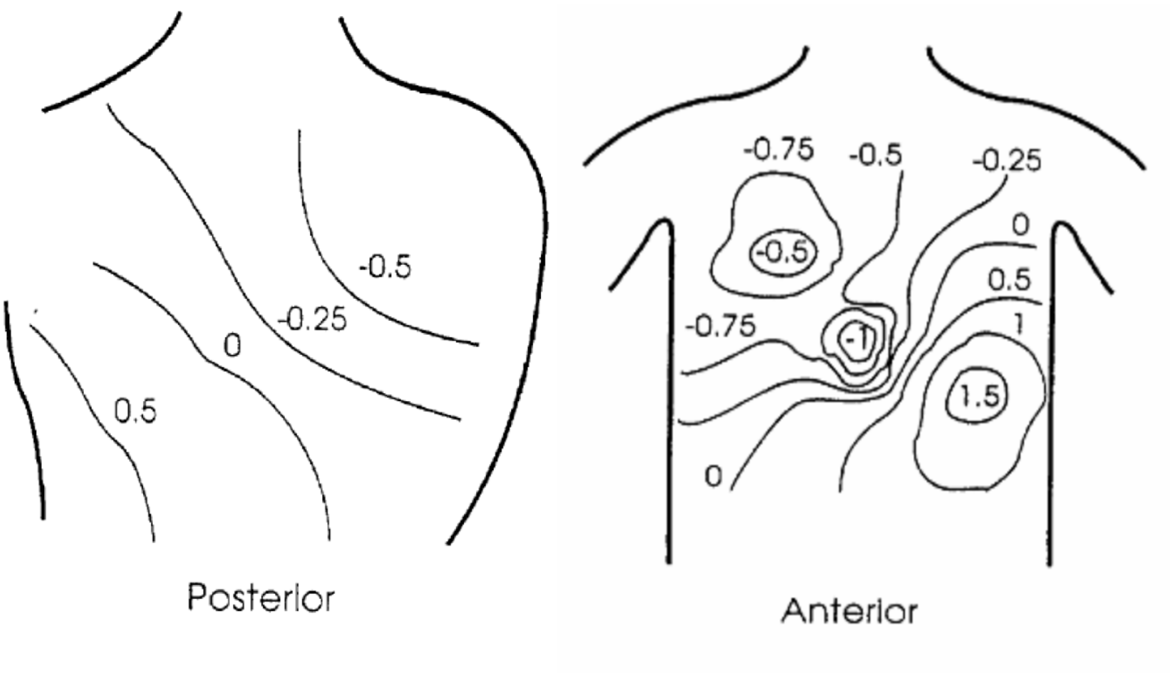

Figure 2.6 Body surface potential mapping at mid-way through QRS complex [7]**.**

The idea of integrating an ECG signal over a predefined interval was first conceived by Wilson. Using this mathematical integration over all ECG signals recorded over the body surface, allows maps to be constructed which present the body surface as lines which join area possessing the same integral values. The integrations are performed over pre-defined time intervals of the ECG. Such iso-integral maps have shown that there is more information outside the spatial scope of the standard 12 lead ECG, which could be used by a clinician to improve patient management. These iso-integral maps have proved their ability to provide as accurate diagnosis in acute instances where the standard 12 leads was equivocal. However, to see the whole electrical "picture" requires the viewing of successive maps at successive time instants throughout at least part of the cardiac cycle [7].

2.1.4 Volumetric conduction

An electric model of a volumetric electric conduction can be represented by injecting a current I at a point on the skin surface. This integral form of Poisson's equation gives us the potential ϕ at distance r as [8]

$$\phi = \frac{1}{4\pi\sigma}\int \frac{I_v}{r}\, dV \tag{2.1}$$

Where,

σ = Scalar conductivity

I_υ = Current Intensity

V = Volume

If the potential at infinity is fixed at zero, and the tissue is considered to be homogeneous with resistivity ρ at infinity, in extent, then the integration can be performed with the radial distance to obtain.

$$V(r) = I \int_r^\infty \frac{\rho}{4\pi r^2}\, dr = \frac{\rho\, I}{4\pi r} \tag{2.2}$$

This represents how the potential changes with radial distance from a point source of current *I*. It can be extended to study the case of a cylindrical nerve fiber within a uniform conducting medium, which is depicted in Figure 2.7.

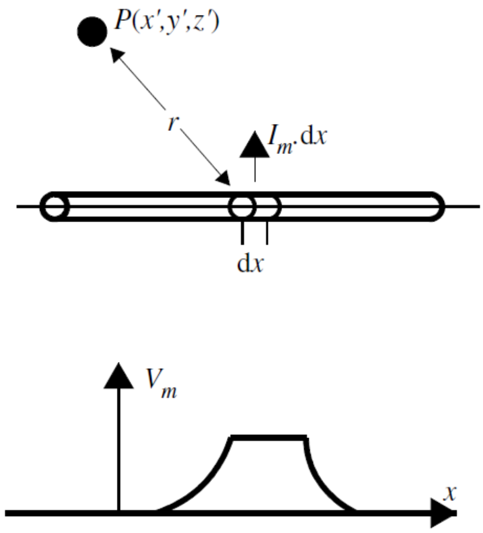

Figure 2.7 A cylindrical nerve fiber set within an infinite-volume conductor and extending in the positive x direction. We calculate the potential at a point P where the coordinates are (x',y',z'). The current emerging from the element dx is of magnitude I_m *dx* and is related to the transmembrane potential V_m [8].

If the current which emerges from an element dx of the membrane is I_m dx then,

$$V(r) = \frac{\rho\, I_m\, dx}{4\pi r} \tag{2.3}$$

If the element I_m is located at (x,y,z), the contribution made to the potential field at point P(x',y',z') can be calculated as illustrated in Figure 2.7 as follows:

$$r = [(x - x')^2 + (y - y')^2 + (z - z')^2]^{1/2} \tag{2.4}$$

and we can integrate along the fiber to obtain the superimposed potential at point P. We will place the fiber along the x-axis such that y = z = 0.

$$\phi(x, y, z) = \int \frac{\rho\, I_m(x)}{4\pi\, [(x - x')^2 + y'^2 + z'^2]^{1/2}}\, dx \tag{2.5}$$

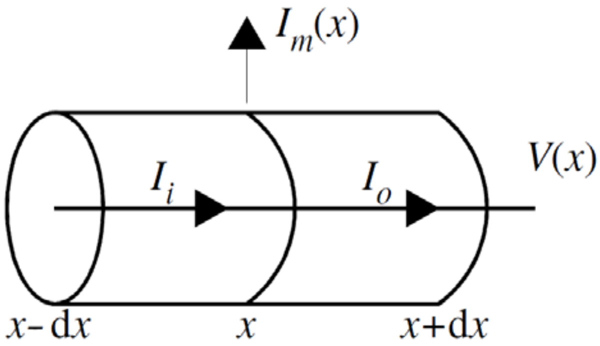

Figure 2.8 The current I_m emerging from an element of a nerve fiber is related to the transmembrane potential V [8].

In order to determine the potential distribution, we need to know I_m. The transmembrane potential was shown in Figure 2.7. This can be related to I_m, as follows, using the notation of Figure 2.8.

$$I_m(x) = I_i - I_o = \frac{[V(x) - V(x - dx)]a}{\rho\, dx} - \frac{[V(x + dx) - V(x)]a}{\rho\, dx} = \frac{2a}{\rho}\frac{d^2V}{dx^2} \tag{2.6}$$

Where

a = cross-sectional area of the fiber

σ = resistivity of the axoplasm.

If the form of the transmembrane potential V_m is known, equation (2.6) and (2.5) can be utilized to ascertain I_m and ϕ at any point respectively.

This calculation is graphed in Figure 2.9, where the potential ϕ has been calculated as a function of x for three different values of y, with z taken as zero. V_m was defined over the time 1-280 and ϕ was calculated for y = 30, 40 and 50. V_m was defined as $(x - 120)^2$ for $120 \leq x < 130$, 100 for $130 \leq x < 150$, $(160 - x)^2$ for $150 \leq x < 160$ and zero elsewhere. The double differentiation for equation (2.6) and integration for equation (2.5) were performed numerically.

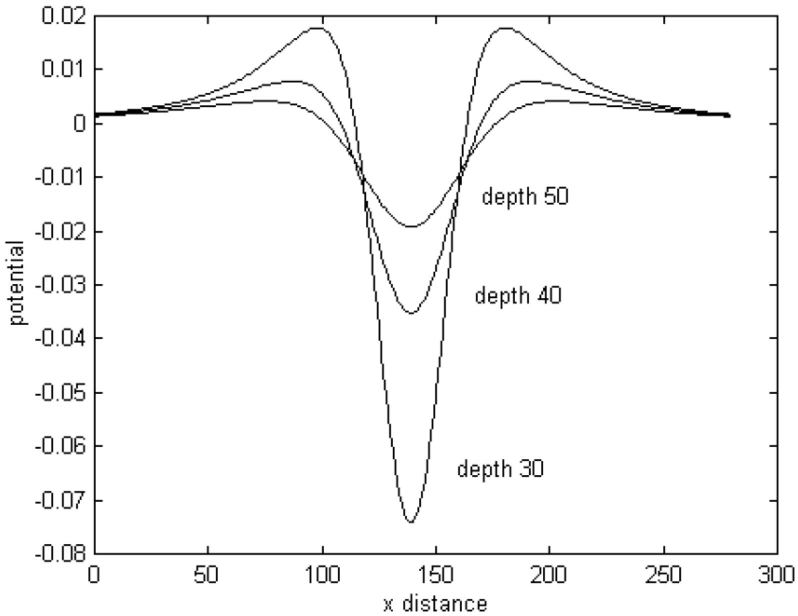

Figure 2.9 The potential field around a nerve at different perpendicular distances from the nerve [8].

The form of the potential shown in Figure 2.9 shows that a triphasic waveform can be expected to be recorded as an action potential is propagated past a recording electrode. It also indicates that the shape of the signal will depend upon the distance between the nerve and the electrode. Here, the size of the signal as well as the timing of the successive peaks vary with distance.

A change in frequency content of the signal is expected as the distance between electrode and the nerve changes. This is demonstrated in Figure 2.10, where the Fourier transforms of the three signals of Figure 2.9 are plotted. It can be observed that as the distance between nerve and recording electrode decreases the amplitude of the high frequency components rises. It was found in practice that when electrodes are moved closer to the source of a bioelectric signal, the bandwidth of the measured signal increases.

Additionally, as the action potential approached an electrode the potential is positive initially, followed by negative and positive inclination respectively.

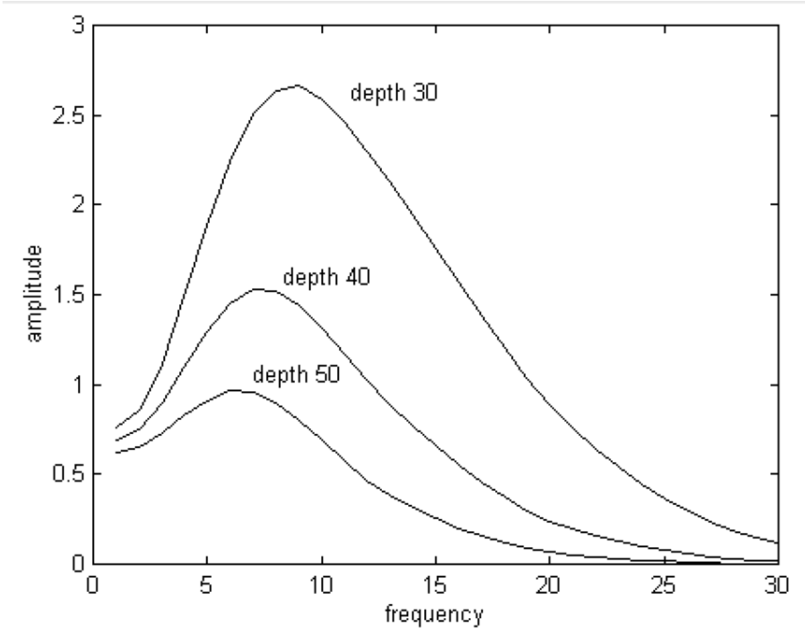

Figure 2.10 This shows the frequency transforms of the three signals given in figure 16.12. Note the increase in high frequency components close to the nerve axon [8].

2.2 Electrocardiography

The Electrocardiogram is a record of electric activity of the heart over time with an electrocardiograph. It shows repolarization and depolarization of the heart muscle and hence depicts diagnostic information related to heart [9].

It was originally observed by Waller in 1887 using a pair of electrodes (Zinc covered by chamois leather and moistened with brine) connected to Lippmann's capillary electrometer [10]. The electrodes were strapped in the front and back of the chest. He indicated the dipole nature of the electric activity and suggested measuring the ECG between various points.

In 1903, Einthoven enhanced the technology by employing the string galvanometer as the recording device [11]. He achieved better signal resolution than earlier studies and made a breakthrough in the ECG measurement technology. Einthoven is chiefly responsible for introducing some concepts still in use today, including the labeling of the various waves (P, Q, R, S, and T), defining some of the standard recording sites (Lead I, II and III) using the arms and legs [12]. We also owe the EKG acronym to Einthoven's native Dutch language, where the root word cardio is spelled with a K. In 1924; he was awarded the Nobel Prize in Medicine for his discovery of the mechanism of the electrocardiogram [13].

The electrocardiogram (ECG) is an electric single with amplitude range (QRS peak) from 0.4 to 2.5 mV [14]. This signal can be acquire by an electric machine called electrocardiograph. A conventional Electrocardiograph consists several parts ranging from an electrode to display / plot.

Electrode : it forms an electric contact (impedance) between the electric circuitry of the Electrocardiograph and the human body to convey the ECG signal to the system. Impedance created because of this contact is called source impedance and it is a very crucial parameter while designing the measurement system.

Amplifier : ECG signals are quite small in amplitude, and are therefore not sufficient for the display or plot. So the signal requires amplification of a factor of 1000 normally.

Filters : while measuring an ECG signal, there is the possibility of have various signal interference like EMG signal from nearby muscle, power line noise etc. These signals can be eliminated using appropriate signal filtering. The quality of a clinical ECG signal can be achieved using a bandwidth of 0.05 Hz to 100 Hz with accurate reproduction of the wave shape and can be 0.5-50 Hz for monitoring purposes . In this case, higher frequency noise beyond the ECG bandwidth are removed. Additionally power line noise (50/60 HZ) are in the range of the ECG and should be removed with a notch filter. In short, any undesirable signal from the ECG should be removed with analog and digital filters in order to represent it interpretable for further use or diagnosis.

Display : Finally the ECG signal can be displayed for useful interpretation with help of devices like oscilloscope, monitor, plotter etc.

In order to record an Electrocardiogram, a differential recording between two points on the body is made. Traditionally, each differential recording is referred to as a Lead [5]. Leads are made up of different combinations of electrodes in order to get an ECG from different views. Thus the different leads are projections of the heart’s depolarization vector onto different axis.

A clinically accepted lead system has been devised and is known as 12 lead system [15]. It consist of electrode combinations for taking the ECG measurement from different part of body like limb, chest, precordial [16]. The limb leads acquire the signal from limbs and called leads I, II and III. Similarly chest leads and precordial leads acquire signals from the combination of limb leads and chest respectively. The chest lead called aVR, aVL and aVF and precordial leads called V1, V2, V3, V4, V5 and V6. These various leads help to diagnose the patient's heart condition significantly.

2.3 Capacitor

A capacitor comprises two electric conductor separated by an dielectric (electric insulator) [17]. A dielectric material is an electric insulating materials like paper, air, oil, plastic etc. A capacitor can be charged by applying voltage across its terminals. The charging of capacitor transfers charges from one side (+Q) of the capacitor to the another side (-Q), maintaining the net charges of the capacitor to zero [18]. Differential of these charges is equal to energy storage of the capacitor, resembling a power source [19]. So, the greater the amount of charges on one side of the capacitor compare to another, the greater the energy the capacitor can hold.

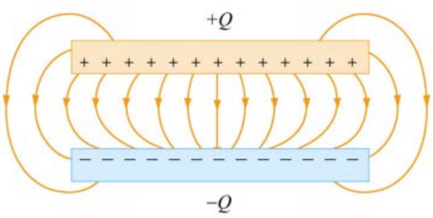

Figure 2.11 A parallel plate capacitor with electric field [21].

The difference of the charges creates an electric field between the side of the capacitor and potential difference as well [20]. The amount of the charges (Q, coulomb) on the capacitor is proportional to voltage (V, volt) across it. The constant of proportionality is called capacitance and has the unit Farad.

$$C = \frac{Q}{V} \tag{2.7}$$

2.3.1 Parallel plate capacitor

One of the basic capacitor configurations is a parallel plate model, consisting of identical parallel plate isolated by a dielectric medium with permittivity ε. The plates are assumed to have uniform area A and a charge density $\pm\rho$ (= $\pm Q/A$) exists on the either surface [17]. The model can be configured as depicted in Figure 2.11, by placing the plates exactly parallel to each other and separating them by a vacuum with distance d. This setup also can be helpful as a basic model to roughly estimate various parameters of other geometries.

It can be seen in Figure 2.11, the electric field at the edges is not straight and the entire electric field is not covered inside the plate. This phenomenon is known as edge effect and non-uniform electric field is called fringing fields [21]. This effect and the non-uniform electric field can be ignored here by considering the ideal situation, where the electric fields are straight lines only.

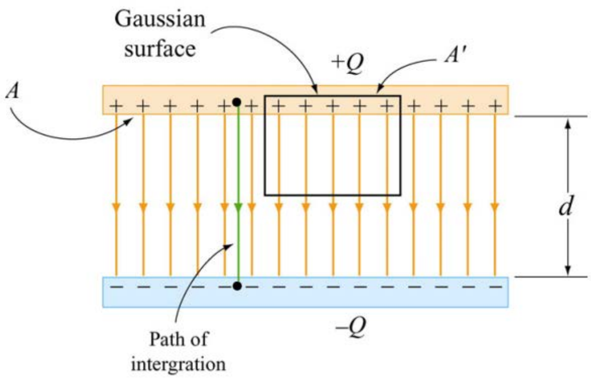

Figure 2.12 Calculation of the electric field between the plate with Gaussian surface [21].

According to Gauss's law for calculating the magnitude of the electric field (E) between the charged parallel plate capacitor is [21].

$$E = \frac{\rho}{\varepsilon_0} \tag{2.8}$$

Considering path of integration to be straight line from positive charged side towards negative charged side as depicted in Figure 2.12 [21]. Because the electric potential lines always follow from higher potential to lower potential. So the potential difference between the plate is [21]

$$V = \int_{+}^{-} \vec{E} \cdot d\vec{s} = -Ed \tag{2.9}$$

Hence,

$$|V| = Ed \tag{2.10}$$

Following the capacitance definition from equation (2.7), capacitance for the parallel plate model separated by vacuum (distance d and dielectric constant =1) is as follows

$$C = \frac{Q}{|V|} = \varepsilon_0 \frac{A}{d} \tag{2.11}$$

Addition of a dielectric material between the plates reduces the electric field between the plates by the dielectric constant of the material [22].

$$E_{new} = \frac{E_{vacuum}}{\varepsilon_r} \ \ and \ \ V_{new} = \frac{V_{vacuum}}{\varepsilon_r} \tag{2.12}$$

Hence the capacitance in the case is

$$C = \varepsilon_0 \, \varepsilon_r \, \frac{A}{d} \tag{2.13}$$

Where,

A = Area of the plates (m^2)

d = distance between the plates (m)

ε_0 = Vacuum permittivity (8.854 X 10^{-12} F/m)

ε_r =Relative permittivity of the dielectric material

Thus increasing area can raise the capacitance and similarly increasing the distance between the plates can reduce the capacitance. Impedance of this capacitance can be achieved (considering ideal capacitor, hence no resistive part) by following equation [23].

$$Z_c = -\frac{j}{2\pi f \cdot C} \tag{2.14}$$

2.3.2 Capacitor with more dielectric materials

In the earlier section, the capacitance formula of a parallel plate capacitor was explained. Now for capacitively coupled measurements, it is crucial to consider more dielectric material than one. Figure 2.13 illustrates a parallel plate capacitor with more dielectric material (k_1,k_2 and k_3) in parallel.

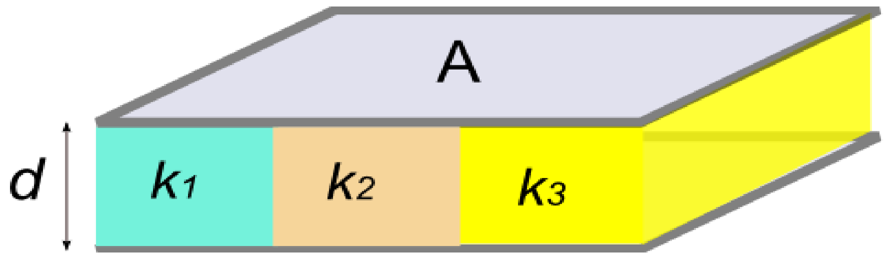

Figure 2.13 A parallel plate capacitor with more dielectric material in parallel

It can be seen in Figure 2.13 that total charges on the capacitor can be represented by accumulation of charges on respected plates (A) of the each dielectric material [24]. Hence this can be described by following equation

$$Q = Q_1 + Q_2 + Q_3 \tag{2.15}$$

Hence the following result can be derived after implementing the equation (2.7) in the above equation.

$$Q = V \cdot C_1 + V \cdot C_2 + V \cdot C_3 \tag{2.16}$$

$$C = C_1 + C_2 + C_3 \tag{2.17}$$

Therefore, the resulting (total) capacitance of the capacitor can be calculated considering the capacitors in parallel with respected dielectric material and area as defined in equation (2.17) [24].

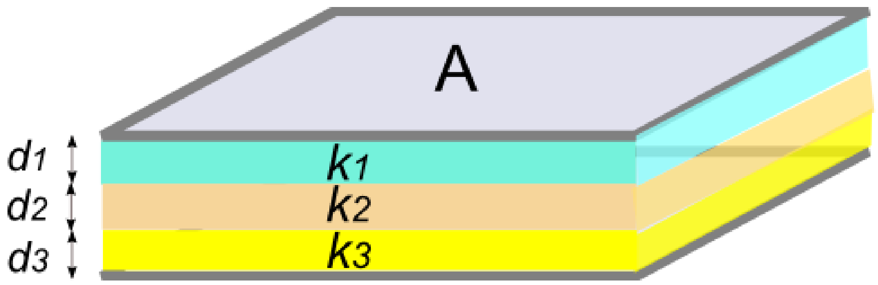

Figure 2.14 A parallel plate capacitor with more dielectric material in series

In a case with more than one dielectric material in series within a capacitor as illustrated in Figure 2.14, voltage across the plates (V) can be defined as follows

$$V = V_1 + V_2 + V_3 \tag{2.18}$$

Hence it can be derived with equation (2.7), [24]

$$\frac{Q}{C} = \frac{Q}{C_1} + \frac{Q}{C_2} + \frac{Q}{C_3} \tag{2.19}$$

$$\frac{1}{C} = \frac{1}{C_1} + \frac{1}{C_2} + \frac{1}{C_3} \tag{2.20}$$

This equation can be simplified with (2.13), considering the dielectric constant of the materials and its thickness as follows

$$\frac{1}{C} = \frac{d_1}{\varepsilon_{r1} \cdot \varepsilon_0 \cdot A} + \frac{d_2}{\varepsilon_{r2} \cdot \varepsilon_0 \cdot A} + \frac{d_3}{\varepsilon_{r3} \cdot \varepsilon_0 \cdot A} \tag{2.21}$$

Thus the total capacitance (C) can be considered as the capacitors in series with respective dielectric and their thickness as represented by equation (2.22).

$$C = \frac{\varepsilon_0 \cdot A}{\left(\frac{d_1}{\varepsilon_{r1}} + \frac{d_2}{\varepsilon_{r2}} + \frac{d_3}{\varepsilon_{r3}}\right)} \tag{2.22}$$

Where,

A = Area of the plates (m^2)

$d_{(n)}$ = Thickness of the dielectric material (m)

ε_0 = Vacuum permittivity (8.854 X 10^{-12} F/m)

$\varepsilon_{r(n)}$ = Relative permittivity of the respective dielectric material

2.4 Various ECG electrodes

2.4.1 Voltage divider

It is very crucial to clear the basics of the voltage (potential) divider rule before explaining the different ECG electrodes to acquire an ECG signals from a body. A voltage divider circuit resembles the input stage of a ECG system. Figure 2.15. depicts a comparison of a voltage divider circuit and a capacitive coupled ECG system (CCECG).

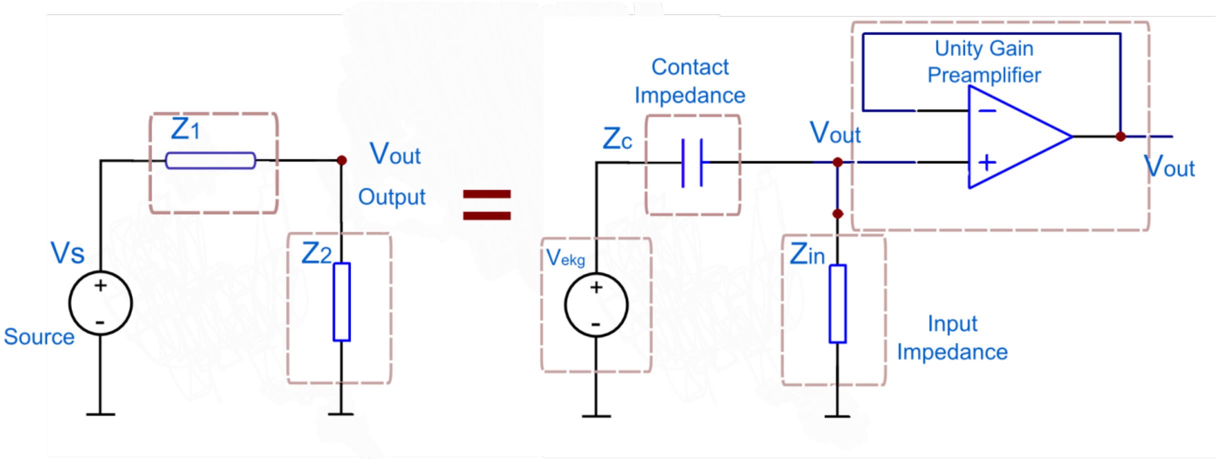

Figure 2.15 Voltage divider circuit compared with input stage of capacitive coupled ECG system (CCECG).

In the figure, Z_1 and Z_2 represent impedances containing any electronic components like capacitor, resistor and inductor. V_s and V_{out} are input (supply) voltage and output voltage across Z_2 respectively. Using Ohm' law [25], the input voltage and output voltage can be defined as follows.

$$V_{in} = I \cdot (Z_1 + Z_2) \tag{2.23}$$

$$V_{out} = I \cdot Z_2 \tag{2.24}$$

Output voltage (V_{out}) can be derived using above equations in terms of Voltage and impedance.

$$V_{out} = V_{in} \cdot \left(\frac{Z_2}{Z_1 + Z_2} \right) \tag{2.25}$$

Similarly to the voltage divider circuit, an equation for the comparable capacitive ECG system can be derived as follows.

$$V_{out} = V_{ekg} \cdot \left(\frac{Z_{in}}{Z_c + Z_{in}} \right) \tag{2.26}$$

Here Z_c and Z_{in} are any contact impedance (in the case capacitive) and input impedance of the preamplifier. While ECG signal and output potential across the input impedance (also output of the preamplifier as unity gain) are represented by V_{ecg} and V_{out} respectively. Transfer function of this circuit can be derived as follows.

$$H = \frac{V_{out}}{V_{ekg}} = \left(\frac{Z_{in}}{Z_c + Z_{in}} \right) \tag{2.27}$$

So the equation (2.26) implies that the higher the input impedance the higher the source signal that can be acquire with it. For example, if Z_{in} is 10 times the input impedance (Z_c), 90.9 % of the input signal can be acquired with the preamplifier as follows.

$$V_{out} = V_{ekg} \cdot \left(\frac{10 \cdot Z_c}{Z_c + 10 \cdot Z_c} \right) \tag{2.28}$$

$$V_{out} = V_{ekg} \cdot \left(\frac{10}{11} \right) = 0.909 \cdot V_{ekg} \tag{2.29}$$

2.4.2 Wet electrodes

The electrical activity of the heart reaches the skin as a potential as explained earlier in section 2.12. In order to pick up this potential, metal plate electrodes with electrolytic layers are used generally to perform electrocardiography.

Our skin is dry and contains dead cells, so to rectify this problem, as dead cells contribute more impedance at contact; we need to use electrolytic gel to reduce the contact resistance. Ag-AgCl electrodes are most commonly used electrodes. Ag-Cl being a non-polarizable material allows easy current passage from the muscle to the junction between the electrolyte and the electrode. This introduces less electrical noise into the measurement, as compared with equivalent metallic electrodes (e.g. Ag) [26]. These kinds of electrodes can also be used in disposable form.

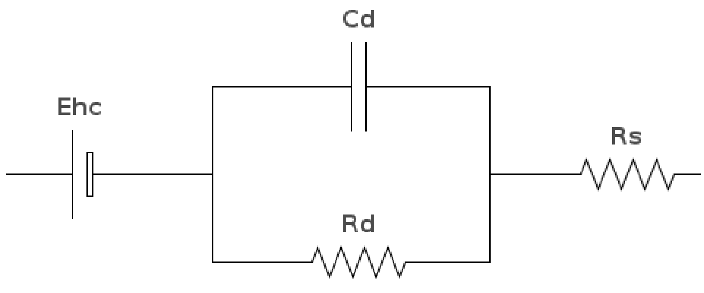

Figure 2.16 Equivalent circuit of a wet electrode.

A biopotential electrode has nonlinear electric characteristic and a function of current density at their surface [27]. So linear representation of the electrode need to require that they be operated at low potential and current [27]. Within the ideal conditions, the electrode can be modeled with the equivalent circuit shown in Figure 2.16 [27]. In the circuit, Cd and Rd designated to the capacitive and resistive components of the impedance of electrode-electrolyte interface. Resistance of electrode material and interface is designated as series resistance Rs and the battery Ehc is associated with half-cell potential.

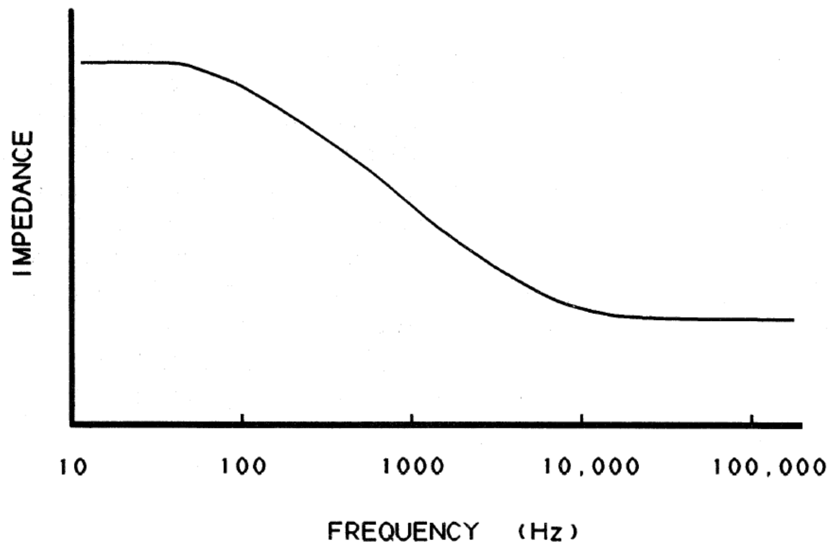

Figure 2.17 An example of biopotential electrode impedance over frequency. Characteristic frequencies will be somewhat different for electrode with various geometry and material [27].

Impedance of the electrode would be frequency dependent as seen in Figure 2.17[27]. So the impedance is influenced by series combination of Rs and Rd at lower frequencies, whereas Cd bypasses the effect of Rd at higher frequency and therefore it is close to Rs. Hence components of the equivalent circuit can be determined by measuring the impedance of an electrode at lower and higher frequencies [27].

Though the signal quality with the electrode is good, it has some drawbacks.

- There are cases where allergic reactions like swelling and skin irritation are reported for some people.

It needs preparation time to remove dead skin or skin hair that could be unpleasant for the patient.

The standard Ag-AgCl gel electrodes are susceptible to dehydrating, which modifies their impedance and can support bacterial growth [28], causing skin abnormalities in long term monitoring. Even the replacement of the gel and cleaning the site needs to remove the electrode, making the process more cumbersome.

The patient needs to do his routines and sometime sports too, in that case the electrodes with electrolytic gel are not comfortable.

2.4.3 Dry electrodes

Conventional wet electrodes have some drawbacks as described above. To overcome some of the problems, electrodes have been implemented without the necessity of any electrolyte. Here contact impedance between the electrodes and the skin would be higher than the standard Ag-AgCl electrodes, hence requiring higher input impedance to obtain the ECG signal [29]. Therefore this system uses higher input impedance amplifier to acquire the ECG signal through the contact impedance to avoid any signal loss. The dry electrodes eliminate some of the problems associated with wet electrodes caused by electrolytes such as need of skin preparation (and time), skin reactions due to the gel (e.g. irritation, swelling, gel dehydration) [30].

Wide ranges of Dry electrodes exist ranging from simple stainless steel discs to micro-fabricated silicon structure with built-in amplifier circuitry [31]. A dry electrode has similar input electronic schematic to capacitive electrode except it doesn’t have as higher input impedance as capacitive electrode. In a dry electrode, the contact impedance is in the range of several mega ohms so the input amplifier need at least 10 times higher input impedance than the contact impedance [32] considering voltage divider (section 2.4.1). *Voltage divider* is a linear circuit that results in a portion of the input voltage [33]. Albeit higher input impedance and other electronic circuit betterment, dry electrodes delivers lower signal quality relative to adhesive electrodes mainly due to its less sturdy interface with the skin [34].

2.4.4 Capacitive electrode

In addition to the wet and dry electrodes, that require direct galvanic contact with the body; there is a possibility to measure ECG without any electrical contact with the body [35]. In a direct contact of skin and metal plate electrode, the contact impedance would be in few kilo ohms to few mega ohms range. While in the non-contact measurement, the body and electrode forms a capacitor (C_{el}) of very low value (1-100 pF) [36] as shown in Figure 2.18 and hence forms very high contact impedance. The capacitive coupling functions on displacement current rather than real charge and hence requiring no direct contact with the body [37]. *Displacement current* is not electric current of moving charges, it is associated with the generation of magnetic field by time-varying electric field [38][39]. In the capacitive coupling, the medium between skin and body works as dielectric material in the capacitor.

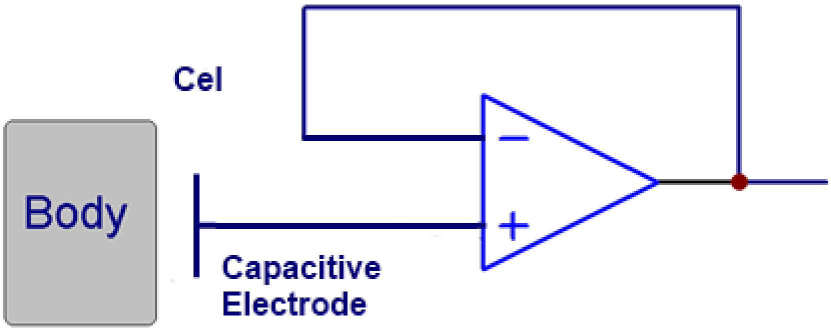

Figure 2.18 Capacitively coupled electrode & ultra-high input impedance preamplifier.

Today it is possible to get op-amps with ultra-high input impedance (e.g. INA116 with 10^{15} Ω and 0.2 pF) and so it is feasible to measure a low amplitude signal from body through very high contact impedance. The inputs of the ultra-high input impedance amplifier are very sensitive to its surroundings, therefore guarding and shielding around the connections can help to minimize the surrounding influences like parasitic effects [40].

Capacitively coupled electrodes provide no galvanic contact to the skin and electrode (no direct contact to the body); hence electrode artifacts do not occur at all [41]. Yet motion artifacts originate from charge separation due to distance changes between skin surface and electrode and skin potential changes [41]. Elaborated description of Capacitively Coupled Electrocardiography (CCECG) can be found in chapter 3.

2.5 Modeling and Simulation Tools

In the course of this doctoral work, various software tools are used. They are used to simulate & model the system to be developed and to support design & measurement process on the other hand. The next paragraphs give an overview over these tools.

2.5.1 Protel (Altium designer)

Protel stands for "Procedure Oriented Type Enforcing Language". It is an electronic design software (EDA) tool for designing and producing electronic systems ranging from printed circuit boards (PCBs) to integrated circuits. It is developed by the Australian CAD/CAE software company, which is now named Altium [42]. This software is used during this doctoral work to design the circuits of the projects.

2.5.2 Cadence Pspice

Pspice is a SPICE (Simulation Program for Integrated Circuits Emphasis) based simulator, which simulates analog and mixed signal electric circuits on a computer. Pspice is developed by Orcad and presently belongs to Cadence [43].

It is one of the widely used powerful tools to simulate an electrical circuit and performs many tasks related to electric circuit simulation like frequency response, Bode Plots, transient response, DC sweeps, component value sweeps, DC bias point/small signal parameters, temperature analysis, Monte Carlo (for component variations), noise Analysis etc. It is used during this doctoral work to perform different simulation for the CCECG circuit.

2.5.3 MATLAB

MATLAB® is a high-level language and interactive environment that enables you to perform computationally intensive tasks faster than with traditional programming languages such as C, C++, and Fortran [44]. Post analysis and graphical presentation of the capacitive electrocardiograms are performed using this platform in this work at various stages.

2.5.4 Simulink

Simulink® is an environment for multi domain simulation and Model-Based Design for dynamic and embedded systems. It provides an interactive graphical environment and a customizable set of block libraries that allow you to design, simulate, implement, and test a variety of time-varying systems, including communications, controls, signal processing, video processing, and image processing [45]. To simulate variation in capacitance between the body and the electrode by the changing distance, Simulink is utilized during this doctoral work.

2.5.5 LabVIEW

LabVIEW is a short form of ”Laboratory Virtual Instrumentation Engineering Workbench“ and a platform and development environment for a visual programming language from

National Instruments. The graphical language is named "G". Originally released for the Apple Macintosh in 1986, LabVIEW is commonly used for data acquisition, instrument control, and industrial automation on a variety of platforms including Microsoft Windows, various flavors of UNIX, Linux, and Mac OS [46].

LabVIEW is a graphical programming environment used to develop sophisticated measurement, test, and control systems using intuitive graphical icons and wires that resemble a flowchart. It offers unrivaled integration with many hardware devices and provides hundreds of built-in libraries for advanced analysis and data visualization – all for creating virtual instrumentation [47]. It is also used for analysis & signal processing, automated test, embedded designing and measurement. As within this work, it is used to analyze and to process the data acquired from CCECG.

Reference

[1] J. Malmivuo and R. Plonsey, Bioelectromagnetism, principles and applications of bioelectric and biomagnetic fields. New York : Oxford University Press.1995, pp.16-19.

[2] Heart Anatomy : http://www.texasheartinstitute.org/HIC/Anatomy/anatomy2.cfm, last accessed on 14 May 2011.

[3] The Heart Image. Source : http://vo-ambulanse.wikispaces.com/sirkulasjonsystemet, last accessed on 14 May 2011.

[4] Electric conduction of the heart. Source : http://www.emergencymedicaled.com/ 215AED.htm, last accessed on 14 May 2011.

[5] J. Bronzino, The Biomedical Engineering Handbook, 2nd edition, vol. 2. Florida: CRC press LLC. 2000, pp. 181-190.

[6] Book (Chapter): Bioelektrische und biomagnetische Signale, pp. 33.

[7] J. Anderson and J. Allen, “Apparatus for body surface mapping,” US patent, No. US2003/0040677 A1

[8] B. H. Brown et al, Medical Physics and Biomedical Engineering, Bristol and Philadelphia: IOP Publishing Ltd. 1999, pp. 521-523.

[9] Electrocardiography. Source : http://en.wikipedia.org/w/index.php?title=Electrocardiography&oldid=466330366. Last accessed on 12 March 2011.

[10] August D. Waller, “A demonstration on man of electromotive changes accompanying the heart’s beat,” The Journal of Physiology, Vol. 8(5), October 1887.

[11] G. E. Burch, N. P. De Pasquale and J. Howell, “A History of Electrocardiography,” Norman Publishing, San Francisco, 1990.

[12] Redmond Shouldice and Gary Bass, "Developments in Electrocardiography – from Bench to Bedside," pp. 1-10. Source : http://dsp.ucd.ie/dspfiles/main_files/pdf_files/original_iei_article_manuscript.pdf. Last accessed on 3 January 2011.

[13] Nobel Prize in Medicine to Einthoven for his discovery of the mechanism of the Electrocardiogram. Source : http://nobelprize.org/nobel_prizes/medicine/laureates/1924/index.html. Last accessed on 11 January 2011.

[14] M. R. Neuman, Analysis and application of analog electronic circuits to biomedical applications. Boca ratoon : CRC press LLC. 2004, pp. 9-11.

[15] N. V. Thakor, "Electrocardiographic monitors," in Encyclopedia of medical devises and instrumentation, J. G. Webster , New York, Wiley, 1988pp. 1002-1017.

[16] N. V. Thakor, " Chapter 74: Biopotentials and Electrophysiological measurements." In the measurement, instrumentation and sensor handbook, Florida: CRC press LLC. 1999.

[17] Capacitor, Source : http://en.wikipedia.org/w/index.php?title=Capacitor&oldid=475598469, last accessed on 08 February 2012.

[18] J. F. Becker, "Capacitor and dielectrics (Chapter 24)," Physics Dept, San Hose state University. Source : http://www.physics.sjsu.edu/becker/physics51/capacitors.htm, Last accessed on 08 February 2012.

[19] T. R. Kuphaldt, Lesson in Electric Circuit Volume I-DC (Chapter 13: Capacitors), Open book, 2006. Source : http://openbookproject.net/electricCircuits/DC/DC_13.html, last accessed on 08 February 2012.

[20] Capacitor Theory, University of Waterloo. Source : https://ece.uwaterloo.ca/~lab100/ls1notes.pdf, last accessed on 08 February 2012.

[21] Capacitance and dielectrics, chapter 5, MIT(web). Source : http://web.mit.edu/8.02t/www/materials/StudyGuide/guide05.pdf, last accessed on 09 February 2012.

[22] Capacitors and dielectric theory part 1, Video lecture by Viken Kiledjian. Source : http://www.youtube.com/watch?v=NZwCrNcrw-k , last accessed on 09 February 2012.

[23] Capacitance Impedance, Wikipedia. Source : http://en.wikipedia.org/w/index.php?title=Electrical_impedance&oldid=479307509, last accessed on 29 February 2012.

[24] G. Hagmann, Grudlagen der Elektrotechnik: das bewährte Lehrbuch für Studierende Elektrotechnik und anderer technischer Studiengänge ab 1. Semester, AULA Verlag, Wiebelsheim, 2010.

[25] Ohm's law, Wikipedia. Source: http://en.wikipedia.org/w/index.php?title=Ohm%27s_law&oldid=479104407, last accessed on 29 February 2012.

[26] J. Duchene and F. Gouble, Surface electromyogram during voluntary contraction: Processing tools and relation to physiological events. Critical Reviews in Biomedical Engineering 21(4):313–397,1993.

[27] M. R. Neuman, "Chapter 48: Biopotential electrodes," in the Biomedical Engineering handbook :2nd edition, J. D. Bronzino, Boca Raton, CRC Press LLC, 2000.

[28] A. Karilainen, S. Hansen and J. Müller, " Dry and capacitive electrodes for long term ECG monitoring," 8th Annual workshop on semiconductor advances 2005, pp. 155-161, 17 November 2005.

[29] G. E. Bergey, R. D. Squires and W. C. Sipple, "Electrocardiogram recording with pasteless electrodes," IEEE Transactions on Biomedical Engg. Vol. 18, No. 3, pp. 206-211, May 1971.

[30] R. P. Bett and B. H. Brown, "Method for recording electrocardiogram with dry electrodes applied to unprepared skin," Medical and Biological Engineering, vol. 13, pp. 313-315, May 1976.

[31] Y. M. Chi, T. P. Jung and G. Cauwenberghs, "Dry-contact and Noncontact biopotential electrodes : Methodological review," IEEE Reviews in Biomedical Engg., vol. 3, pp. 106-119, 2010.

[32] Al Keltz, "High and low impedance signals". Source : http://whirlwindusa.com/support/tech-articles/high-and-low-impedance-signals/, last accessed on 24 February 2012

[33] Voltage Divider, Wikipedia. Source : http://en.wikipedia.org/w/index.php?title=Voltage_divider &oldid=475984238, last accessed on 24 February 2012.

[34] H. de Talhouet and J. G. Webster, "The origin of skin-stretch caused motion artifacts under electrodes," Physiological Measurement, vol. 17 (81), pp. 81-93, 1996.

[35] Richardson, P. C., "The Insulated Electrode," In Proceedings of the 20th Annual Conference on Engineering in Medicine and Biology. Boston, MA (USA), p. 157, 1967.

[36] R. J. Prance, A. Debray, et al, "An ultra-low-noise electrical-potential probe for human-body scanning," Meas. Sci. Technol. 11, pp. 291-297, January 2000.

[37] C. J. Harland, T. D. Clark and R. J. Prance, "Electrical Potential probes – new directions in the remote sensing of the human body," Meas. Sci. Technol., vol. 13, pp. 163–169, 2002.

[38] Displacement current, Wikipedia. Source : http://en.wikipedia.org/w/index.php?title=Displacement_current&oldid=473445260, last accessed on 15 February 2012.

[39] R. Fitzpatrick, "Classic Electromagnetism: An intermediate level course," University of Texas. Source : http://farside.ph.utexas.edu/teaching/em/lectures/node46.html, last accessed on 15 February 2012.

[40] A. Rich, "Shielding and Guarding, how to exclude interference-type noise, what to do and why to do - A rationale approach," Analog Dialogue 17-1, pp. 124-129, 1983.

[41] J. Ottenbcaher, L. Jatoba, U. Großmann, W. Stork and K. Müller-Glaser, "ECG Electrodes for a context-aware cardiac permanent monitoring system," World Congress on Medical Physics and Biomedical Engineering 2006, IFMBE Proc. vol. 14/2, pp. 672-675, July 2006.

[42] Protel (Altium Designer). Website : www.altium.com. Last accessed on 20 January 2011.

[43] Cadence pSpice. Website : http://www.cadence.com/products/orcad/pspice_simulation/pages /default.aspx. Last accessed on 20 January 2011.

[44] MATLAB. Website : http://www.mathworks.com/products/matlab/, last accessed on 20 January 2011.

[45] Simulink. Source : http://www.mathworks.com/products/simulink/, last accessed on 20 January 2011.

[46] LabVIEW Wikipedia. Source : http://en.wikipedia.org/w/index.php?title=LabVIEW&oldid=465039969. Last accessed on 20 January 2011.

[47] LabVIEW. Website : http://www.ni.com/labview/. Last accessed on 20 January 2011.

3 Capacitive Electrocardiography

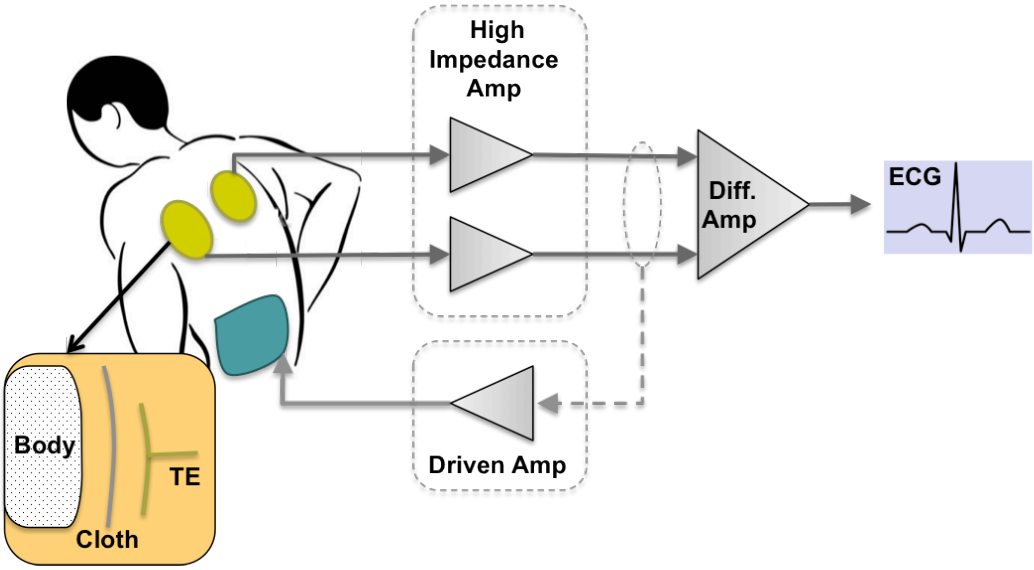

Figure 3.1 Capacitively coupled Electrocardiography system

Unlike conventional ECG systems that use low impedance electrical contacts to acquire electrical signals from the body‘s surface, CCECG systems require a capacitive (very high impedance) contact. Hence body and the capacitive electrode (TE) form a capacitor to couple the potential from the body to a ultra-high input impedance preamplifier [1][2] as shown in Figure 3.1. The input amplifier with ultra-high input impedance works as a buffer to transfer the signal from a high impedance source to its low impedance output for the next stage of signal processing. Signals from the buffers are fed to differential amplifiers to minimize common mode signals and to amplify the differential signal [3]. Here clothes, air and/or any material between the two surfaces act as dielectric material of the capacitor as shown in the Figure 3.1 (insert).

Further improvement in the common mode cancellation can be achieved by a driven seat circuit [4][5]. The circuit uses the unity gain signals from the buffer to feed it back to the body through a driving amplifier to a driven seat electrode after adding and amplifying the signals [6].

3.1 State of the art

The conventional way to measure Electrocardiogram uses Ag/AgCl electrodes directly attached to the body [7] as explained in section 2.4.2. This kind of electrodes need skin preparation and an electrolyte in form of electrode paste and gel to reduce contact impedance. In long term monitoring, skin-electrode interaction can cause irritation when drying out of electrolyte gel. This requires a requirement of regular replacement of the electrolyte, which can be discomforting during repetitive skin preparation.

The first capacitive recording of an ECG signal without conductive body contact as described by Richardson [8] represents a possible solution to this problem. The surfaces of his capacitive electrodes were electrically insulated and remained stable for long-term monitoring. In 1969, Wolfson and Neuman designed a capacitive coupled Electrocardiography using a high input impedance amplifier with a MOSFET [9]. David and Portnoy (1972) used an integrated arrangement of an insulated electrode and an impedance matching configuration (to acquire signal from high source/contact impedance) with a Fairchild μA 740 operational amplifier enclosed in a plastic housing [10].

Betts and Brown (1976) built a conductive plastic electrode in place of metal electrode with bandwidth of clinical ECG (0.1 to 100Hz) [11]. These electrodes were circular disc shaped and they conducted a study on 200 patients while comparing the ECG signal with wet pad system of electrodes. An integrated unit of an electrode and an Amplifier were designed by Luca et al. (1979) to use the unit in front end of a standard bio-potential measurement [12]. The module enclosed in a metal shell which worked as housing and ground contact as well.

In 1994, Clippingdale et al presented an array of ultrahigh ohmic sensors for Heart Imaging at University of Sussex [13]. The array comprises 25 spring-mounting sensors, arranged in five rows of five unit, with 32 mm distance between sensors. It was set into a bench on which the patient reclined; face down, so that the array faced the chest area without requiring any physical contact. The spring-mounted array pressed the sensor against the body to conform the contour of the chest. An insulating spacer, approximately 3 mm thick was placed between the sensor electrode and the body for electrical isolation.

The same group, R. J. Prance et al published in 2000 a study on a potential probe for human body scanning [14]. The probe was designed for ultralow noise (2 μV $Hz^{-1/2}$ at 1 Hz) with an instrumentation amplifier INA116 (Burr Brown) [15] and adjusted bandwidth of 0.01 – 100 kHz to detect wide range of electric activity from the body. At this noise level it should prove possible to resolve even the smallest electrical signals generated by the body. Further advancement in the probe with remote sensing of human body was demonstrated by Harland et al in 2002 [16]. They presented the sensing of a high resolution Electrocardiogram up to a distance of 1 meter from a clothed body.

The term *capacitively coupled non-contact electrode* (CCNE) was introduced in 2002 by Lee et al. at the QUASAR (Quantum Applied Science and Research, San Diego) research team. Their compact sensor was claimed to be able to record ECG signals without any galvanic contact through clothing [17]. They observed that sensors were able to measure the ECG of a fully clothed person standing within a range of about 25.4 cm. The following year, they developed a miniature version of the sensor termed the capacitively-coupled noncontact electrode (CCNE), specifically to measure ECG through clothing. This first version of the ECG electrode, including all amplification electronics, was approximately 25.4 mm square with a thickness of 8.89 mm.

3.2 Capacitive Coupling

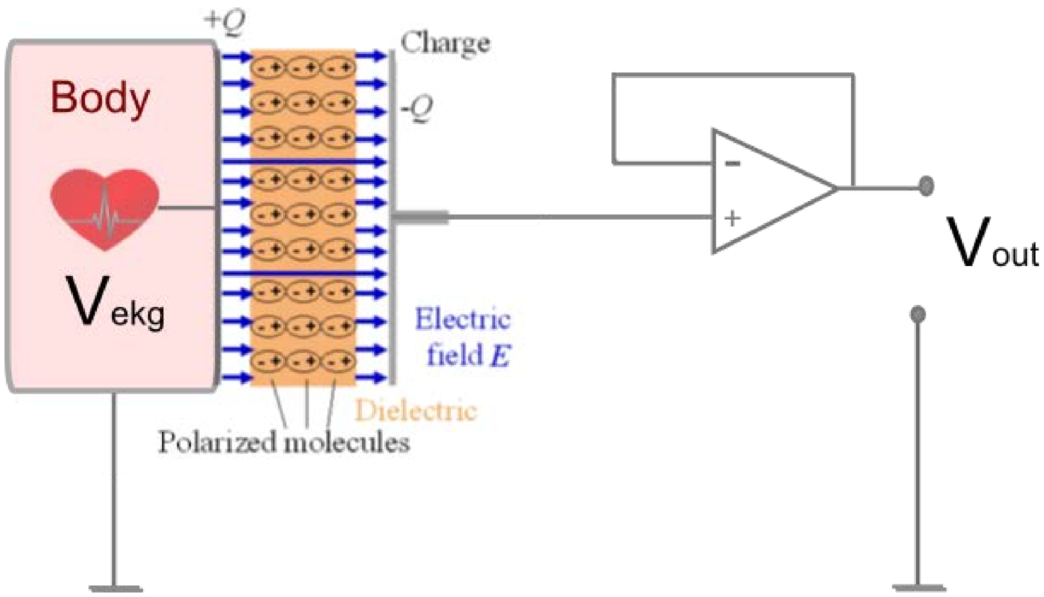

Figure 3.2 Capacitance formation between body and electrode.

Potentials generated by the heart are referred to as body surface potential mapping (section 2.1.3), is conducted by body tissues from the heart and brought to the epidermis (outer skin layer) [18]. Conventional Electrocardiography uses a galvanic contact with the skin to acquire these potentials [19]. However, the body surface can work as a conductive plate and if there is a conductive surface close to the body, they will form a capacitor according to equation (3.1) [13]. Clothes work as dielectric material between the plates. Figure 3.2 illustrates formation of capacitance between body and electrode. The capacitance formed between a human body and the electrode is in approximate range of 1-100 pF [14].

$$C = \varepsilon_0 \, \varepsilon_r \, \frac{A}{d} \tag{3.1}$$

Where,

C = capacitance in Faraday

ε_0 = Vacuum permittivity (8.854 E-12 F/m)

ε_r = Relative permittivity of the dielectric material

A = Area of the plate (m^2)

d = Distance between the plates (m).

In a case of several dielectric material layers in the capacitance (C_{el}) formed by the body and the electrodes, the equation of capacitance will be as follows.

$$C = \frac{\varepsilon_0 \cdot A}{\left(\frac{d_1}{\varepsilon_{r1}} + \frac{d_2}{\varepsilon_{r2}} + \frac{d_3}{\varepsilon_{r3}}\right)} \tag{3.2}$$

Where,

A = Area of the plates (m^2)

$d_{(n)}$ = Thickness of the dielectric material (m)

ε_0 = Vacuum permittivity (8.854 X 10-12 F/m)

$\varepsilon_{r(n)}$ = Relative permittivity of the respective dielectric material

Both plates of the capacitor contain some amounts of charges. So when the heart signal is displayed on the body surface, it produces potential difference across the capacitor. This potential difference creates flow of charge from one plate to another as indicated in the Figure 3.2. This flow produces current in the circuit in opposite direction to the flow of charge. The capacitor operates on the displacement current rather than real charge and hence eliminates the need for direct contact with the body [14]. Capacitance formed by electrodes over the distance is graphed in Figure 3.3.

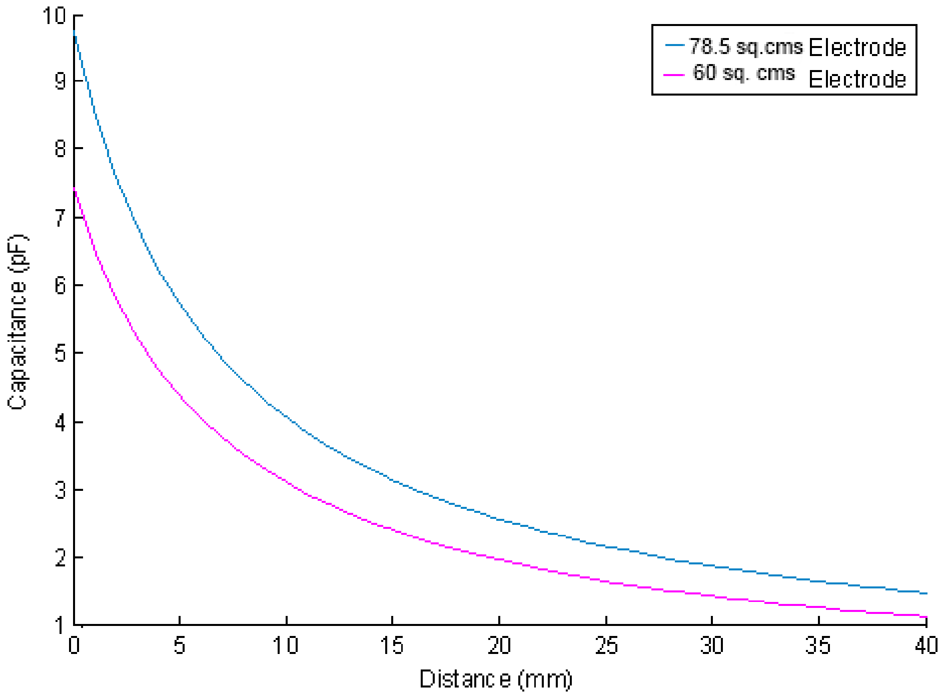

Figure 3.3 Capacitance Vs Distance for the electrodes for two different electrode area.

Earlier Electrocardiography, the principal of capacitively coupled measurement has also been applied in various biosignals measurements. Electroencephalography (EEG) [20][21][22][23][24] and Electromyography (EMG) [25][26][27] are two other vital parameters on which various studies are conducted using the same capacitively coupled measurement.

3.3 Impedance matching and the signal

To achieve a signal from its source with minimal loss, it is very crucial to have impedance matching of its source and the sensor as per voltage divider rule (section 2.4.1). A *Voltage divider* is a linear electronic circuit that produces a portion of the input voltage [28]. It helps to estimate a proportionate value of the input impedances (with respect to contact / source impedance) in order to acquire signals from the source with appropriate value or minimum loss.

Various technical components, those come after the capacitive coupling and before the differential amplifier are elaborated in this section. These components are very crucial for the capacitive coupling as they provide technical platform to acquire the ECG signal. The components are highlighted in Figure 3.4 with dotted blocks.

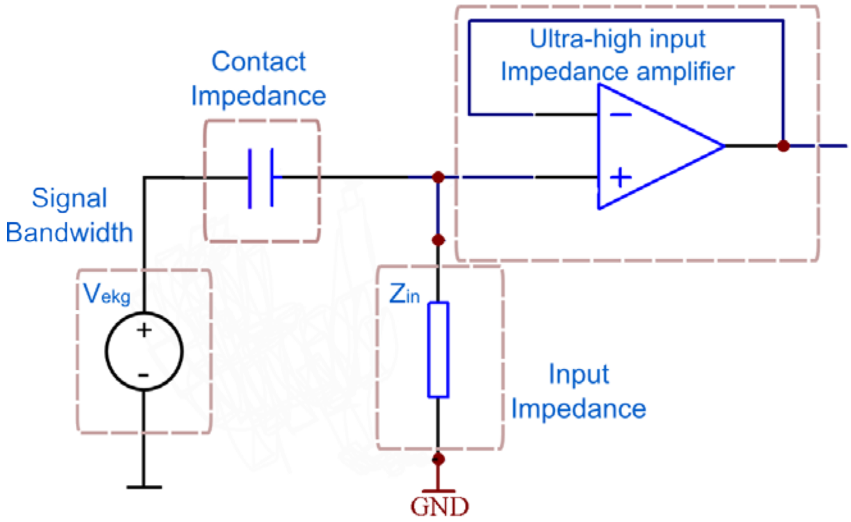

Figure 3.4 Components of the impedance matching.

3.3.1 Bandwidth considerations

The peak amplitude of an ECG signal (QRS) is typically in the range of ±2 mV for normal human on the body surface [1]. Figure 3.5 shows three bandwidths used for different applications in electrocardiography [29]. The clinical bandwidth used for recording the standard 12-lead ECG is 0.05–100 Hz. For monitoring applications, such as for intensive care patients and for ambulatory patients, the bandwidth is restricted to 0.5–50 Hz. In these environments, rhythm disturbances (i.e. arrhythmias) are principally of interest rather than subtle morphological changes in the waveforms. Thus the restricted bandwidth attenuates the higher frequency noise caused by muscle contractions (electromyographic or EMG noise) and the lower frequency noise caused by motion of the electrodes (baseline changes) [29].

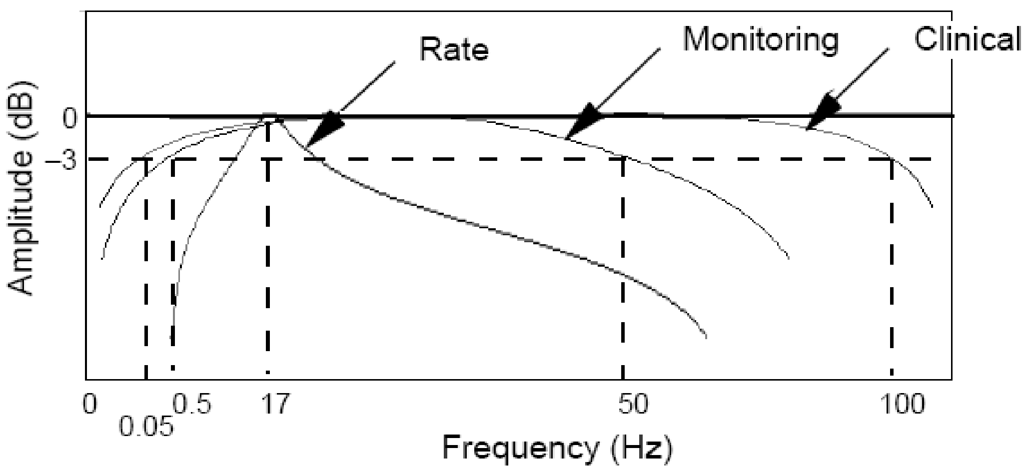

Figure 3.5 Electrocardiography bandwidths used in various applications [29].

A third bandwidth used for heart rate meters (cardio-tachometers) uses a simple band pass filter centered at 17 Hz with a Q (center frequency / bandwidth) of about 3 or 4. It maximizes the signal-to-noise ratio for detecting the QRS complex. Such a filter passes the frequencies of the QRS complex while rejecting noise including non-QRS waves in the signal such as the P and T waves. This filter helps to detect the QRS complexes but distorts the ECG so much that the appearance of the filtered signal is not clinically acceptable [29].

3.3.2 Impedance of the input stage

Figure 3.6 shows the input stage of a capacitive electrode that also constitutes the input stage of the CCECG system. This input stage is very crucial for the capacitive measurement as its impedance plays a significant role in acquiring the signal. A voltage divider (section 2.4.1) has been formed between the source, the capacitive electrode and the preamplifier input. Impedance of each component of the stage affects measured signal at preamplifier output. Since the contact impedance is very high, it is necessary to deploy an impedance transformation circuit [30]. A typical impedance transformation circuit has a high input impedance (section 2.4.1), matched with the contact impedance and very low output impedance. Low output impedance helps the next stage of the circuit to acquire the signal without having significant input impedance.

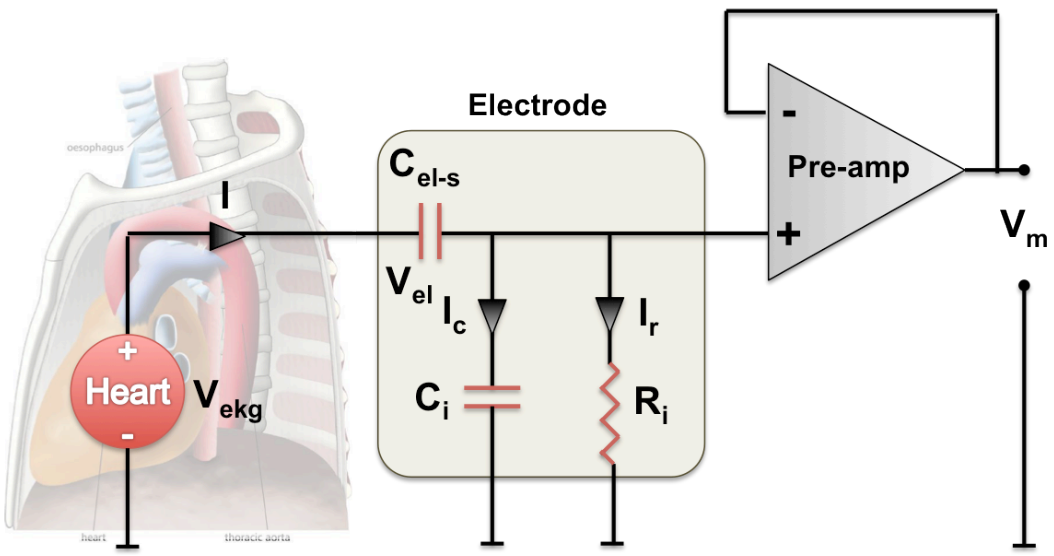

Figure 3.6 Input stage of the Capacitive coupled Electrocardiography.

According to the Kirchhoff's voltage law [31], potential distribution in the loop would be as follows. Here V_m represents potential across C_i, Ri and the potential measured at output of the preamplifier (as it is unity gain amplifier).

$$V_{ekg} = V_{el} + V_m$$

$$V_{ekg} = \frac{1}{C_{el-s}} \int I dt + V_m$$

$$V_{ekg} = \frac{1}{C_{el-s}} \int (I_c + I_r) dt + V_m$$

$$V_{ekg} = \frac{1}{C_{el-s}} \int \left(C_i \frac{dV_m}{dt} + \frac{V_m}{R_i} \right) dt + V_m$$

$$V_{ekg} = \frac{C_i}{C_{el-s}} V_m + \frac{1}{R_i} \int \frac{V_m}{C_{el-s}} dt + V_m$$

$$V_m = V_{ekg} - \frac{C_i}{C_{el-s}} V_m - \frac{1}{R_i} \int \frac{V_m}{C_{el-s}} dt \tag{3.3}$$

Here R_i would be an effective resistance of the preamplifier and $C_{el\text{-}s}$ is the resultant capacitance from series connection of the capacitances C_s (series capacitor) and C_{el} (capacitance between the body and the electrode) as explained in section 3.5.1.1. C_i is an overall capacitance considering input capacitance of the amplifier and practical parasitic capacitance. Table 3.1 describes all the parameter related to the circuit and the equations.

Parameter	Description
R_i	Parallel connection of bias resistance (R_b) and input resistance of the preamplifier (R_{in})
C_i	Parallel connection of parasitic capacitance and input capacitance of the preamplifier
V_{el}	Potential across the capacitive contact
V_m	Output signal of the preamplifier

I_c	Current across the aggregated input capacitor (C_i)
I_r	Current across the aggregated input resistor (R_i)
C_{el-s}	Resultant capacitor of C_s (Series capacitor) and C_{el} (capacitance between body and the electrode)

Table 3.1 Description of various circuit parameter.

It can be implied from the equation (3.3) that two conditions are necessary to minimize the signal attenuation with respect to parameters like resistance and capacitance. Followings are the two conditions (3.4) and (3.5), where $Z_{Cel\text{-}s}$ is the impedance of the capacitance $C_{el\text{-}s}$ (equation (2.14) in section 2.3.1).

$$C_i << C_{el-s} \tag{3.4}$$

$$R_i << Zc_{el-s} \tag{3.5}$$

It means aggregated input capacitance and effective input resistance are very crucial to achieve the signal without minimal attenuation. With lower input capacitance, comes higher input resistance, which in turn means a better signal acquisition.

3.3.3 Contact Impedance

The capacitance formed between a human body and the electrode is in approximate range of 1-10 pF for the electrodes sizes 78.5 cm^2 and 60 cm^2 as seen in the Figure 3.3. Hence the contact impedance of the source would be in range of Giga Ohms with the following equation (section 2.3.1).

$$Z_c = \frac{1}{2\pi f \cdot C} \tag{3.6}$$

Where,

Z_c = Impedance of the capacitor (Ω)

f = Frequency of the input signal (Hz)

C = Capacitance of the capacitor (Farad)

Figure 3.7 shows the contact impedance of the electrodes R10 (78.5 cm^2) and S6X10 (60 cm^2) for various frequencies. The normal amplitude of an ECG signal is in the range of 1 to 2 mV, but this amplitude decreases when acquired through capacitively coupled measurements. So in this case, an ultra-high impedance amplifier with appropriate input capacitance would be required to satisfy the conditions (3.4) and (3.5). More on the requirement of the ultra-high impedance amplifier is explained in section 3.3.4.

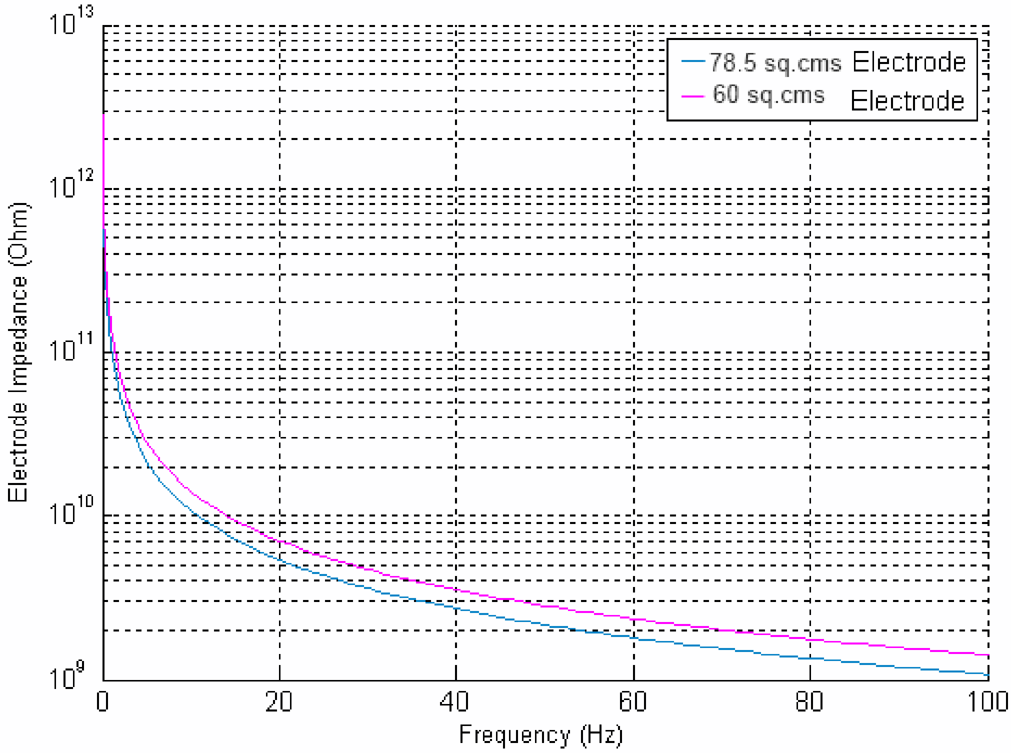

Figure 3.7 Impedance Vs frequency for the electrodes

3.3.4 Ultra High input Impedance Amplifier

To acquire ECG signal from the high impedance source (capacitive contact), a preamplifier with higher input impedance than the source must be used in order to minimize attenuation of the signal as voltage divider (section 2.4.1) and equations (3.4) and (3.5). Under this condition, the input capacitance of the amplifier plays a very important part. If the preamplifier satisfies formula (3.7), the attenuation would be considerably low.

The equation (3.7) shows the relation between the two capacitances of the input stage of the circuit. Capacitance ‘C_{el-s}’ is the series combination of contact capacitance (C_{el}) and series capacitance (C_s), and ‘Ci’ is the input capacitance of the preamplifier. Lower value of Ci in relation to C_{el} results in quite higher impedance for Ci than $C_{el\text{-}s}$. This proportion increases the input impedance of the buffer and reduces signal loss in the acquisition.

$$C_i \ll C_{el-s} \tag{3.7}$$

Where,

$C_{el\text{-}s}$ = resultant series capacitance of Cs and Cel

C_i = input capacitance of the amplifier.

An ultra-low input bias current instrumentation amplifier INA116 from Texas Instruments [15] has been used in this case. It has very high input resistance (10^{15} Ω) and the lowest input capacitance (0.2 pF) available in the market [15] to fulfill the above mentioned requirement.

To stabilize the input stage circuit, we have used biasing. The biasing provides steady current for the amplifier and makes it stable to obtain the signal. The bias resistor (R_b) should be of a very high value to match the source impedance for frequencies below 10 Hz (see Figure 3.7). Hence bias resistance of 200G Ω is implemented to do so. It should also be noted here that a high impedance circuit is prone to receive noises as it is capable of picking low amplitude signal. Here the amplifier has been configured as unity gain buffer for the application by grounding the negative input of the INA 116 amplifier.

3.3.4.1 Parasitic capacitance

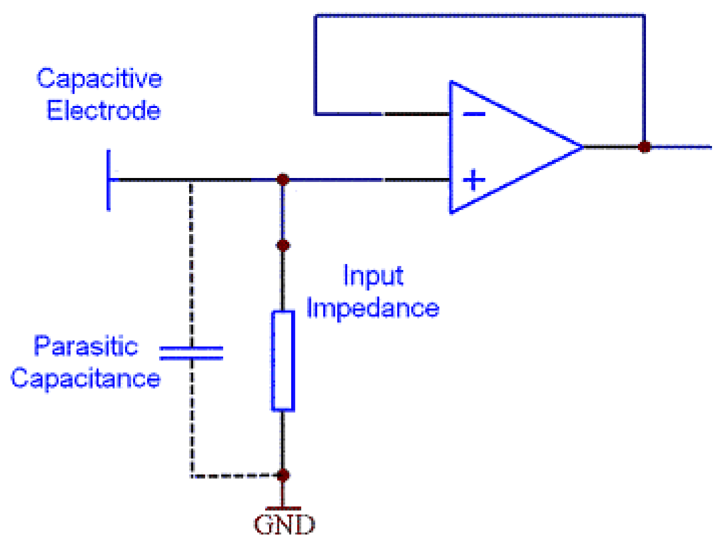

Figure 3.8 Parasitic capacitance at the input stage.

When a potential difference exists across two wires lying adjacent in close proximity to each other at different potentials, they are affected by each other's electric field. They act like the plates of a capacitor and store charge [32].

This kind of parasitic capacitor lies parallel to the input impedance of the preamplifier as depicted in figure 3.8. This arrangement increases the effective input capacitance and reduces over all impedance of the preamplifier. It is frequently observed in closely placed wires and on a Printed Circuit Board (PCB).

3.3.4.2 Guarding

Guarding is a technique used to protect the input impedance of the amplifier from the parasitic effects. In this method, surrounding of the input terminal is driven by the same potential as the input signal to avoid forming a parasitic capacitance between input terminal and the surroundings [33]. So the input signal is shielded all around throughout from capacitive sensor to the INA116 amplifier [15] by the same potential. The instrumentation amplifier also has inbuilt guarding connections to protect the signal from any parasitic effects. These pins give unity amplified input signal to provide exactly the same potential. Various electrical conducting surroundings are implemented and elaborated in section 4.3.2 of the chapter system implementation.

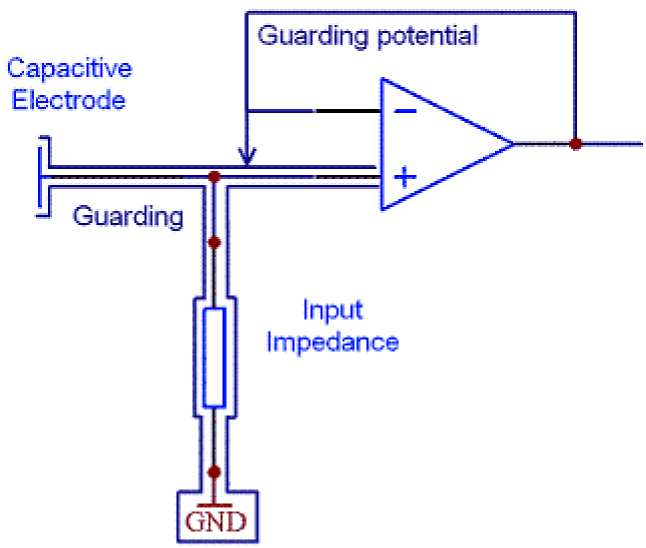

Figure 3.9 Guarding for the input signal.

In a noisy ambience, another layer of shielding around the inputs helps to minimize the noise reception in the signal further [34]. Hence a 3rd layer on the capacitive electrodes is implemented and is connected to circuit ground.

3.4 Signal Conditioning

3.4.1 Baseline and DC removal

An Electrocardiogram contains very low frequency components in its spectrum. At the same time, there is some low frequency interference in the ECG signal e.g. breathing signal, inherent DC offset from the amplifier etc. Breathing signal or low frequency signal creates base drifting of the ECG signal, which can cause the amplifier to go into saturation. DC offset elevates the signal base potential and makes it difficult to amplify the signal (amplification of the signal can force the differential amplifier into saturation).

Hence it is very crucial to filter these low frequency interferences from the ECG signal. A high pass filter with cutoff of 0.159 Hz has been employed after the pre-amplification stage to eliminate the interferences.

3.4.2 Differential amplification

After obtaining the two signals from the high input impedance amplifiers, the signals must be fed to a differential amplifier [3]. The signals contain many unwanted signals that should be distinguished from the desired signal for clear display, and hence we need to filter noise and common mode signals. The ECG signals are also very small in magnitude and need amplification for further processing, to accomplish these requirements, an instrumentation amplifier is the preferred option, because it rejects common mode signals as well as amplifying the differential signal.

A FET-input, low power instrumentation amplifier INA 121 from Texas Instruments is used here because it has a high common mode rejection ration (CMRR) of 106 dB at a gain of 100 or more [35]. The gain 200 is set here with only one resistor.

The differential amplifier equation is given by

$$V_{in+} - V_{in-} = AV_{out} \tag{3.8}$$

Before feeding the electrode signals to the instrumentation amplifier, a high pass filter has been used to remove DC offsets with a cut-off frequency of 0.159 Hz..

At output of the differential amplifier, an anti-aliasing filter, has been used with theoretical cut-off frequency of 50 Hz. It restricts the bandwidth to sample the signal without aliasing. A data acquisition system (NI USB-9162 with NI9215) [36][37] from National Instruments is used here to sample the signal for further digital analysis in a visual programming language, LabVIEW [38].

3.4.3 Anti-aliasing

The signal from the CCECG system has a large bandwidth as there is no limiting of the frequency. The digitization of the wide bandwidth signal can create distortion artifact in the signal known as aliasing. A low pass filtering technique called anti-aliasing is employed before the digitization to avoid such distortion artifact. This anti-aliasing filter attenuates high-frequency components buried in the analog input and prevents them from being aliased into the signal frequency band [39].

An analog to digital conversion is sampled at nyquist rate which is twice the input signal band. The anti-aliasing filter transition band must be very narrow and its stop band must have enough suppression of the out-of-band noise [39].

In some cases, a first order anti-aliasing low pass filter is implemented to limit higher frequency components from the signal. To restrict the signal, a theoretical cutoff frequency of 50 Hz has been used.

3.4.4 Digital Signal Processing

Generally the resulting signal of the CCECG system is very noisy due to its sensitivity to acquire any signal capacitively in vicinity. Minimizing these noises is a very important task in order to achieve a signal with interpretable quality. In this work, various digital and analog signal processing techniques have been utilized. LabVIEW programs and analog hardware filters are applied for digital and analog signal processing respectively.

Considering different measurement scenarios (see chapter 5), a versatile digital and analog signal processing method had to be developed. The contactless ECG signal needs advanced signal manipulation because of its extreme noise sensitivity. Following are some of the techniques used to the signal digitally, in additionally to standard filters

3.4.4.1 Filtering

A signal without filtering from the CCECG system can be seen in Figure 3.10. Considering the noise in the signal filtering of the signal was crucial.

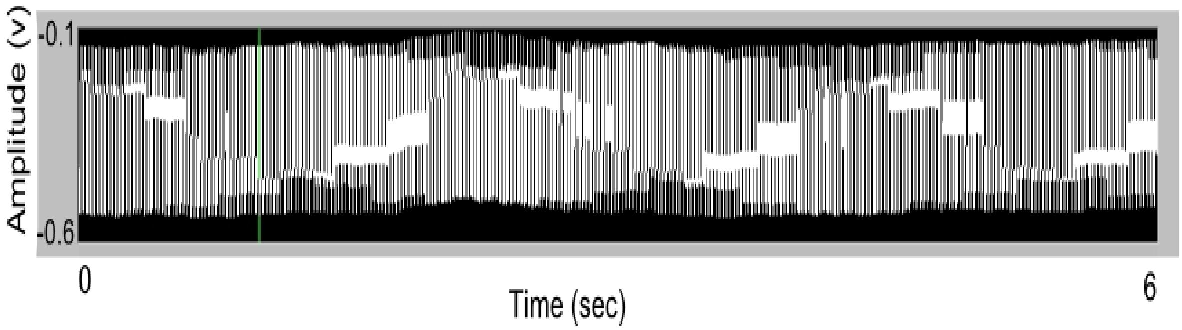

Figure 3.10 an signal acquired by the CCECG without filtering.

Digital filters can be classified into various groups as per the criteria used for the classification [40]. Major type are infinite impulse response (IIR) digital filters and finite impulse response (FIR) digital filters [40].

Infinite impulse response (IIR) digital filters have non zero over an infinite length of time impulse response [41]. It has z-transform transfer function defined in equation (3.9) [42].

$$H(z) = \frac{B(z)}{A(z)} = \frac{b_0 + b_{1Z}^{-1} + \cdots + b_{LZ}^{-L}}{1 + a_{1Z}^{-1} + \cdots + a_{LZ}^{-L}} \tag{3.9}$$

General characteristic of such digital filters are as follows [42].

- Very sharp cutoff

- Narrow transition band
- Low order structure
- Low processing time

Finite impulse response (FIR) digital filters are referred to linear filtering operator with finite length impulse response [43]. A z transform transfer function of the system can be described by using unity denominator in the equation (3.9) [42].

$$H(z) = B(z) = b_0 + b_{1Z}^{-1} + \cdots + b_{LZ}^{-L} \tag{3.10}$$

General characteristic of finite impulse response digital filters are as follows [42].

- Many coefficients
- Designed to have exact linear phase characteristics
- Implementation via fast convolution

3.4.4.2 Wavelet Transform

The concept of wavelet is discussed as early as the 1980s. The wavelet transform is a tool to decompose data or functions into separate frequency components and then to study each component with a resolution matched its scale (at specific time scale) [45]. Hence it represents the signal in the time and frequency domain at the same time, unlikely Fourier transform which holds only the frequency domain presentation of the signal.

The idea behind these time-frequency joint representations is to cut the signal of interest into several parts and then analyze the parts separately [46]. The wavelet transform intelligently adapts itself to capture features across a wide range of frequencies and thus has the ability to capture events that are local in time or transient [47]. This makes the wavelet transform an ideal tool to study non-stationary or transient time series.

A wavelet is a function of zero average [48] [49].

$$\int_{-\infty}^{+\infty} \psi\,(t)\; dt = \; 0 \tag{3.11}$$

It is dilates with a scale parameter s, and translated by u [48];

$$\psi_{u,s}\;(t) \;=\; \frac{1}{\sqrt{s}}\;\psi\left(\frac{t-u}{s}\right) \tag{3.12}$$

At the scale s and position u, the wavelet transform *f* is computed by correlating *f* with a wavelet atom [48].

$$Wf\;(u,s)\;=\int_{-\infty}^{+\infty} f(t)\;\frac{1}{\sqrt{s}}\;\psi\left(\frac{t-u}{s}\right)\,dt \tag{3.13}$$

Similar to a windowed Fourier transform, a wavelet transform can measure variation in time-frequency of spectral components, but with different time-frequency resolution [48]. it is called **time-frequency measurement**.

The wavelet transform, by zooming across scales can also find and characterize transients [48]. This **Multiscale Zooming** capability not only locates isolated singular events, but can also characterize more complex multifractal signals with non-isolated singularities [48].

3.4.4.2.1 Wavelet Denoising

Wavelet Denoising is a one of the many uses of wavelet transform aimed to remove noise from signals and images. Following is the method for applying the wavelet denoising [50][51][52][53].

- Apply wavelet transform to decompose the noisy signal for achieving wavelet coefficients using averaging filters and others that produce details.
- Select suitable threshold limit at each level and threshold method (hard or soft thresholding) for the noise removal.
- Reconstruction of the denoised signal by inverse wavelet transform using the thresholding wavelet coefficients.

In the procedure of wavelet denoising, selecting the thresholding method is very crucial with respect the noise in signal. Hard thresholding is set to zero coefficients that are less than or equal to a particular threshold [54]. Hardware thresholding estimator is implemented with following expression [48]. Where d_m is thresholding functions and T is threshold.

$$d_m(x) = \begin{cases} x & if\ |x| > T \\ 0 & if\ |x| \leq T \end{cases} \tag{3.14}$$

In the case of soft threshold, it subtracts the threshold from coefficients and hence moves the time series towards zero [55]. It implements an attenuation to decrease all the noisy coefficients by T the amplitude [48]. Following is the estimator for soft thresholding [48].

$$d_m(x) = \begin{cases} x - T & if\ x > T \\ x + T & if\ x \leq T \\ 0 & if\ |x| \leq T \end{cases} \tag{3.15}$$

A Result of the wavelet denoising can be observed in the Figure 3.11. In the figure, the raw signal (top) with noise can be seen and consequently denoised signals after the wavelet denoising procedure are depicted. Result of hard and soft thresholding can be compared (middle and bottom) in the figure.

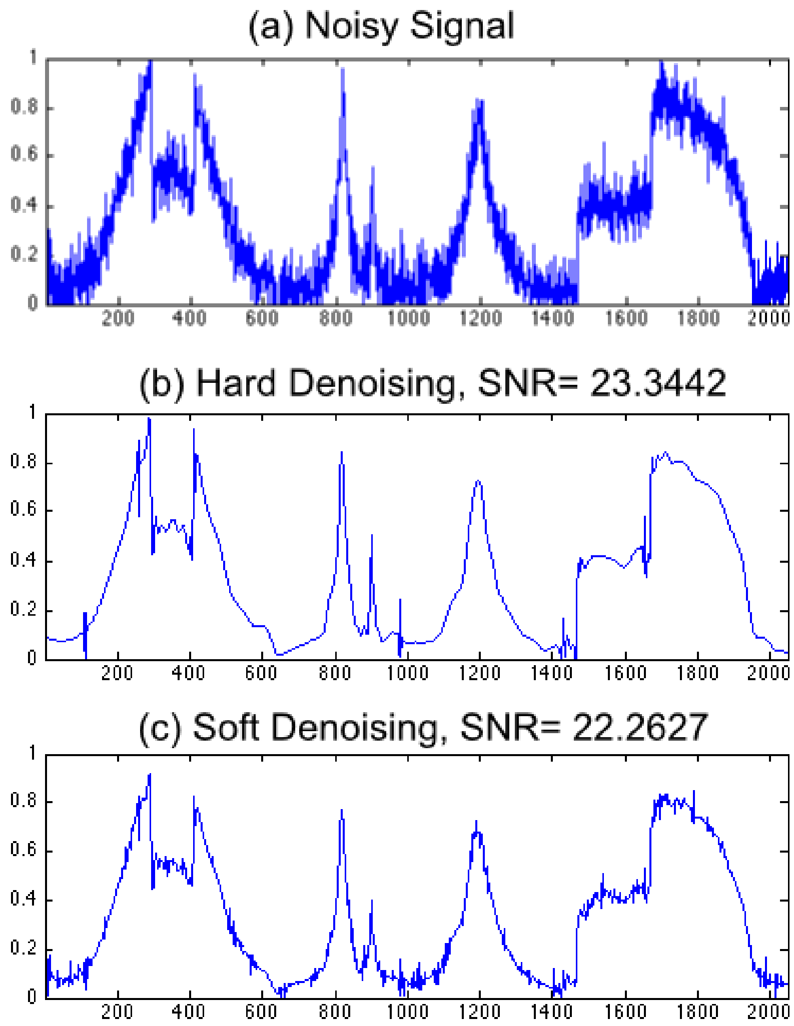

Figure 3.11 Wavelet denoising : noisy signal (top), Hard denoising of the signal (middle) and soft denoising of the signal (bottom) [56].

3.4.4.2.2 Wavelet Detrend

Time signals often contain components such as seasonal and cyclical components, trends and irregularities, if an additive decomposition model is assumed [57]. These trends of the input signal are the slow-varying part of the signal that mainly contributes to the approximation coefficients. Wavelet detrend applies the following steps to implement the detrend function on the signal [58].

- Apply the Discrete Wavelet Transform (DWT) to the input signal.
- Set the approximation coefficients to zeroes.
- Reconstruct the signal based on all the detail coefficients

Discrete Wavelet Transform is implemented using discrete filter banks for computing discrete wavelet coefficients [59]. A common and an efficient way to implement the DWT is using two channel perfect reconstruction (PR) filter banks [59], the a typical two channel PR filter banks can be seen in Figure 3.12.

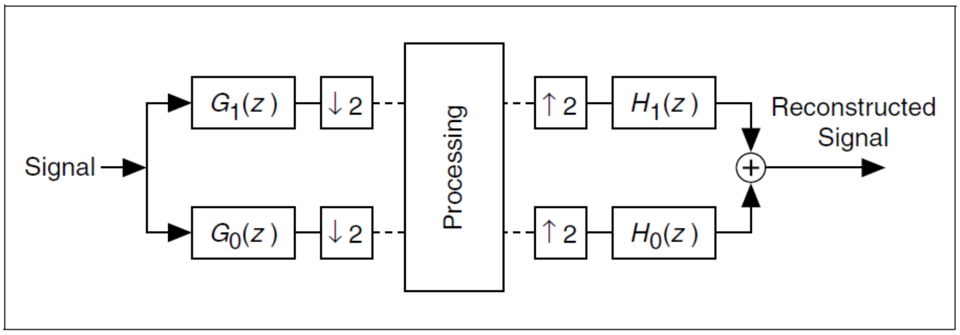

Figure 3.12 Two-Channel Perfect Reconstruction Filter Banks [59].

A trend removal from a graph of daily closing stock prices by wavelet detrending can be seen in Figure 3.13. Difference in original signal (blue) and detrended signal (pink) is evident in the figure. Similarly, one of the uses of the detrending is to reduce baseline wandering in ECG signal [60].

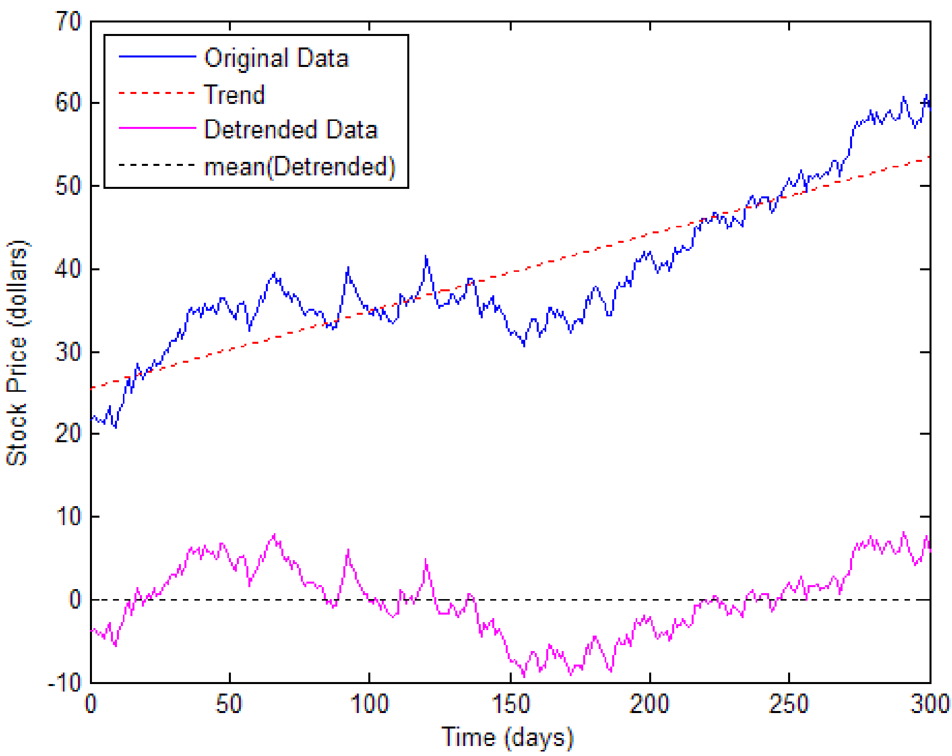

Figure 3.13 Example of trend removing from daily closing stock prices [61].

3.5 Artifacts

3.5.1 Movement artifacts

Movement artifacts are one of the critical distortions in contact or non-contact Electrocardiography. Lacking physical stabilization in contactless measurement, this capacitively coupled ECG system is strongly prone to movement artifacts.

One of the factors that contribute to the motion artifacts is the triboelectric effect. When the capacitive sensor and the subject come into contact and are than separated (like rubbing, friction etc), it produces static charges in the materials by the so called triboelectric effect [62]. The polarity and strength of the charges produced depends up on the material, the surface roughness, separating speed and other properties [63].

Also there is probably the leading artifact sources are movements. The artifacts are induced by the changing distance between the capacitive electrode and the subject. This issue of movement artifacts from capacitance fluctuation is addressed in the following section in details.

3.5.1.1 Movement compensation

Figure 3.14 shows the input stage of the capacitive electrode that constitutes the input stage of the CCECG system illustrated in section 3.2.1. This stage is very crucial for measurement as its impedance plays a significant role in measuring the signal, because it is forming a voltage divider (section 2.4.1) between the source, the capacitive electrode and the op-amp input.

Figure 3.14 Cel and Cs in series and resultant of these capacitance Cel-s

The capacitance between body and electrode changes when the body moves forth and back as shown in Figure 3.3. This movement varies the capacitance value in few pF to some pF as per the equation (3.1) with the change in the distance. Because of variance in the value of C_{el}, its impedance will be also changed which varies the amplitude of the output signal (refer to equation (3.3)).

The use of another capacitor (C_s) in series with the coupling electrode can help to reduce the overall capacitance change. If Cel ≥ Cs, the resulting capacitance, according to equation (3.16) , is kept in the range of $C_s / 2 < C_{el\text{-}s} < C_s$. To compensate this variance a capacitor (C_s) of 5 pF (2pF in the pilot study) is placed in series with C_{el} as shown in Figure 3.14, so the resulting capacitance will be near to 5 pF (2pF in the pilot study) as it is the lower value. As per the formula (3.16), the resultant capacitance will be 2.5 pF (1 pF in the pilot study) if the C_{el} is 5 pF (2pF in the pilot study, very low range). Hence the resultant capacitance will be always between 2.5 to 5 pF (1 pF to 2 pF in the pilot study).

Resultant capacitance of C_{el} & C_S ($C_{el\text{-}s}$) can be calculated with following formula.

$$C_{el-s} = \frac{C_{el} \cdot C_S}{C_{el} + C_S} \qquad (3.16)$$

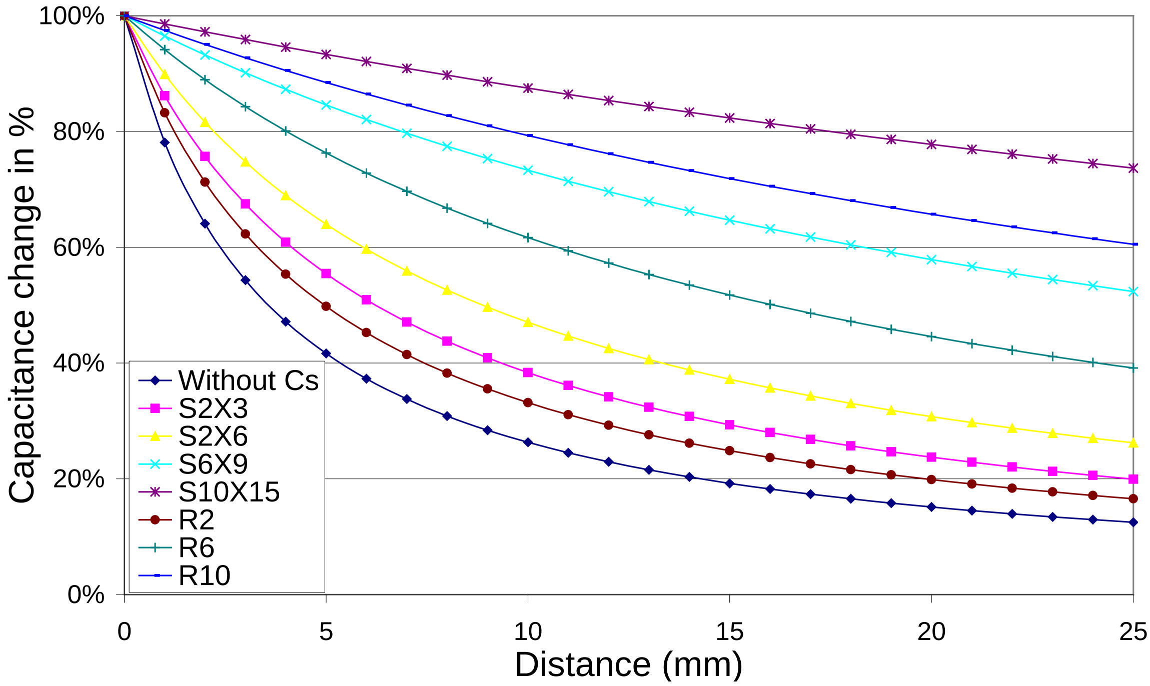

Figure 3.15 Variation in resultant capacitances of each stiff CCECG electrode over the distances.

The aim of the movement compensation is to defy the large variance in the signal amplitude against body movement (separating electrodes from body). It helps to get the output signal as constant as possible independent of the body movement, though the amplitude of the output signal is low.

This effect is shown in Figure 3.15 with series capacitor of 2pF during the pilot study. It shows the change in percent of the resulting capacitance with and without a series capacitor of 2 pF over an increasing air gap. Whereas the change in capacitance without the series capacitor is around 87.5 % (independent of the electrode area), it can be decreased by using C_s. In the case of the R10 electrode, it has a value of only 40 % (for 0 to 25 mm)as shown in the Figure 3.15. Electrode naming and its description can be seen in Table 3.2.

Naming	Description of the electrode (Area)
S2X3	Square electrode with area of 2 cm by 3 cm (6 cm^2)
S2X6	Square electrode with area of 2 cm by 6 cm (12 cm^2)
S6X9	Square electrode with area of 6 cm by 9 cm (54 cm^2)
S10X15	Square electrode with area of 10 cm by 15 cm (150 cm^2)
R2	Round electrode with diameter of 2 cm (3.14 cm^2)
R6	Round electrode with diameter of 2 cm (28.27 cm^2)
R10	Round electrode with diameter of 2 cm (78.5 cm^2)

Table 3.2 Electrode naming and its description.

Thus, limiting the impedance ratio (capacitive contact impedance) to a certain range and consequently the variation in the output amplitude of the input stage is also reduced. It should be noted that only the effect on the ECG amplitude due to capacitance change (due to distance variation) is considered here.

3.5.1.2 Simulation of the movement compensation

To visualize the movement compensation graphically with mathematic derivation of the input stage (3.3), a mathematical simulation with MATLAB-Simulink has been performed. The equation is employed in to the simulation tool using its Graphical User Interface (GUI) as seen in Figure 3.16.

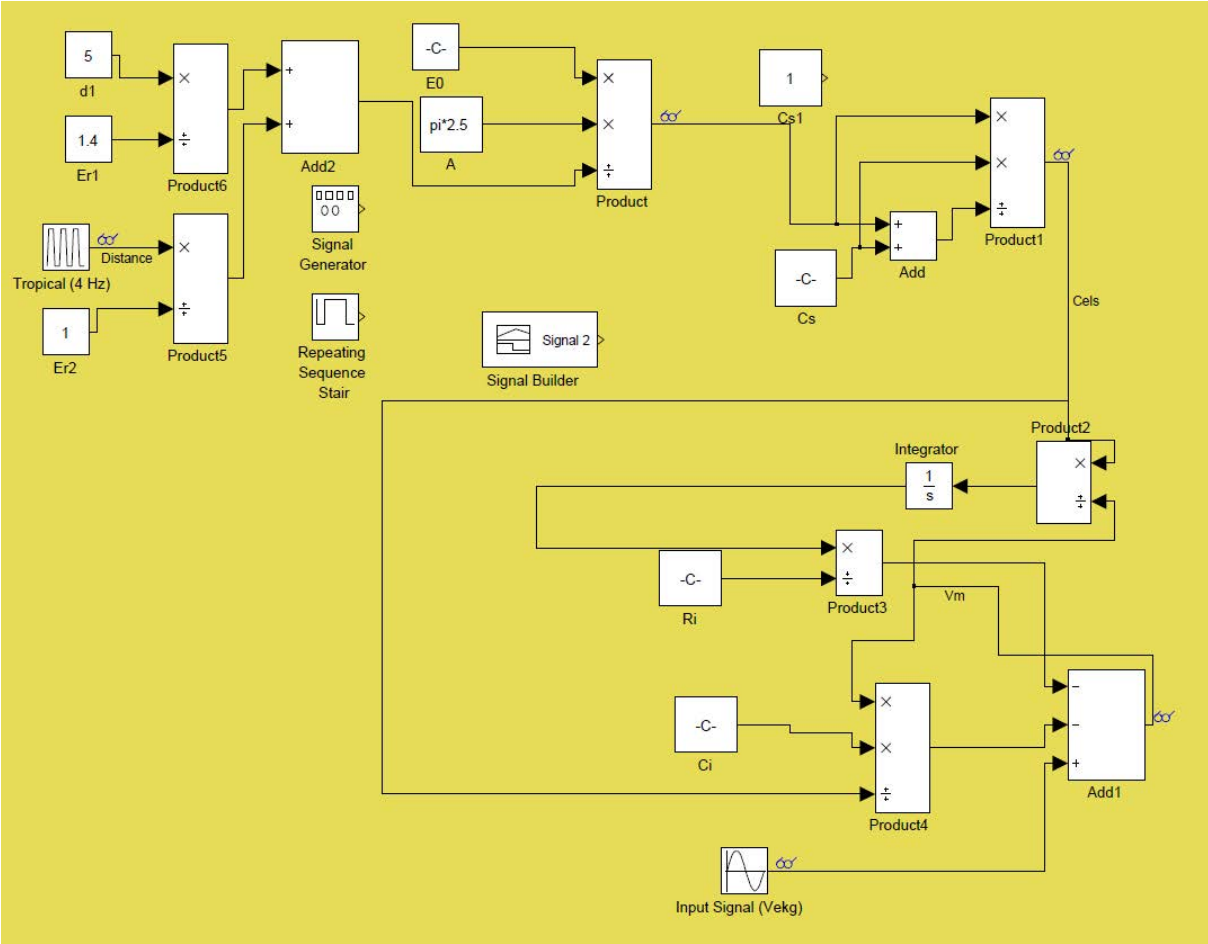

Figure 3.16 Simulink model for CCECG input stage as derived in equation (3.3).

In the equation, R_i is the effective input resistance of the op-amp, formed by the parallel connection of the op-amp input resistance (R_{in}) and the bias resistor (R_b).

So, $R_i = R_{in}$, OP || R_b, (parallel connection of these two resistance)

$$R_i = 10^{15}\ \Omega \parallel 200\ \text{G}\Omega \approx 200\ \text{G}\Omega$$

$C_{el\text{-}s}$ is the resultant capacitance from series connection of the capacitances C_s (2 pF) and C_{el}. The op-amp input capacitance (C_{in}) is 0.2 pF but we have considered a total input capacitance (C_i) ≈ 1 pF (possible hypothetic value) as it is approximately equal to the total practical value including parasitic capacitances, mentioned in section 3.2.4.1. The result of the simulation obtained through Simulink without and with the series capacitor is shown in Figure 3.17 and Figure 3.18 respectively. A real life situation is considered while simulating the coupling capacitance. So, the electrode capacitance has been modeled as a plate capacitor with an area of 78.53 cm^2, a relative permittivity of air ε_{r1} (=1) with the varying distance (1-50 mm) and a relative permittivity of subjects' cloth ε_{r2} = 1.4 (cotton) with fixed distance of 5 mm.

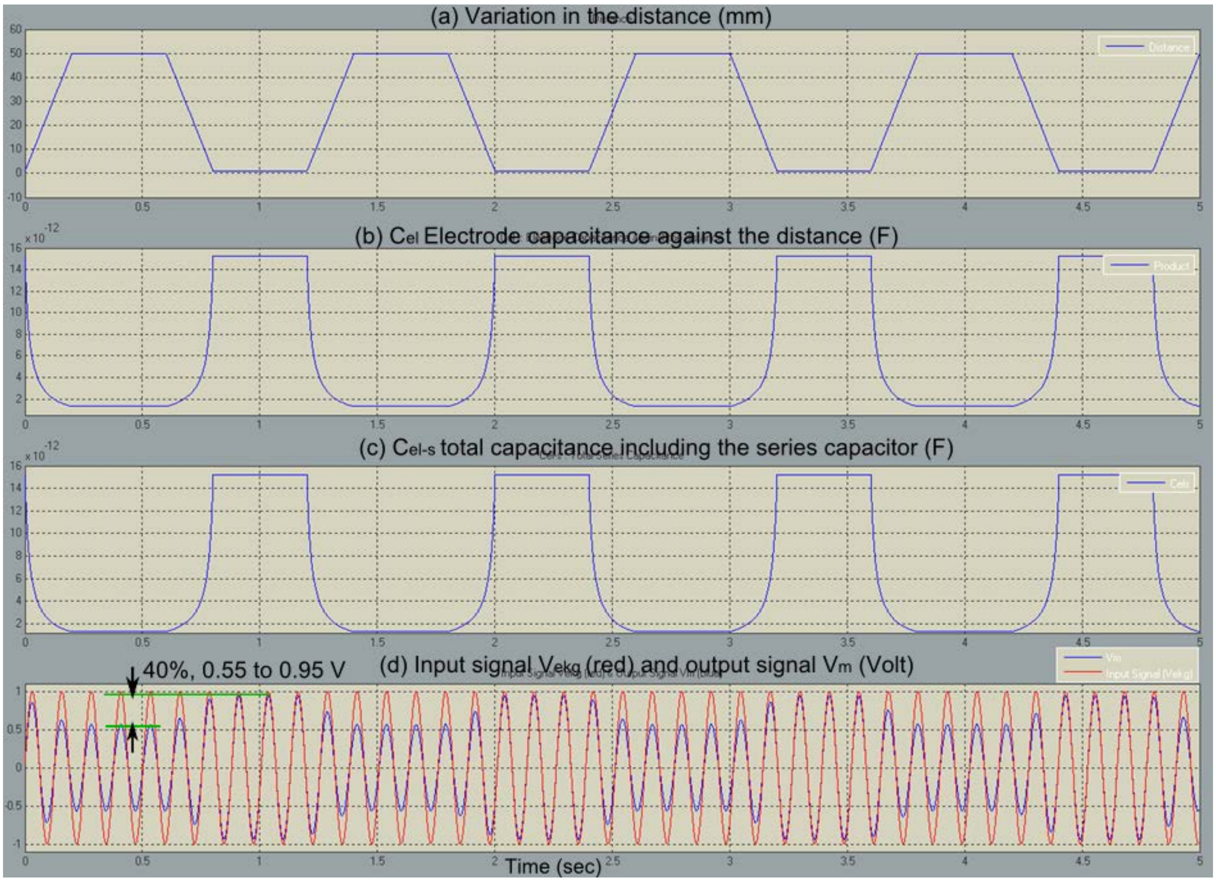

Figure 3.17 Simulation result by Simulink without a series capacitor (C_s)

In Figure 3.17, the 1st graph shows the change in the distance of the capacitance C_{el} (distance between the body & electrode). The corresponding change in the electrode capacitance and resultant capacitance C_{el-s} are shown in 2nd and 3rd graph respectively. The 4th graph shows the input signal (V_{ekg}) plotted in red and output or measured signal (V_m) in blue while varying the distance.

It can be observed in Figure 3.17 that variation in the amplitude of the output signal is from 0.55 to 0.95 V (maximum variation of 40 %). Now, it can be seen in Figure 3.18, the variation in the amplitude of the output signal is reduced from 0.45 to 6V (maximum variation of 15 %) after employing the series capacitor. The resultant improvement in the signal due to the series capacitor is the effect of the movement compensation. It should be noted here that movement compensation reduces the amplitude of the output signal. Here, the maximum relative signal losses are 5 % and 40 % for without series capacitor and with series capacitor configuration respectively. Similarly, the compensation effect reduces the amplitude of the movement artifact signal and hence limits variation in the amplitude of movement artifacts.

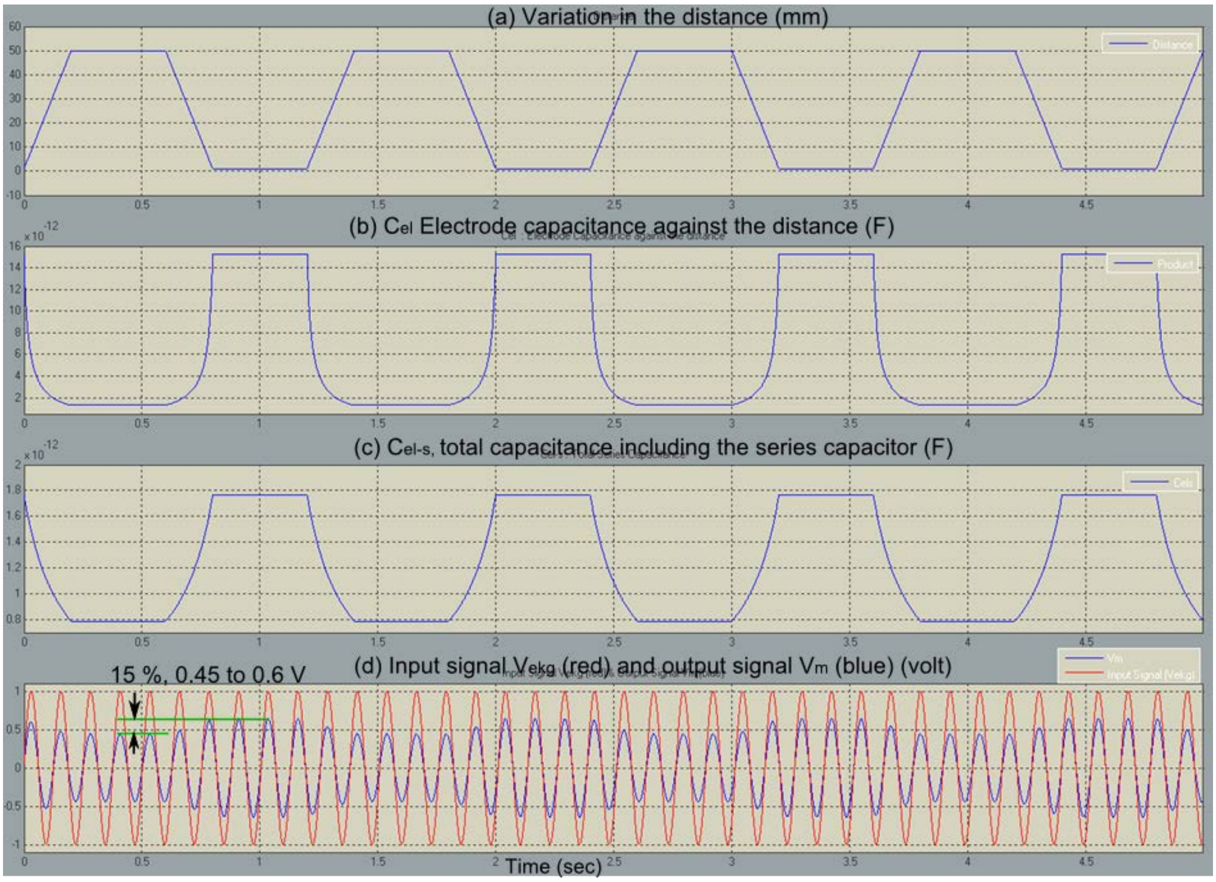

Figure 3.18 The simulation response with the series capacitor (C_s), (a) variation in the distance of the contact capacitance (C_{el}), (b) C_{el} Electrode capacitance against the distance, (c) C_{el-s} total capacitance including series capacitor, (d) Input signal (V_{ekg}) and output signal (V_m)

3.5.2 Power line and common mode noises

During measurement, the body also forms different capacitances with its surroundings (e.g. earth, power line etc) as sketched in Figure 3.19. In the figure, C_b, C_e and C_p represent capacitance between body and earth, circuit ground and earth and body and power line respectively. The capacitance C_P adds power line noise into the measurement through the body [4].

Power lines and surrounding electronic devices couple to the CCECG through the body and are the main source of common mode noises. The power line noise is so intense that sometimes it just masks whole ECG signal [64] because of it large amplitude compared to ECG signal. In early capacitive electrocardiography systems, capacitive ground (C_b) used to be employed to the body to reduce common mode noises [1]. Still the common mode signals were high enough to saturate the differential amplifier. This averts higher gain and higher cut-off frequency of the low pass filter. Filtering in such a case with reduced cut-off frequency distorts the ECG signal as some components of the ECG signal are sacrificed, which leads to lower ECG resolution and sharpness. Direct contact (resulting in low impedance contact) of the body to ground can have dangerous implications in a case of leakage current as the patient must be protected from currents higher than 20 uA [65] and according to German norms [66].

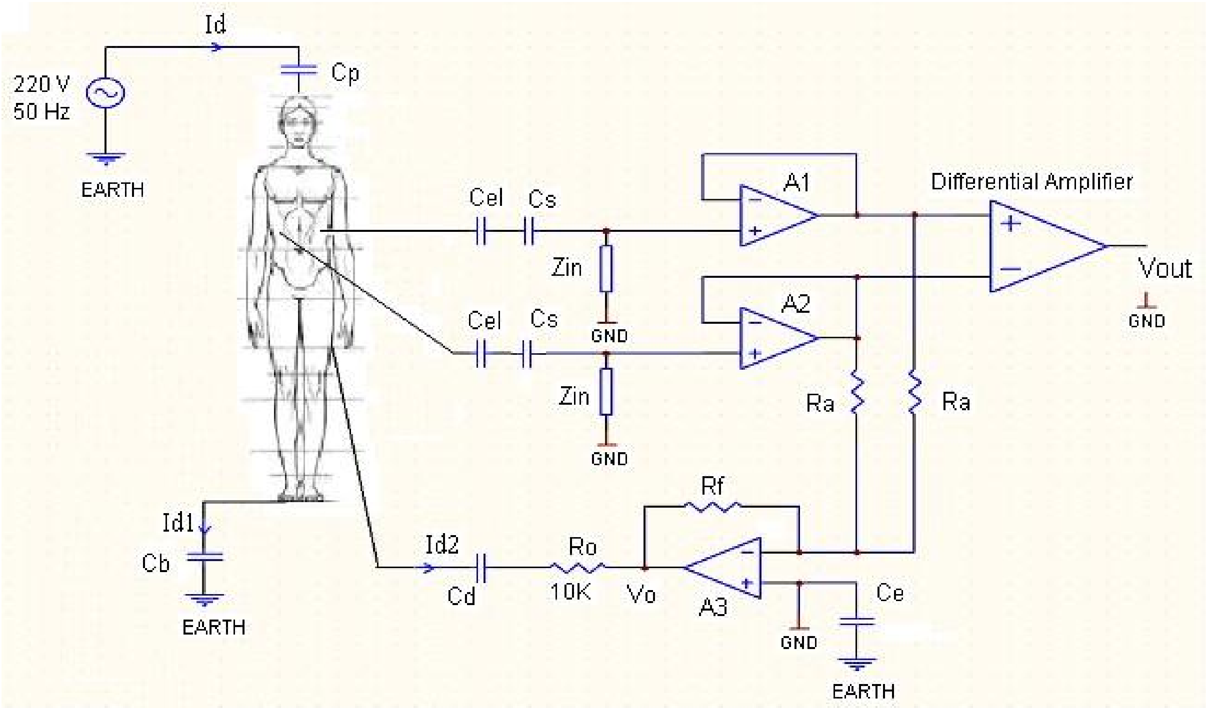

Figure 3.19 Power line and other common mode interference in CCECG[4].

Having mentioned above problems, it is crucial to have a configuration in capacitive electrocardiography to minimize common mode noises. Here we explain two main current methods to cope with the common mode signals, 1) differential amplifier with high common mode rejection ratio and 2) Driven Seat Circuit (analogous to driven right leg circuit to reduce common mode noises at the body surface) [4][5].

3.5.2.1 Input Differentiation

As part of differential signal amplification, signals from the two electrodes were fed to the differential amplifier (INA121) as explained in section 3.3.1. During the amplification, the instrumentation amplifier also removes the common mode signal to certain extent.

Figure 3.20 shows the graph of common mode rejection versus input frequencies of INA121 for various gains. The rejection of common mode signal is 106 dB at a gain of 100 or more with flat rejection band for conventional ECG bandwidth (0.5 - 100 Hz) [35]. Such common mode rejection ration (CMRR) will reduce power line noise to -106 dB. The gain of the amplifier is set to 200 for appropriate amplification in some cases.

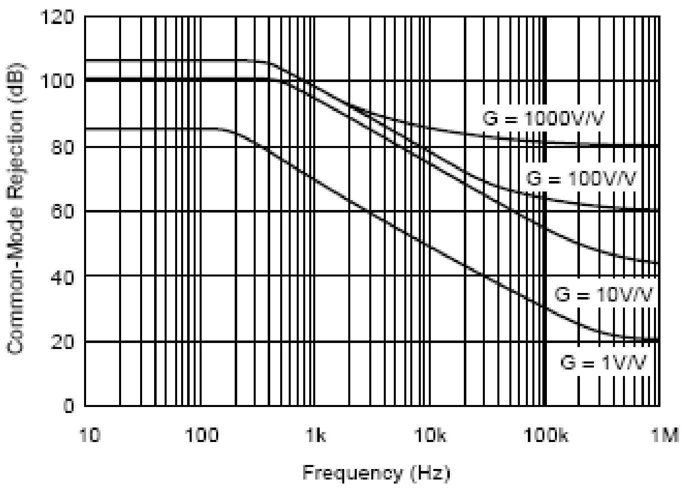

Figure 3.20 Common mode rejection Vs input frequencies [35]

3.5.2.2 Driven Seat Circuit

Another way to reduce the common mode signal effectively is by minimizing the potential directly at the source (the subjects' body) [67] [4]. The common mode voltage (V_c) is transformed into an interfering differential voltage (V_i) according to equation (3.17) [68] and fed back into the body.

$$V_i = V_c \left(\frac{1}{CMRR} + \frac{Z_d}{Z_c} \right) \tag{3.17}$$

Where,

Z_d = difference between the two electrode impedances

Z_c= common mode impedance

CMRR = Common mode rejection ratio

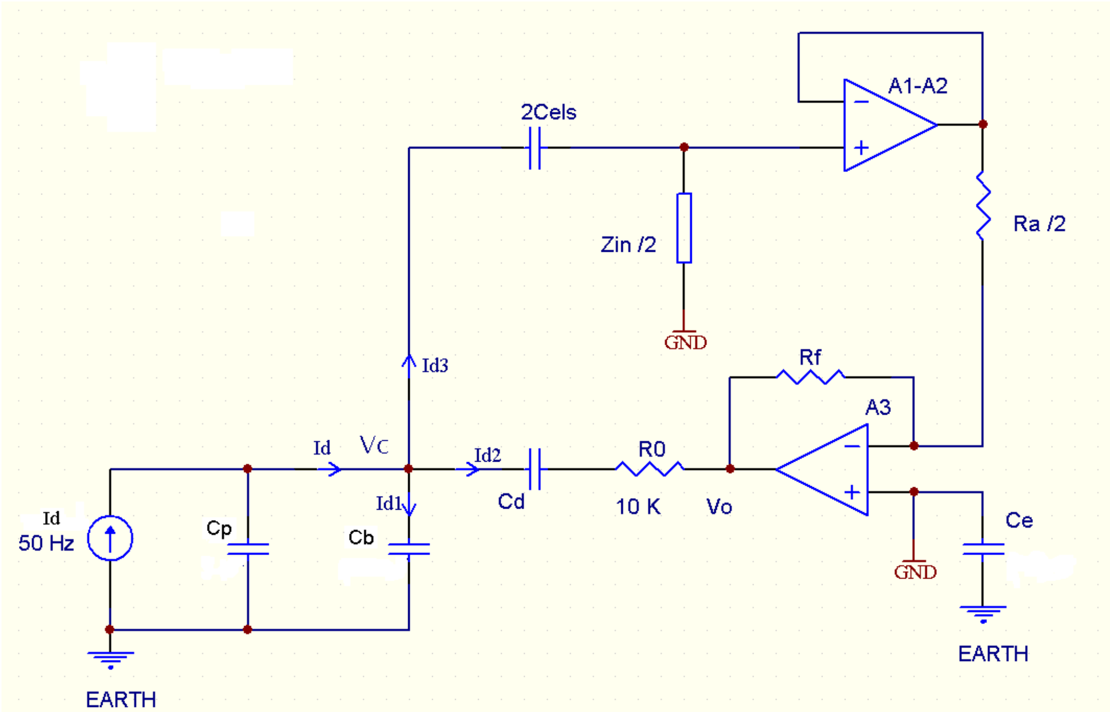

Figure 3.21 Equivalent circuit of driven seat circuit in Figure 3.19

Figure 3.21 shows the equivalent circuit of Figure 3.19 [69]. We can derive the following equation from the figure. We have assumed C_{el1} equal to C_{el2} to ease the calculation.

$$V_O = G \cdot V_C \tag{3.18}$$

$$G = 2\frac{R_f}{R_a} \tag{3.19}$$

$$V_C = V_O - R_O i_{d2} - \frac{1}{C_d}\int i_{d2}\, dt \tag{3.20}$$

G is the gain of the inverting amplifier (A_3), R_o and C_d are current limiting resistor and contact capacitance of driven circuit respectively. A low-noise JFET-input general-purpose operational amplifier TL071 from Texas Instruments is used here as A3.

Now from equations (3.18), (3.19) & (3.20), the magnitude of the common mode signal would be as follow.

$$V_c = \frac{R_o}{G+1} i_{d2} + \frac{1}{C_d\left(G+1\right)} \int i_{d2} dt \tag{3.21}$$

We can figure out from the equation (3.21) that by increasing the gain (G) of inverting amplifier we can further reduce the common mode signal [69][6]. Hence if we attach the additional capacitive electrode (C_d) as shown in Figure 3.21, we can reduce the common mode signal [4][5]. It can also be deduced from the equation (3.21) that maximizing electrode-body capacitance (increasing size of the driven electrode) will also yield in reduction of the common mode signal [6]. The driven seat circuit actively drives the electrode to a tenth of a millivolt to reduce the effective impedance of the electrode [67]. Implementing such a capacitive coupling system avoids current injection due to its isolated electrodes.

References

[1] Y.G. Lim, K.K. Kim, and K.S. Park, "ECG measurement on a chair without conductive contact," IEEE transactions on bio-medical engineering, vol. 53, pp. 956-9, May 2006.

[2] W. Portnoy, R. David and L. Akers, "Insulated ECG Electrode," in H. A. Miller and D.C. Harrison (Eds), Biomedical Electrode Technology, Acad. Press, New York, 1974.

[3] A. Lopez and P.C. Richardson, "Capacitive Electrocardiographic and Bioelectric Electrodes," IEEE Trans. Biomed. Eng., vol. 16, pp. 99, January 1969.

[4] K. Kim, Y. Lim, and K. S. Park, "Common mode noise cancellation for electrically non-contact ECG measurement system on a chair," Proc. 2005 IEEE Engg in Med. & Bio. 27th annual conference, Shanghai, China, September 2005.

[5] A. Aleksandrowicz, M. Walter, and S. Leonhardt, "Ein kabelfreies , kapazitiv gekoppeltes EKG-Messsystem Wireless ECG measurement system with capacitive coupling," Biomedizinische Technik, 2007, pp. 185-192.

[6] K.M. Lee, S.M. Lee, K.S. Sim, K.K. Kim, and K.S. Park, "Noise Reduction for Non-Contact Electrocardiogram Measurement in Daily Life," Computers in Cardiology, vol. 36, pp. 493-496, 2009.

[7] J. Bronzino, The Biomedical Engineering Handbook, 2nd edition, vol. 2. Florida: CRC press LLC. 2000, pp. 181-190.

[8] Richardson, P. C., "The Insulated Electrode," In Proceedings of the 20th Annual Conference on Engineering in Medicine and Biology. Boston, MA (USA), p. 157, 1967.

[9] R. N. Wolfson and M. R. Neuman, "Miniature Si-SiO_2 insulated electrode based on semiconductor technology," Proc. 8th Int. Conf. Med. Bio. Engg. Chicago, Carl Gorr , Paper No. 14-6, 1969.

[10] R. M. David and W. M. Portnoy, "Insulated electrocardiogram electrodes," Med. & Bio. Eng. vol. 10, 742, 1972.

[11] R. P. Betts and B. H. Brown, “Method for recording electrocardiograms with dry electrodes applied to unprepared skin,” Med. & Bio. Eng., pp. 313-315, May 1976.

[12] C. J. De Luca, R. S. Le Fever and F. B. Stulen, “Pasteless electrode for clinical use,” Med. & Bio. Eng. and Comput., vol. 17, 387, 1979.

[13] A. J. Clippingdale, R. J. Prance, T.D. Clark, and C. Watkins, “Ultrahigh impedance capacitively coupled heart imaging array,” Rev. Sci. Instrum. 65, pp. 269-270, January 1994.

[14] R. J. Prance, A. Debray, et al, “An ultra-low-noise electrical-potential probe for human-body scanning,” Meas. Sci. Technol. 11, pp. 291-297, January 2000.

[15] Burr-Brown corporation, “INA 116, an ultra-low input bias current instrumentation amplifier,” Datasheet, pp. 1-9, March 2011.

[16] C. J. Harland, T. D. Clark and R. J. Prance, “Electrical Potential probes – new directions in the remote sensing of the human body,” Meas. Sci. Technol., vol. 13, pp. 163–169, 2002.

[17] J. M. Lee, F. Pearce, A. D. Hibbs, R. Matthews & C. Morrisette, “Non-contact (through-clothing) Electrode for ECG monitoring and Life Science Detection for the Objective Force Warfighter,” Presented at the RTO HFM Symposium on “Combat Casualty Care in Ground Based Tactical Situations: trauma technology and Emergency Medical Procedure,” St. Pete beach, USA pp. 16-18, August 2004.

[18] J. Malmivuo and R. Plonsey, Bioelectromagnetism, principles and applications of bioelectric and biomagnetic fields. New York : Oxford University Press.1995, pp.16-19.

[19] R. S. Khandpur, Handbook of Biomedical Instrumentation, New Delhi, Tata McGraw-Hill Publishing. 2000, pp. 3-30.

[20] C. J. Harland, T. D. Clark and R. J. Prance, “Remote detection of human Electroencephalograms using ultrahigh input impedance electric potential sensor,” Appl. Phys. Lett. , vol. 81, pp. 3284-3286, October 2002.

[21] T. Matsuo, K. Iinuma and M. Esashi, “A Barium-Titanate-Ceramic Capacitive-Type EEG Electrode,” IEEE Trans. on Bio. Eng., BME-20, pp. 299-300, July 1973.

[22] L. J. Trejo et al “Multimodal Neuroelectric Interface Development,” IEEE Trans. on Neur. Sys. & Rehab. Eng., vol. 11, pp. 199-203, July 2003.

[23] N. von Ellerieder, E. Spinelli and C. H. Muravchik “Capacitive Electrodes in Electroencephalography ,“ EMBS 2006, 28th Annual Internation Conference of the IEEE, pp. 1126, August 2006.

[24] M. Oehler et al “Extraction of SSVEP signals of a capacitive EEG helmet for Human Machine Interface,” 30th Annual International Conference of the IEEE, pp. 4495-4498, August 2008.

[25] G. R. Langereis, C.P. Oy, A. Spaepen, K.U. Leuven, and T. Linz, “Context: contactless sensors for body monitoring incorporated in textiles,” FiberMed06 : Conf. on Fibrous Products in Medical & Healthcare, Tampere, Finland, 7-9 June 2006.

[26] L. Gourmelon and G. Langereis, “Contactless sensors for Surface Electromyography,” Proc. of the 28th IEEE EMBS Annual International Conference, New York City, USA, pp. 2514-2517, August 2006.

[27] T. Linz, L. Gourmelon, and G. Langereis, “Contactless EMG sensors embroidered onto textile,” BSN2007 : Body Sensor Network, 4th International Workshop on Wearable and Implantable Body Sensor Networks, Aachen, Germany, 26-28 March 2007.

[28] Voltage Divider, Wikipedia. Source : http://en.wikipedia.org/w/index.php?title=Voltage_divider &oldid=475984238, last accessed on 24 February 2012.

[29] W. J. Tompkins, Biomedical Digital Signal Processing. New Jersey: Prentice Hall. 1993, pp. 24-54 (43).

[30] W. H. Ko, M. R. Neuman, R. N. Wolfson and E. T. Yon, “Insulated Active Electrodes,” IEEE Tras. on Indu. Elect. & Contl. Inst., vol. 17-2, pp. 195-198, April 1970.

[31] Kirchhoff’s Voltage law ,Wikipedia. Source: http://en.wikipedia.org/w/index.php?title=Kirchhoff%27s_circuit_laws&oldid=478277822, last accessed on 29 February 2012.

[32] Parasitic Capacitance : http://en.wikipedia.org/w/index.php?title=Parasitic_capacitance&oldid=467868292. Last accessed on 6 December 2011.

[33] R. Pallas-Areny and J. G. Webster, Analog Signal Processing. Newyork : Wiley-Interscience Publication 1999, pp. 482-484.

[34] A. Rich, “Shielding and Guarding, how to exclude interference-type noise, what to do and why to do - A rationale approach,” Analog Dialogue 17-1, pp. 124-129, 1983.

[35] Burr-Brown corporation, “INA 121, FET-input low power instrumentation amplifier,” Datasheet, pp. 1-9, March 2011.

[36] National Instruments: NI USB-9162, “C series USB Single module Carrier,” Datasheet, 2010.

[37] National Instruments: NI 9215, “ Ni9215 with BNC 4 Channel ± 10V, 100kS/s per Channel, 16 bit, simultaneous sampling differential analog input,” Datasheet, 2010.

[38] LabVIEW website. Source : http://www.ni.com/labview/, accessed on 05 March 5, 2012.

[39] V. K. Medisetti and D. B. Williams, The Digital Signal Processing Handbook, CRC press LLC. 1998, pp. 5-10.

[40] Z. Milivojevic, Digital filter design, Mikroelektronika. Source : http://www.mikroe.com/eng/chapters/view/71/chapter-1-basic-concepts-of-digital-filtering-and-types-of-digital-filters/, last accessed on 05 March 5, 2012.

[41] Infinite impulse response, Wikipedia. Source : http://en.wikipedia.org/w/index.php?title=Infinite_impulse_response&oldid=480265851, last accessed on 05 March 5, 2012.

[42] C. S. Lessard, Signal processing of random physiological signals (synthesis lectures on biomedical engineering), Morgon and Claypool publishers, 2006, pp. 118-121.

[43] R. Aster and B. Borchers, “Dgital filtering,” 27 September 2011. Source : http://www.ees.nmt.edu/outside/Geop/Classes/GEOP505/Docs/Filter.pdf, last accessed on 05 March 5, 2012.

[44] L. Debnath, “Wavelet transforms and their applications,” Birkhäuser, Bostron, 2001, pp. 12-17.

[45] I. Daubechies, “Ten lectures on wavelet,” Society for Industrial and Applied Mathematics, Philadelphia, 1992, pp. 1-16.

[46] C. Valens, “A really friendly guide to wavelets,”, Source : http://www.polyvalens.com/blog/?page_id=15#1.+Introduction, Last accessed on 31 December 2011.

[47] R. Gencay, F. Selcuk and B. Whitcher, “An Introduction to wavelets and other filtering methods in finance and economics,” Academic press, London, 2002, pp. 1-12.

[48] S. Mallat, a Wavelet tour of signal processing, Academic press, London, 1998.

[49] D. B. Percival and A. T. Walden, “Wavelet method for time series analysis,” Cambridge university press, 2000, pp. 1-19.

[50] A. Graps, “An introduction to wavelets,” Computing in Science and Engineering, vol. 2, no. 2, pp. 50-61, June 1995.

[51] B. Vidakovic and P. Muller, “Wavelets for Kids,” unpublished, 1994.

[52] M. Fomitchev, “An Introduction to wavelets and wavelet transforms,” 1998. Source : http://www.smolensk.ru/user/sgma/MMORPH/N-4-html/1.htm, last accessed on 06 March 6, 2012.

[53] S. S. Tsai, “Power transformer partial discharge acoustic signal detection using fiber sensros and wavelet analysis, modeling and simulation,” Master thesis at Virginia Polytechnic Institute and

State University, 2002. Source: http://scholar.lib.vt.edu /theses/available/etd-12062002-152858/, last accessed on 06 March 2012.

[54] I. Kaplan, “Applying the haar wavelet transform to time series transform,” Source : http://www.bearcave.com/misl/misl_tech/wavelets/haar.html. Last accessed on 2 March 2011.

[55] D. L. Donoho, “De-nosing by soft thresholding,” IEEE Transaction on Information theory, Vol. 41 (3), pp. 613-627, May 1995.

[56] Signal denoising with wavelets in MATLAB tool box. Source : http://www.mathworks.com/matlabcentral/fileexchange/9554-a-numerical-tour-of-signal-processing/content/numerical-tour/denoising_wavelet_1d/index.html, last accessed on 06 March 2012.

[57] F. Mhamdi, M. Jadane-saidane and J. M. Poggi, “Empirical mode decomposition for trend extraction. Application to Electrical data,” 19th Internation Conference on Computational Statistics, COMPSTAT2010, Paris-France, August 22-27 August 2010.

[58] National Instruments, LabVIEW WA Detrend. Source : http://zone.ni.com/reference/enXX/help/371419B-01/lvwavelettk/wa_detrend/. Last accessed on 31 December 2011.

[59] Advanced Signal Processing toolkit user manual, LabVIEW (National Instruments). Source : http://www.ni.com/pdf/manuals/371533a.pdf, last accessed on 06 March 6, 2012.

[60] M. Faezipour, T. M. Tiwari, A. Saeed, M. Nourani and L. S. Tamil, “Wavelet-based denoising and beat detection of ECG signal,” Life Science System and Applications Workshop, 2009, LiSSA 2009, pp. 100-103.

[61] Detrending data, MATLAB. Source : http://www.mathworks.de/help/techdoc/data_analysis/bqm3i7n-13.html, last accessed on 06 March 6, 2012.

[62] B. Feddes, L. Gourmelon, M. Meftah, and T. Ikkink, “Reducing motion artefacts of capacitive sensors,” Proc. 29th Annu. Int. Conf. IEEE Eng Med. Biol. Soc. (EMBS), 2007, Lyon, Oct. 2007, p. 1532.

[63] T. Wartzek, T. Lammersen, B. Eilebrecht, M. Walter and S. Leonhardt, "Triboelectricity in Capacitive Biopotential measurements,” IEEE Trans. on Biomedical Engineering, vol. 58(5), pp. 1268- 1277, May 2011.

[64] A. K. Ziarani and A. Konrad, “A nonlinear adaptive method of elimination of power line interference in ECG signals,” IEEE Trans. On Biomedical Engg. Vol. 49 (6), June 2002, pp. 540-547.

[65] “Safe use of electricity in patient care areas of hospital,” Nat. Fire Protection Ass., Quincy, MA, NFPA-76B, 1980.

[66] Medizinische elektrische Gerate, Besondere Festlegungen für die Sicherheit von Elektrokardiographen (IEC 60601-2-25:1993 + A1:1999), German Version DIN EN 60601-2-25:1995 + A11999.

[67] B.B. Winter and J.G. Webster, “Reduction of interference due to common mode voltage in biopotential amplifiers,” IEEE transactions on bio-medical engineering, vol. 30, Jan. 1983, pp. 58-62.

[68] J. H. Huhta and J. G. Webster, “60-Hz Interference in Electrocardiography, ” IEEE Trans. Biomed. Eng., vol. 20, Mar. 1973, pp. 91-101.

[69] Bruce B. Winter, John G. Webster, “Driven right leg circuit design,” IEEE Transaction on biomedical engg., vol. 30, pp. 62-66, January 1982.

[70] R. Pallás-Areny, “On the reduction of interference due to common mode voltage in two-electrode biopotential amplifiers,” IEEE transactions on bio-medical engineering, vol. 33, Nov. 1986, pp. 1043-6.

4 CCECG System Implementation

4.1 Hardware CCECG System

To prove the principle of capacitively coupled Electrocardiography and to conduct a feasibility test, a pilot study was carried out with stiff PCB electrodes. A study was also done to find suitable capacitive electrodes, including verification of the shape and size of the capacitive electrodes. This section provides details of the CCECG system with the stiff PCB electrodes of various shapes and sizes.

4.1.1 Capacitive electrode

A pilot study to prove the principle of capacitive electrocardiography was conducted with a stiff PCB CCECG system (electrode + electronics). In this study, various shapes of capacitive electrodes with common electronics were examined from square electrode with area of 150 cm^2 to round electrode with area of 6 cm^2. This examination can help to find best electrode shape among the electrodes that can be implemented for further development in the study of capacitive electrocardiography.

Conducting layers in the electrodes are copper-plated to a thickness of approximately 35µm and fused with a 6µm -10µm tin film, protecting the tracks and pads during the final etching process.

Each of these electrodes forms different capacitance with the body in standard comparable situations. They couple the ECG signal in various amount by cohering with body surface potential mapping (refer section BSPM).

4.1.2 Electronics Unit

One of the main goals of this work is to compare the performance of different shapes and sizes of the electrodes. In order to be able to do this, a modular concept is implemented. Figure 4.1 shows the block diagram of the CCECG electronics units.

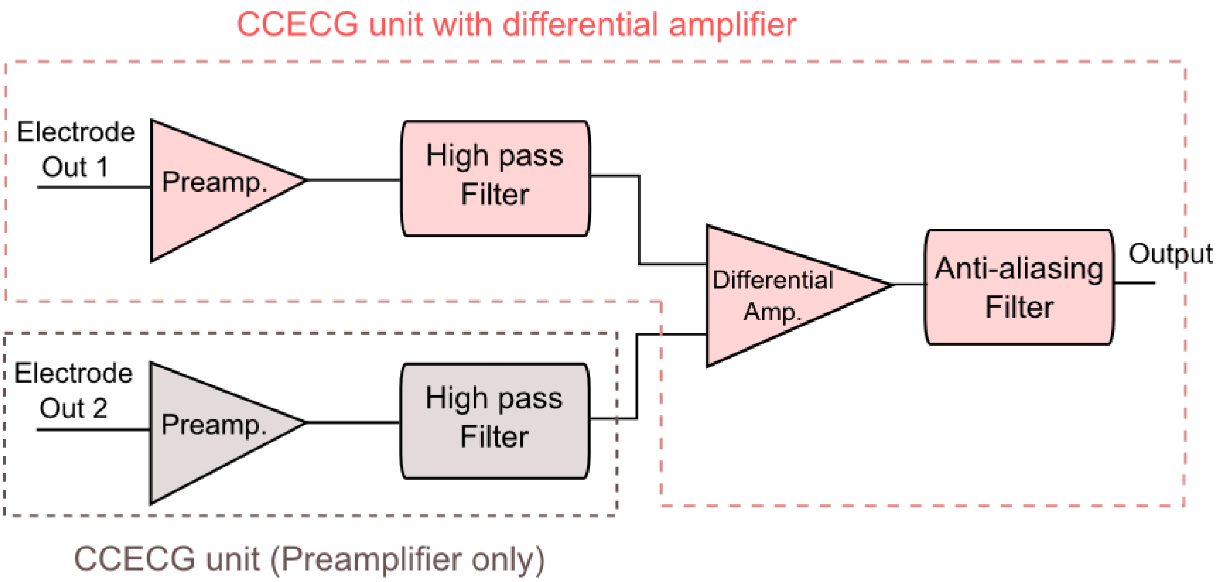

Figure 4.1 The CCECG Electronics units.

In the figure, two different electronic units can be seen. While both units contain preamplifiers (unity gain), one has an additional differential amplifier. The unit with only a preamplifier is connected to the unit with additional differential amplifier via coaxial cable as shown in depicted in Figure 4.1. Here the printed circuit board (PCB) layout of both units are designed identical and differential amplification circuit implemented in one of the units.

4.1.3 PCB CCECG Electrode module

Section 3.2.1 describes different bandwidths for different ECG applications. For our ECG sensors, we have tried to achieve a bandwidth suitable for monitoring the heart activity. A final PCB CCECG module integrated with electrode and electronic unit is sketched in Figure 4.2. We have used locking connector strips (SFML-120-T2-S-D-LC [1] & TFML-120-01-S-D-LC [2], Samtec) to get firm mechanical and electrical contact between the electrodes and the electronic unit.

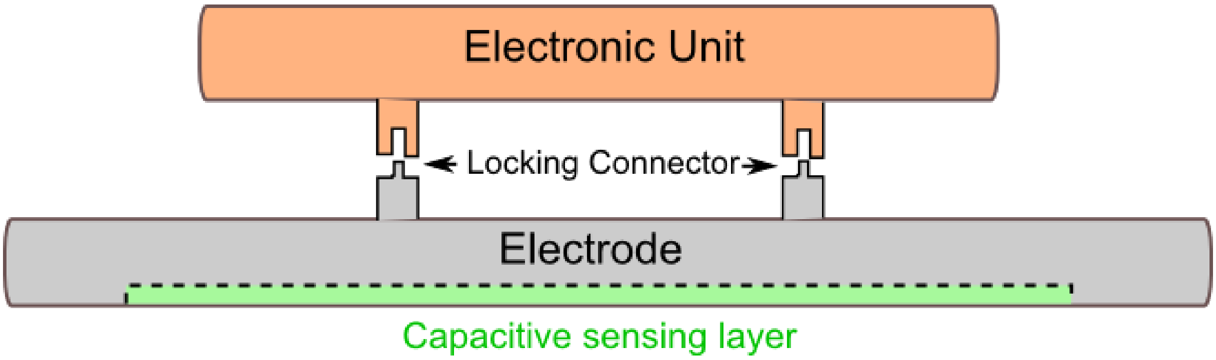

Figure 4.2 PCB CCECG module with electrode and electronic unit.

Minimizing of the common mode signal is performed using driven seat circuit as explained in the section 3.5.2.2. A capacitive (metal plate) electrode as driven seat electrode to reduce common mode signal is shown in Figure 4.3 with driven seat circuit. The capacitive electrode is a thin tin plate with an area of 650 (26X25) cm^2 and thickness of 0.45 mm. This tin plate electrode couples with the lower part of the body (buttocks) and provides capacitive connection for the driven seat circuit.

Figure 4.3 Driven Seat electrode and circuit of the system.

The body and the driven seat electrode form a capacitance of approximately 161 pF between them considering the subject wearing 5 mm thick cotton pants (dielectric material, ε_r =1.4). In the pilot study, the electrode was implemented only to verify the theory of the driven seat circuit; hence comfort of the subject with the electrode was not taken under consideration.

Figure 4.4 shows the simulated frequency response of the system at different stages of the circuit with pspice simulation. The bandwidth of the system is shown in green in the 2nd graph and has range of 0.412 Hz to 49.36 Hz. Gain of the differential amplifier is set to 50, yet the overall output of the system is 46 mV with input of 1 mV signal. Thus, total system gain is

46, the attenuation of -0.7 dB is produced by the passive filters. Turquoise (1st graph, top), yellow and blue lines (2nd graph, bottom) show the frequency response of the preamplifier, high pass filter frequency response and frequency response of the differential amplifier respectively.

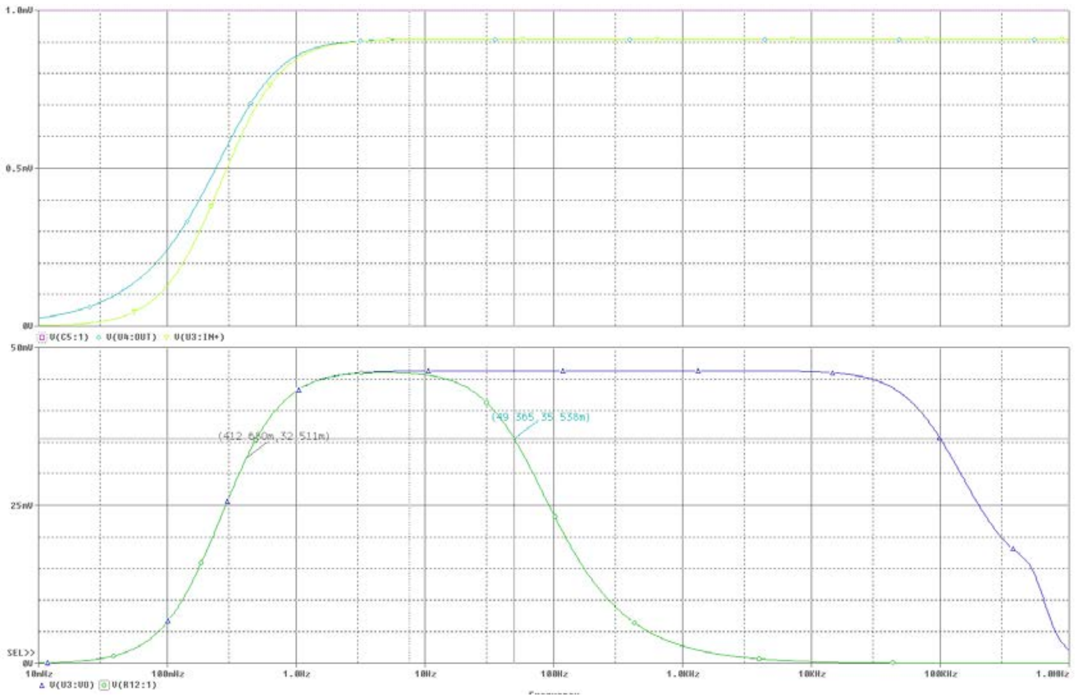

Figure 4.4 Frequency response of the system at various stages through PSpice simulation.

The simulated PSpice circuit of the CCECG system can be seen in Figure A 21 in the annex. For comparison with real system, let's see the actual measured frequency response of the system. Figure 4.5 shows the actual frequency response of the system at different stages. Blue, pink and yellow represent the frequency response of the preamplifier, differential amplifier, and system respectively.

Here, the actual bandwidth of the overall system is 0.3 Hz to 75 Hz. This is higher than the simulated one, which can be caused by the tolerance of the components, especially the capacitors which had a tolerance of +/-15%. Lower cutoff frequency of the preamplifier (buffer) is 0.3 Hz, similar to frequency response of the whole system (also similar to frequency response of differential amplifier), while simulation result showed 0.412 Hz..

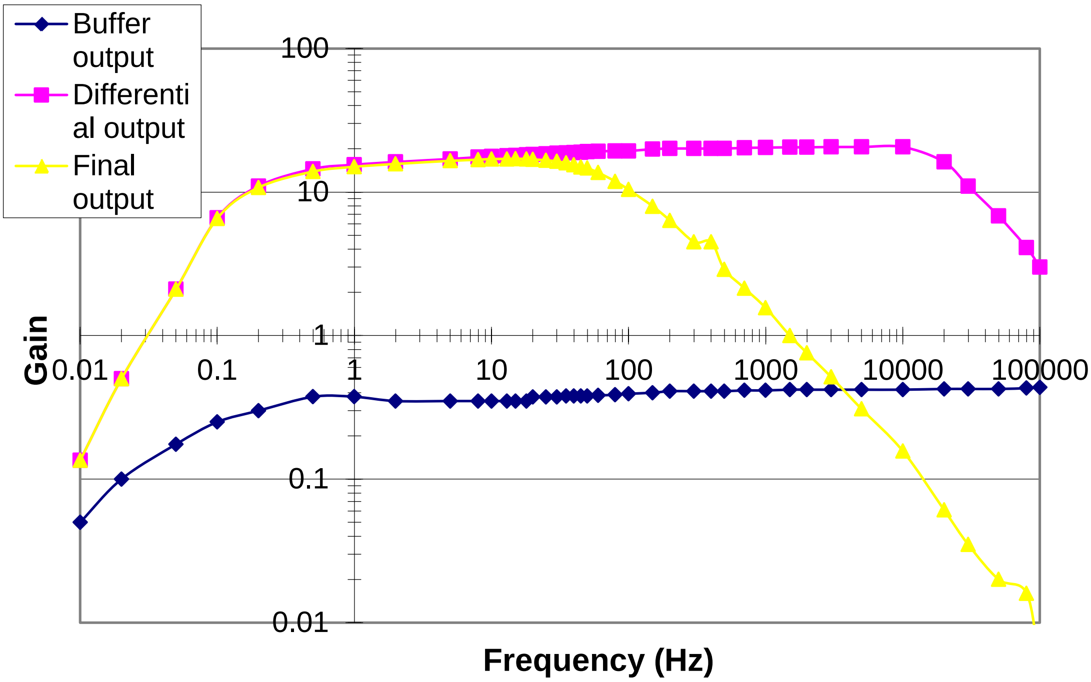

Figure 4.5 Actual frequency response of the system at various stages

4.2 1st Generation Textile CCECG System

As part of the project, the main application was to realize using technical textile (conductive textile). So the next step, after developing the pilot system with stiff PCB electrodes was to transform the stiff system into a textile form. As part of the transformation process, a first version of the textile electrodes and semi flexible (star-flex) electronics was implemented. Following sections describe the realization of the system in details.

4.2.1 Textile Capacitive electrode

Several version of the textile electrodes have been constructed within this doctoral work with help from TITV (Institut für Spezialtextilien und flexible Material), Greiz [3]. All the electrodes were manufactured using printed textile technology (images of the each version can be found in the Appendix I). The first prototype contained textile co-axial cable as shown in Figure 4.6 to carry the signal from the electrode to the electronics. Shielding of the coaxial cable was driven with active guarding pins of the INA116 [4] (refer Figure A 8) to protect the signal from parasitic effects.

Figure 4.6 Textile coaxial cable used in the textile electrodes.

But soon after the realization of the textile electrode with textile coaxial cable, it was very complex to solder the textile conductive wires onto a PCB without special soldering equipment. The connection stability of the wires was also weak compare to standard wires due to its conductive textile threads, it was prone to breakage. The wires need special solder treatment to make contact with a PCB solder pad, as standard method resulted in very weak contact (prone to breakage). So this textile coaxial cable (Figure 4.6) was replaced with conventional coaxial cable to ease the connection problem.

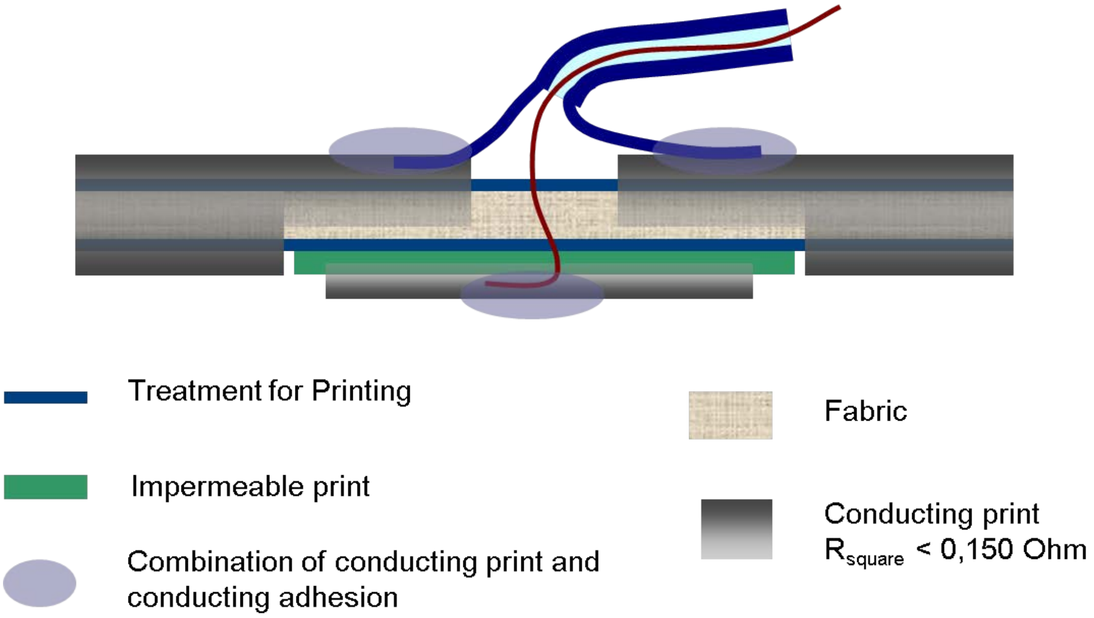

Figure 4.7 Structure of the 2 layer textile electrode.

After improvements, the 3rd version of the electrodes as shown in Figure 4.7 was designed and implemented. It shows the structure of the 2 layer textile electrode containing the front (sensor) and rear layer of the electrode. The rear layer is used as guarding plane to prevent any parasitic effect and is connected to the shield of the coaxial cable to guard the input signal [5]. These guarding connections are driven with the same potential as the signal. Insulation of the rear layer was done by anti-static polythene as shown in the Figure 4.9.

Electrode	**Capacitance (nF)**	**Impedance (kΩ)**
Module 1 (GRD-IN)	1.9211	920.2
Module 2 (GRD-IN)	1.7465	968.4

Table 4.1 Capacitance and impedance between the electrode layers.

Electrode properties like capacitance and absolute impedance between the layers are measured with a LCR meter 4263B (Hewlett-Packard) at frequency of 100Hz. Values of these parameters can be seen in Table 4.1, here GRD-IN means measured between the guarding and input (sensing area) connection. The silver printed textile electrodes are prone to their conductive surface degradation and hence their capacitance and impedance values tend to vary to a greater extend even possible disconnection or layer short circuit.

4.2.2 Flexible Electronics Unit (Star-flex)

Capacitive coupling of the system depends on the distance between the subject and the system, as per the capacitance formula, and hence better capacitive coupling can be achieved by having flexible textile CCECG module, which can be better conformed to body contour. This flexible structure can cohere to the body contour to yield better capacitive coupling and hence provide a bigger contact capacitance. To accomplish the design, the electronics also was implemented in star-flex form. Star-flex is a type of PCB design which is a semi flexible PCB with combination of hard and flexible circuit boards. The star-flex design is shown in the Figure 4.8, where the flexible part is highlighted in red. Guarded solder joint can also be seen in the figure, where the textile electrode is connected (soldered) to convey the ECG signal into the preamplifier.

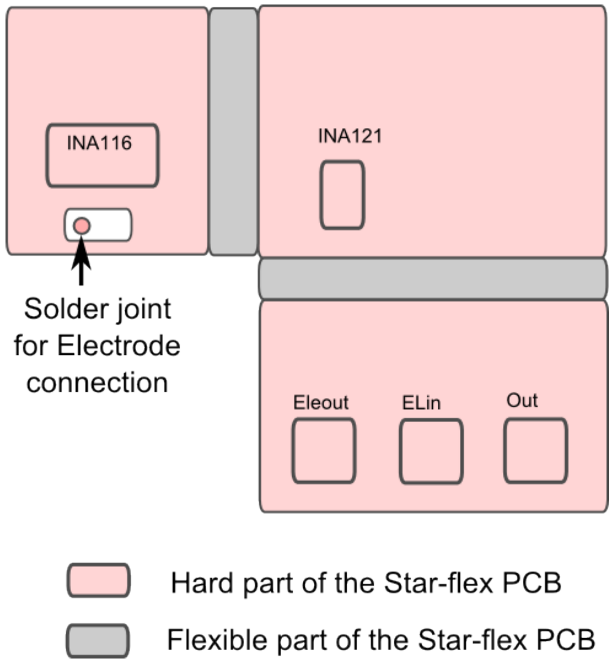

Figure 4.8 A sketch for star-flex PCB design of the electronic unit.

In my CCECG system, each electrode has its own electronics. Design and printing of this star-flex PCB was similar for both of the electrodes. In one of the electronic modules, a differential amplifier circuit was employed to perform the differential amplification and anti-aliasing filtering. The CCECG signal from the other electrode (the electrode with buffer only), after its pre-amplification, was fed to this differential amplifier (INA121) [6] through a gold plated coaxial socket (SMD, SMA, Multicomp) [7] on the PCB and a thin coaxial cable. Series capacitor of 5.1 pF is utilized at the input of the preamplifier to compensate for the movement artifact as explained in section 3.4.1.1.

4.2.3 1st Generation textile CCECG module

The above mentioned electrode and electronics form the textile CCECG module which is demonstrated in Figure 4.9. In the figure, both modules of the textile CCECG can be seen. The left side of the figure shows the electrode with only a preamplifier and how the electronics are fastened to the electrode by a Velcro fastener. The right side of the figure shows the second textile electrode fastened to the electronics with the differential amplifier circuit.

The two conductive layer textile CCECG system is submitted to patenting (DE102008049112A1) [8] and the patent is pending.

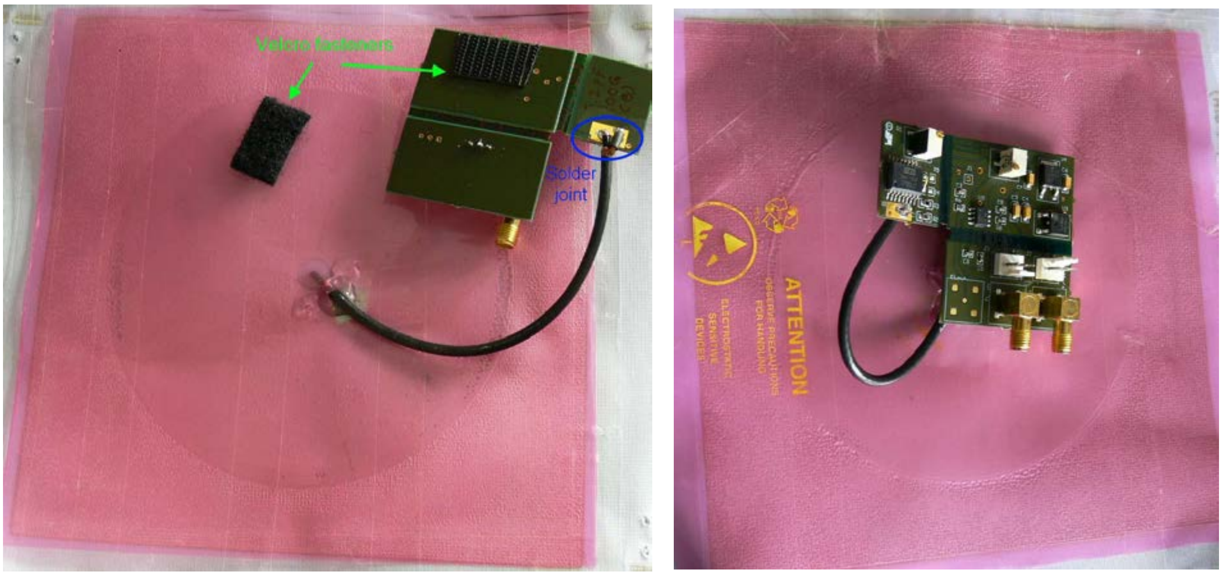

Figure 4.9 1st Generation of the textile CCECG module.

4.3 2nd Generation Textile CCECG System

4.3.1 Textile Capacitive electrode

After trying stiff capacitor plates and 2 layer textile electrodes in earlier work, an improved textile electrode was designed as the results were still not satisfactory. The new electrode design contains 3 conductive and 3 isolating textile layers (PES-Knitted substrate-7058, Thorey) [10]. The silver gel to print the electrodes were made up of 75% silver solvated in 2-butoxyethanol (Silver ink, D & D Puhl GmbH) [11]. The structure of the electrode can be seen in the Figure 4.10. The three layers are highlighted with three different colors, Sensing layer (Sin, red), Guarding layer (GR, blue), Grounding layer (GN, Green).

The guarding layer and the grounding layer work as active and passive shields for the sensor layer. Guarding is a technique used to actively shield a surface against any parasitic effect (e.g. coupling with surrounding noises) by driving the shield (GR) with common mode voltage [5]. This same surrounding potential will avoid coupling with any potential nearby helping to keep the high input impedance of the amplifier intact.

Grounding the layer on top of the guarding layer further shields the input [12]. Each layer of the electrode is connected with the preamplifier through a conductive snap fastener (DAO 12, YKK) as seen in the implemented electrode design (Figure 4.12). The snap fasteners were made up of steel and brass galvanized.

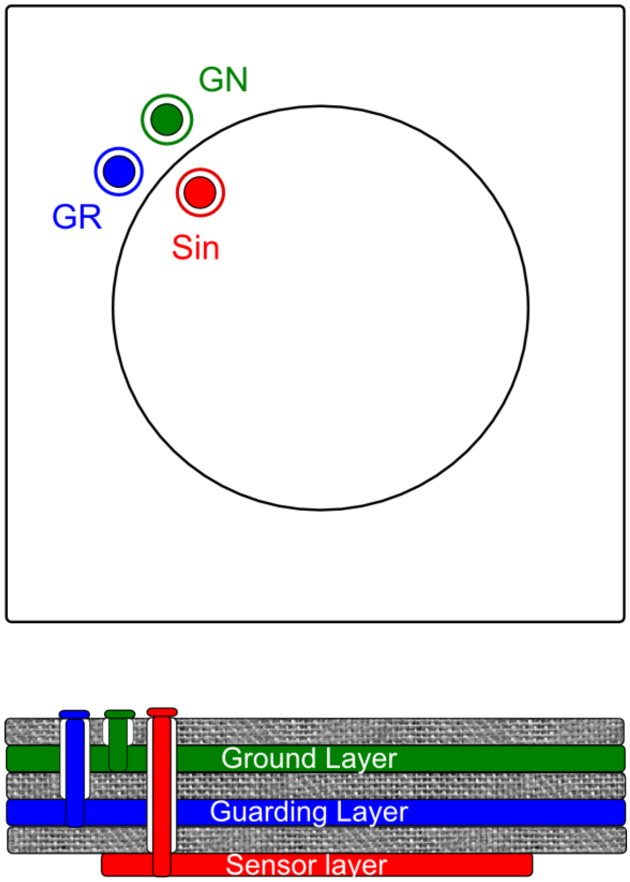

Figure 4.10 The textile electrode structure: top view (top), side view (bottom).

Table 4.2 shows electrode properties like capacitance and absolute impedance between the layers, here GND-GRD means measured between guarding and grounding layer. The values are measured with a LCR meter 4263B (Hewlett-Packard) at frequency of 100Hz.

Electrode	**Capacitance (nF)**	**Impedance (KΩ)**
Module 1 (GND-GRD)	2.1828	746
Module 1 (GRD-IN)	1.461	1172.3
Module 2 (GND-GRD)	1.9489	842.8
Module 2 (GRD-IN)	0.9846	1720.3

Table 4.2 Capacitance and impedance values between the electrode layers

The silver printed textile electrodes are prone to their conductive surface degradation and hence their capacitance and impedance values tend to vary greatly leading to possible disconnection or layer short circuit.

4.3.2 Buffer Module

As explained in the section 3.2.2, a high input impedance amplifier with biasing is needed to couple the ECG signal. An ultra-low input bias current instrumentation amplifier INA116 (Burr Brown Corporation, USA) has been identified for this application. It has a very high input resistance ($10^{15}\ \Omega$) and a very low input capacitance (0.2 pF) [4] thus nicely coping with the requirements. A modular design containing preamplifier (INA116) PCB and an actively shielded aluminum case are shown in the Figure 4.11.

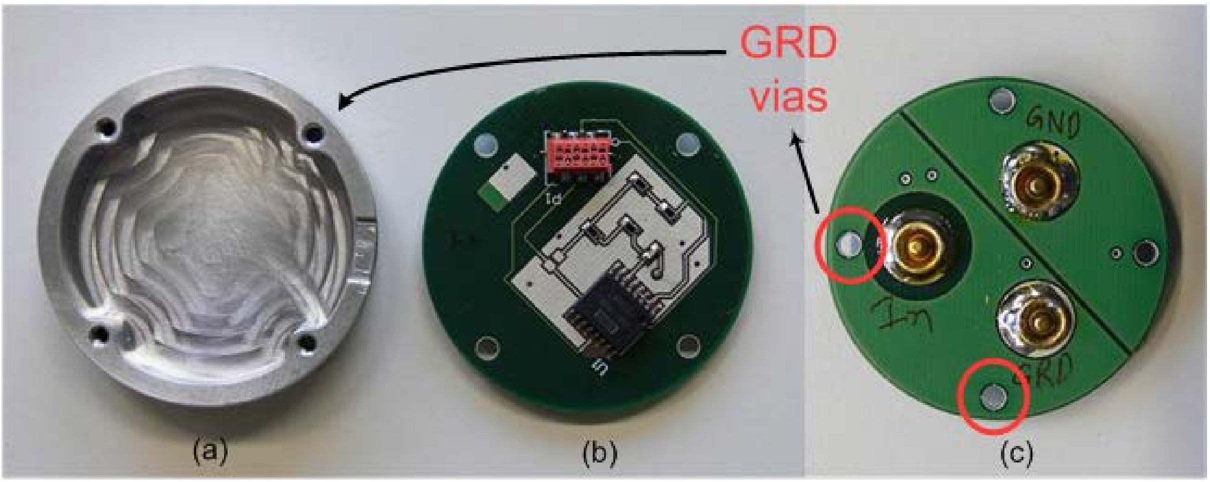

Figure 4.11 Pre-amplifier module: module housing (a), top view of the electronics circuit (b), snap connection to the electrode (c).

A four layer printed circuit board (PCB) was used to shield the input signal from the textile electrode through conductive snap fasteners. The snap fasteners (DAK 112.001, YKK) were made up of galvanized steel and brass. Guarding and grounding layers were also implemented in the PCB on top of the bottom layer (connecting layer) as shown in the figure. These shielding layers help to minimize parasitic effect as described in the section 3.3.4.2, Guarding.

Two holes (left and bottom) seen in the Figure 4.11 (c) are built as conducting pathway to connect to the aluminum housing. This connection added to the guarding plane on the top layer of the PCB (silver colored) ultimately joins guarding pins on the INA116; so does the guarding layer of the textile electrode. As mentioned earlier, driving the housing with the common mode voltage guards the input by avoiding coupling of surroundings.

4.3.3 2nd Generation textile CCECG module

The whole system of the 2nd generation CCECG module can be seen in the Figure 4.12. The buffer module is fastened to the three layer capacitive electrode by the conductive snap fasteners. The three snap fastener connections of the electrode and the electronics can be seen in the middle figure. The connection is quite firm mechanically to hold it for a longer time in various situations. The right hand side of the Figure 4.12 shows two test points; these are electrical connection of the guarding and grounding layer as they are completely isolated and not accessible otherwise.

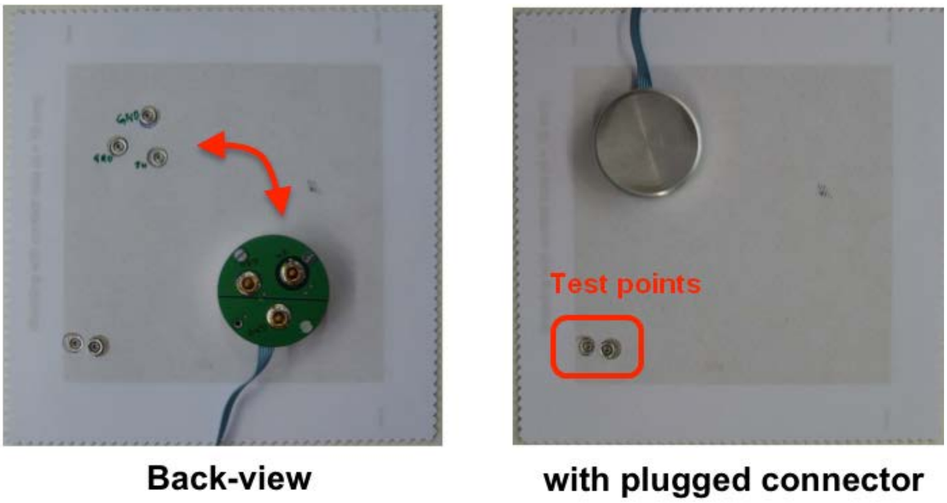

Figure 4.12 A three layer capacitive electrode configuration.

The 6 layered (3 conductive, 2 substrate and 1 covering, as shown in Figure 4.10) structure of the electrode inhibited its flexibility, making it less flexible than 2 layered structure which has only one layer of substrate. The three layer textile CCECG system is submitted for patenting (DE102010023369A1) [9] and the patent is pending.

Reference

[1] Samtec SMD locking socket strip connector, SFML-120-T2-S-D-LC. Source : http://www.samtec.com/ProductInformation/TechnicalSpecifications/Overview.aspx?series=SFML, last accessed on 02 March 2011.

[2] Samtec SMD locking terminal strip connector, TFML-120-01-S-D-LC. Source : http://www.samtec.com/ProductInformation/TechnicalSpecifications/Overview.aspx?series=TFML, last accessed on 02 March 2011.

[3] TITV (Institut für Spezialtextilien und flexible Material), Greiz. Website : www.titv-greiz.de.

[4] INA 116 Datasheet, Burr-Brown corporation, “INA 116, an ultra low input bias current instrumentation amplifier,” Datasheet, pp. 1-9, 2008.

[5] R. Pallas-Areny and J. G. Webster, Analog Signal Processing. New York : Wiley-Interscience Publication 1999, pp. 482-484.

[6] INA121, Burr-Brown corporation, “INA 121, FET-input low power instrumentation amplifier,”, 2008.

[7] SMA Coaxial connector datasheet, Multicomp, Datasheet.

[8] Bhavin Chamadiya and Manfred Wagner, “Textile electrode with integrated electronics to measure body functions and/or vital parameter for automotive application”, Patent Registration No. DE102008049112A1. Web-link: http://www.patentde.com/20090507/DE102008049112A1.html, last accessed on 08 March 2012.

[9] Bhavin Chamadiya and Manfred Wagner, “Capacitive electrodes to measure biological parameter for driver and /or passengers”, Patent Registration No. DE102010023369A1. Web-link : http://www.patent-de.com/20101230/DE102010023369A1.html, last accessed on 08 March 2012.

[10] Thoray Gera Textilveredelung GmbH, “PES-Gewirke Artikel 7058,” 2009, http://www.thotex.de/, last accesed on 24 September 2009.

[11] D & D Puhl GmbH, “Silver ink 392.000,” Technical Datasheet, 2009.

[12] A. Rich, “Shielding and Guarding, how to exclude interference-type noise, what to do and why to do - A rationale approach,” Analog Dialogue 17-1, pp. 124-129, 1983.

5 Various Measurement Environments

5.1 Driving Environment

Automotive safety is a crucial topic, with human mobility difficult to imagine without individualized automobiles. Even though a growing number of passive car safety solutions have been implemented over the past decades that have led to a decrease in fatalities, the human driver still remains the primary cause of accidents.

A number of biomedical and monitoring systems have been incorporated in automobiles for healthcare [1] as well as safety [2] improvement. However, physiological monitoring is still a nascent tool for real automotive healthcare and safety, mainly due to difficult handling of monitoring equipment outside a laboratory.

As such, non-contact measurements of driver's vital parameters by unobtrusive monitoring might improve general traffic safety immensely. Consequently the focus of this study was to integrate capacitive electrodes for electrocardiography in a real automotive environment. Vital sign recordings have been performed while driving in several real world situations and in the laboratory as well. Daimler AG is already working towards this subject, e.g. in the BMBF funded project INSITEX, the goal of which is to improve driver safety with intelligent textiles [3].

Lim at el. presented contactless ECG measurement on an office chair in 2006 [4]. They implemented PCB CCECG electrodes (4X4 cm), clad with copper and plated with gold. The electrodes were imbedded to the backrest of a chair parallel to each other and a large seat mounted conductive sheet to ground the body without direct skin contact. Later this conductive sheet amended to “Driven Seat Ground” with driven common mode potential, which is equivalent to “Driven Right Leg” to improve common mode rejection with negative feedback [5]. Furthermore, the effect of different clothing material on the frequency response of the system was displayed.

Parallel to the work of the INSITEX project in 2008, Leonhardt and Aleksandrowicz presented their study on capacitive ECG for Automotive application [6] and in 2011 [7]. They integrated the CCECG stiff electrodes into a co-driver's seat to measure non-contact ECG in automotive environment. The electrodes and the driven ground plane (analogous to driven right leg) were placed on the backrest of the car seat. The electrodes were fixed diagonally with center to center distance of 12 cm vertically and 13 cm horizontally. The system was wirelessly (Bluetooth) connected to the laptop for further signal display and storing in LabVIEW. The measurements were performed with various automotive scenarios.

Same year, Matsuda and Makikawa did a similar study to incorporate capacitive ECG into a car seat [8]. A single ended amplifier embedded electrode and a ground plane were developed. The electrode was imbedded to the seat cushion while the ground plane was imposed on the steering wheel to have bare skin direct contact. In addition to the measurement on the driving scenario, they also tested the effect of varying the value of the bias resistor of the preamplifier on the frequency response.

Collaboration study of university of Aachen and Ford research center Aachen GmbH in beginning of 2011, showed further work of development and evaluation to integrate CCECG system into a driving seat [9]. An array (2X3) of the capacitive electrodes (stiff) was embedded into the back rest of the seat and a driven seat electrode on the cushion. In addition to these electrodes, an accelerometer was mounted on the backrest to record acceleration of the vehicle in 3 dimensions, which can be utilized for signal processing. A pressure mate was applied to the backrest to examine contact pressure on the electrodes, ultimately selecting better contact electrode combination. Measurement on various driving surfaces was performed by integrating the system into Ford S-max.

In this chapter, the realization of various seat integrated capacitively coupled ECG systems will be described. It will explain different steps that we followed to transform the concept to a real system.

5.1.1 Textile CCECG Systems in Lab

Goal of the INSITEX project was to finally implement textile electrode in the automobile after the pilot study [3]. As the first part of the work, the electrodes have been implemented and tested in the laboratory. During this study, various versions of textile CCECG systems were designed and developed. Application, implementation and integration of these textile electrodes are elaborated in this subdivision. Measurements taken under various conditions using these textile electrodes are also presented.

5.1.1.1 1st Generation textile CCECG System

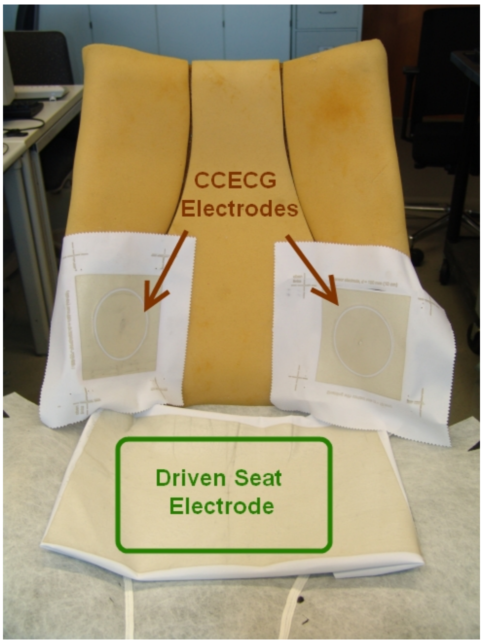

Figure 5.1 Experimental seat with 2nd generation textile electrodes

Electronic unit and electrode design in the first version of the textile CCECG was similar to the pilot work with the PCB CCECG system. Design and development of this textile CCECG system is detailed in section 4.2. In this case, two textile electrodes, silver printed with printed textile technology (TITV, Greiz) [10] as described in section 4.2.1, are connected to ultra high input impedance amplifiers (INA116, Texas Instruments) [11] and receive ECG signals through capacitive coupling from the body and feed them to a differential amplifier. This differential amplifier removes common mode signals and amplifies the ECG signal for further processing. In addition, a “driven seat circuit” (DSC) is used to further reduce common mode noise [5][12]. This circuit is analogous to “driven right leg circuit” in standard ECG system [13].

Round Textile electrodes with diameter of 10 cm were fixed to a stripped experimental car seat by conceiving the specific S-class (Mercedes Benz W221) car seat. Figure 5.1 shows the arrangement of two textile electrodes in the lumbar region of the passenger and one textile electrode for the driven seat circuit on the cushion. Capacitance versus distance graph for this electrode from a simulation can be seen in Figure 3.3.

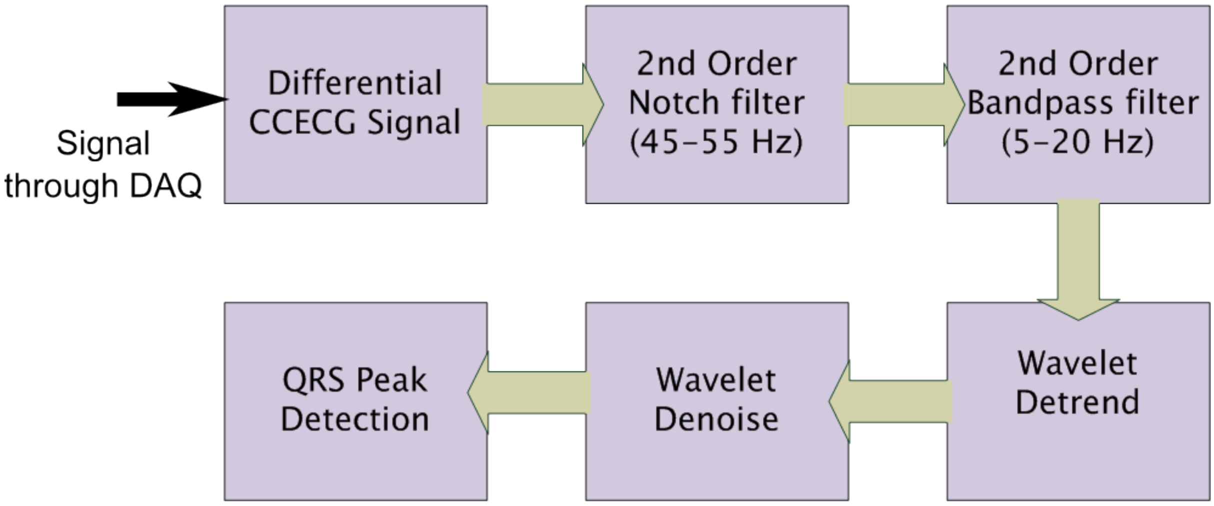

Figure 5.2 Sequence of the signal processing stages of the CCECG system.

Amplified signals are acquired through a data acquisition system (NI USB-9162 & NI-9215) into a LabVIEW program after its digitization. The CCECG signal is prone to encounter variety of noises ranging from severe high frequency noises to movement artifacts. A customized filter program made in LabVIEW helps to minimize these noises, sequence of the signal processing stages is illustrated in Figure 5.2. In that LabVIEW program, the ECG signal was processed in 5 stages, a 2nd order Butterworth notch filter (45-55 Hz), a 2nd order Butterworth band-pass filter (5-20 Hz), wavelet detrend, wavelet denoising and QRS peak detection respectively. A raw CCECG signal and its results with the different stages of the signal processing can be seen in the Figure 5.19 and Figure 5.20.

Fully dressed subjects (cotton t-shirt with thickness of 0.45 mm and jeans with thickness of 0.85 mm) were seated in the experimental seat in our lab resembling seat of series W221. Figure 5.3 shows unfiltered (top) and filtered (bottom) CCECG readout from the system. It is clearly visible, that appropriate filtering is needed to yield recognizable ECG data for further analysis like Heart Rate (HR) or its Variability (HRV). Though we could couple the ECG signal capacitively, the reproducibility of the system was very low. It was very difficult to couple the ECG signal continuously in the system.

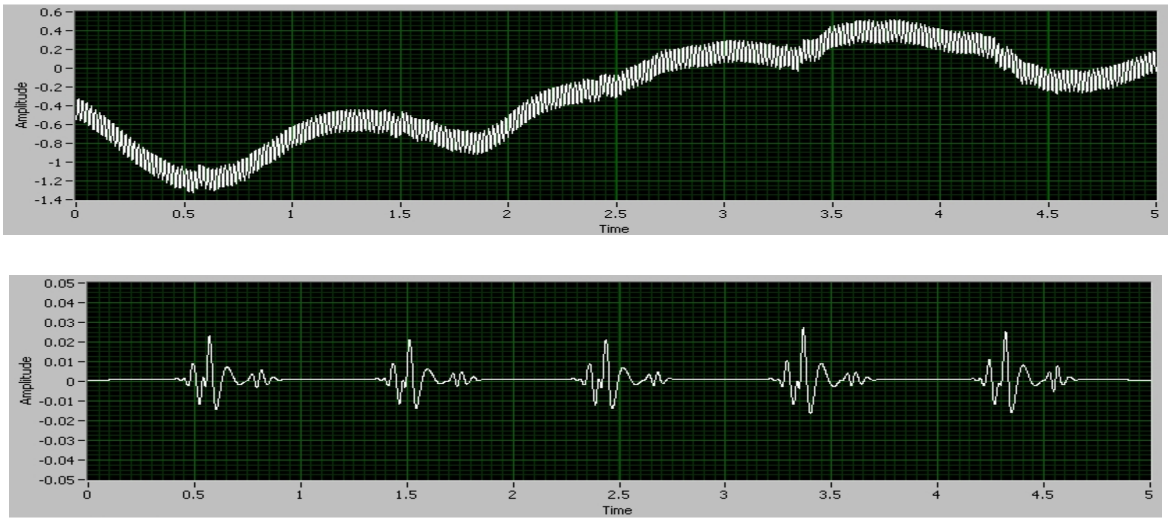

Figure 5.3 Capacitive ECG with the textile electrodes before filtering (top) Capacitive ECG after filtering (bottom).

5.1.1.2 2nd Generation Textile CCECG System

First version of the textile electrodes was examined and used for the capacitive ECG measurement. It was learnt that there is still room for improvement of the textile electrode structure and preamplifier PCB design. As part of this improvement, 2nd version of the textile CCECG electrodes was designed and developed. In this version, an additional conductive textile layer was deployed on top of the guarding layer (refer Figure 4.10) of the 1st version of the textile electrodes (refer Figure 4.7) to have better shielding against noise pickup. This layer is connected to grounding of the circuit so the coupled noise into the layer can be removed [14]. The input signal connection of the electrode is also guarded thoroughly to avoid any parasitic effect that can impact the input impedance of the preamplifier (refer Figure 3.9) [15].

Detail structure of the textile CCECG electrodes and the preamplifier module can be found on the section 4.3. Unlike the electronics of 1st version, where the differential amplifier was also mounted on one of the preamplifier PCB, the preamplifier module of this system contains only a preamplifier. Differential amplification and further signal processing like filtering are performed separately. This configuration enables more options in the signal processing. In this configuration, each parameter of the analogue signal processing can be customized and adjusted.

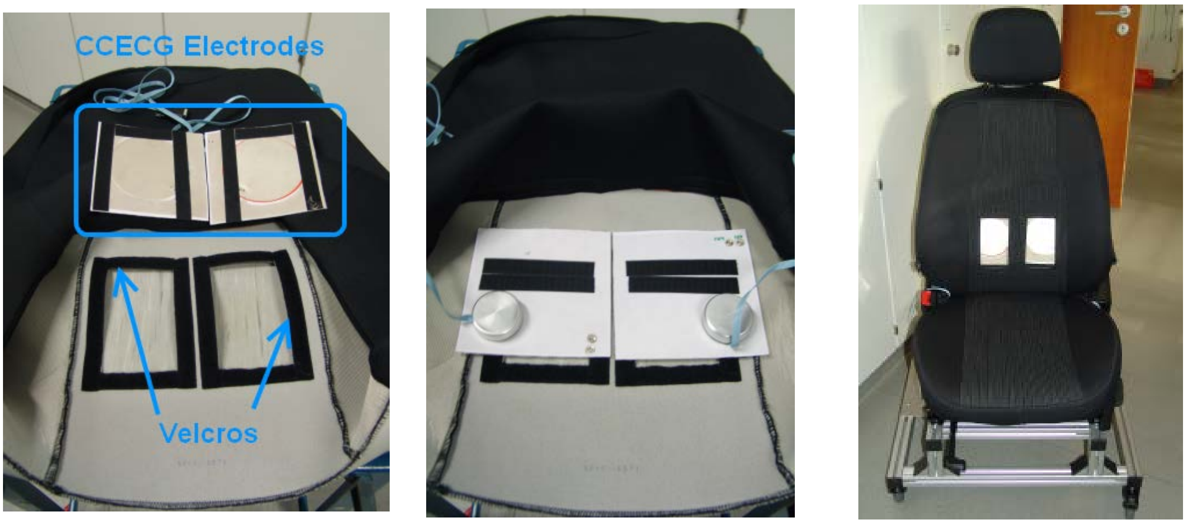

(a) (b) (c)

Figure 5.4 (a) The three layer CCECG electrodes with the seat cover of series W204, (b) the electrodes attached to the seat cover through Velcro, (c) the set cover put on the seat of W204 series.

To make the setup (electrode integration into seats) suitable for an experimental seat in lab and car seat as well, electrodes are fastened into an external seat cover of the Mercedes Benz C-class (W204 series). This external seat cover can be put onto any seat (lab and car) of the Mercedes Benz C-class (W204 series). Figure 5.4 (a) shows the capacitive electrodes and the incision to fasten the electrodes. Next image in the Figure 5.4 (b) represents the fastening of the electrode into the seat cover incision. Complete CCECG system integrated into the seat of W204 series in the lab is pictured in the Figure 5.4 (c), where the capacitive electrode can be seen in the lower backrest region. In the setup, driven seat electrode is placed beneath the cover of the seat cushion.

The external analog signal processing is performed by a programmable signal processing tool box (90IPB, Frequency devices) [16]. The differential CCECG signal was amplified before and after the 8th order elliptical band-pass filtering (1–38 Hz). The processed signal is imported to LabVIEW program through a data acquisition card (NI USB-9162 and NI-9215). In LabVIEW, initially the signal is filtered with notch filter (2nd order Butterworth filter with bandwidth of 46-54 and 80-120 Hz) to remove 50 Hz power line interference and its harmonics. Successively the signal is passed through a 2nd order Butterworth filter with bandwidth of 1-40 Hz and signal derivation.

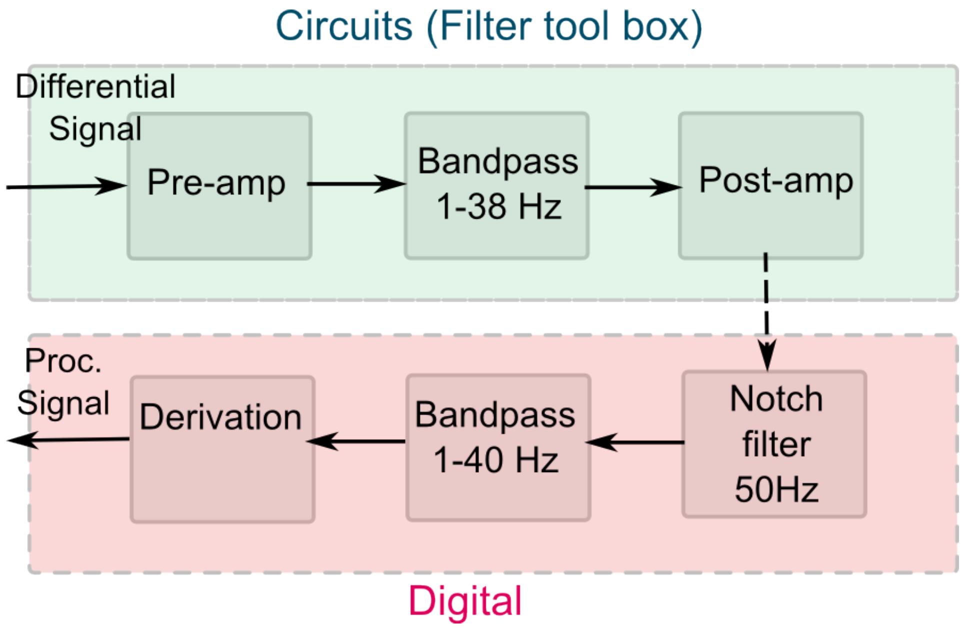

Figure 5.5 Signal processing of 2nd generation textile CCECG system.

Measurement is performed with a 28 years old subject with height and weight 175 cm and 78 kg respectively. The subject is wearing a 100% cotton shirt with thickness of 0.34mm and a 100% cotton pant with thickness of 0.28 mm. He was seating on an original customized car seat of Mercedes Benz C class of series W204 for laboratory use.

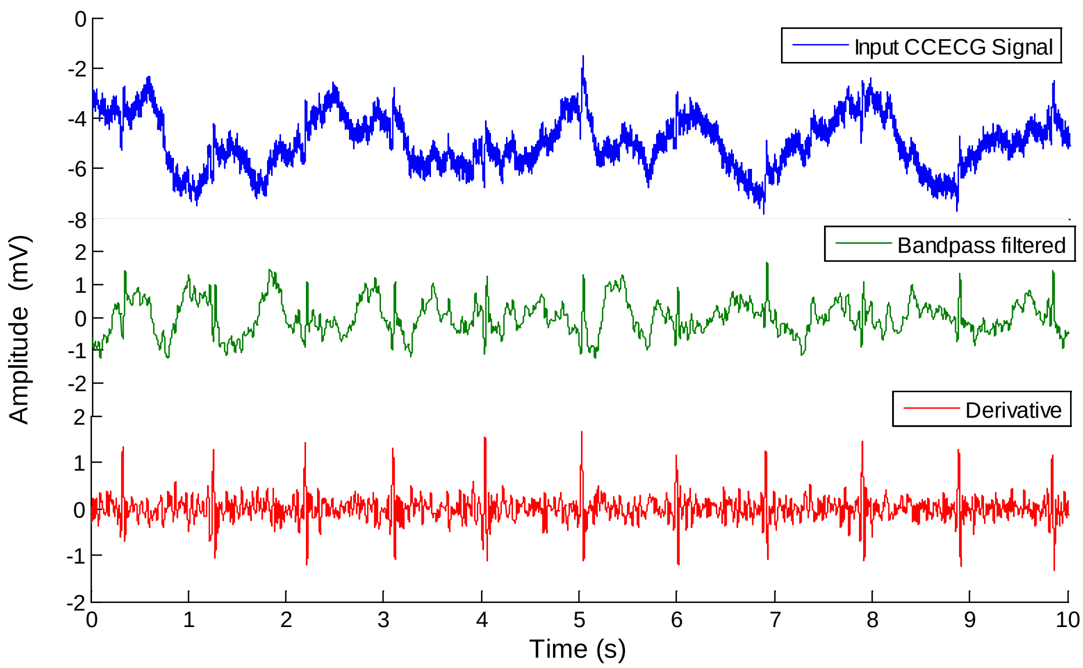

Figure 5.6 Result of the CCECG system.

Measurement result with the textile CCECG system is presented in the Figure 5.6. In the figure, signal with blue color depicts input signal into the LabVIEW program (after the analogue filtering). Even after the hardware band pass filtering, the signal contains low frequency and 50 Hz power line noises. Additional digital band pass filter narrows the signal bandwidth further to minimize unwanted noise while maintaining ECG frequency components (green colored signal in middle of Figure 5.6). Finally the signal in red depicts the CCECG signal after its derivation. An extended version (60 second) of this CCECG signal can be seen in the Figure 5.7.

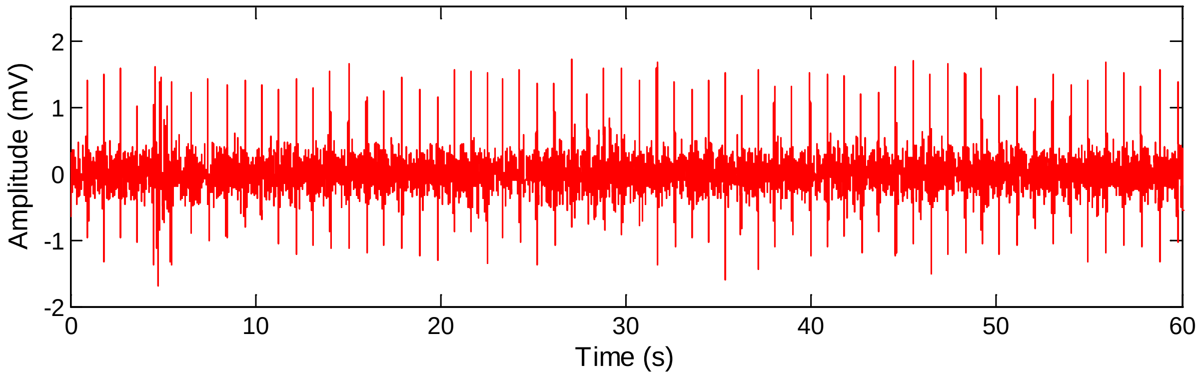

Figure 5.7 60 second long signal with the textile CCECG system.

5.1.2 Textile Capacitive ECG system in Car

Electrodes of for this system are also made up of three layers of conductive textile for electrode (sensor area), guard and ground respectively [17]. The conductive layers are isolated against each other with insulating PU films. The textile used in the electrodes is washable and breathable E-Blocker (Novonic®, W. Zimmermann GmbH & Co. KG) [18]. The three conductive layers of the assembly are attached to the preamplifier module by their respective connection through three conductive snap fasteners. Detail of the textile CCECG system is elaborated in a collaborative literature work [19].

5.1.2.1 System Integration & Experimental Setup

Integration of the textile electrode is done in way to use the system in laboratory and in real car as well. A seat cover of the Mercedes Benz C-class (W204 series) is tailored with two rectangular incisions to adhere the electrode into it (refer Figure 5.8 (left)). The edges of incisions and the textile electrode are equipped with Velcro to be able to have removable configuration by fastening and unfastening the electrodes from the seat cover. Hence it maintains a stable, robust and yet flexible configuration. Signals from the electrodes are taken through the visible blue ribbon cables to commercial 9 pin D-sub connectors (Figure 5.8 (left)).

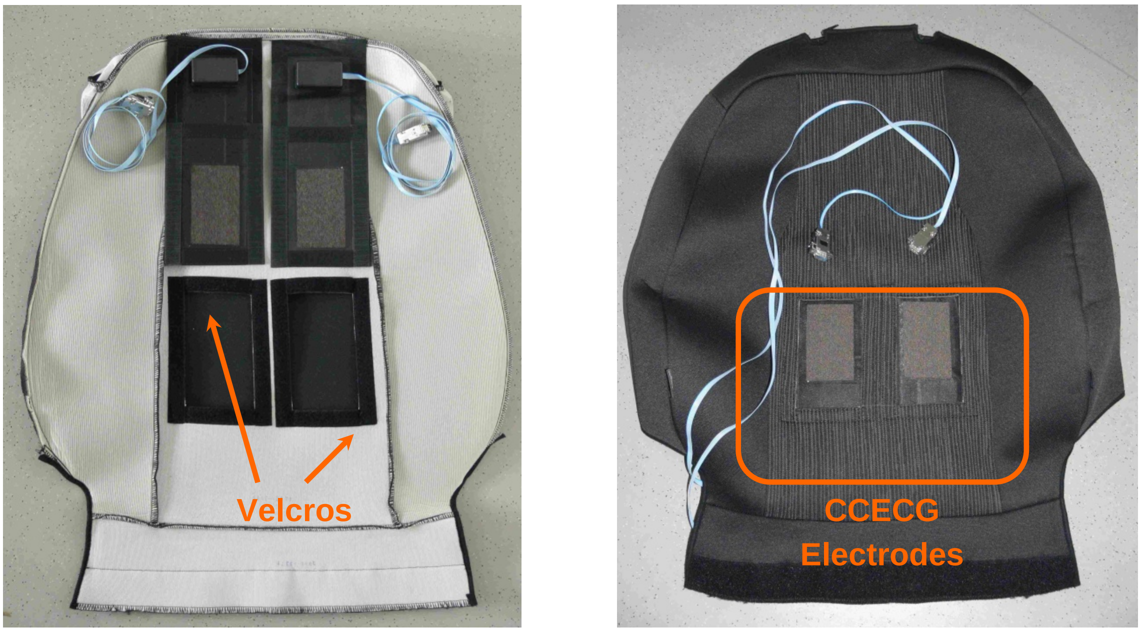

Figure 5.8 The electrodes and incised seat cover with Velcro (left), the electrodes when fastened into the seat cover (right).

The seat cover is applied to a C class car seat both in lab and in a real car as well; Figure 5.9 shows the arrangement inside a Mercedes Benz C class (W204 series). The driven seat textile electrode is spread beneath the cushion cover of the car seat to reduce common mode noise.

Figure 5.9 the seat cover applied on the car seat

Each of the electrodes is connected with only a preamplifier. The outputs of these preamplifiers are fed to an externally designed signal processing box, what does amplification and other signal processing of the signal [17]. Both inputs to the box are filtered with high pass filter (0.8 Hz) to remove baseline drift and DC offset. The differential of the signal is further filtered with a band pass and 50Hz notch filter before any amplification [19]. The pre-processed analog signal is digitized with a data acquisition card (NI USB-9162 and NI-9215) for further processing and final display in LabVIEW.

5.1.2.2 Measurement results

The CCECG measurement system has successfully gathered data for various real life driving situations. Measurements in conditions like driving on highways, surface street driving, enabling car functions while driving, by putting on different clothes on the subject etc. have been performed. Non-contact ECG recordings under different road conditions are displayed in the Figure 5.10.

During all the measurements, the driving subject wore a t-shirt (100% cotton) with 0.68 mm thickness and a pant (wool and polyester) with 0.29 mm thickness. The subject was 56 years old with height and weight, 182 cm and 92 kg respectively

5.1.2.2.1 Impact of the road condition

Considering real life driving situations, it is very crucial to perform measurements while driving on various roads. Different road surfaces like highway, city street (in good condition), uneven city street are taken into account while conducting the Electrocardiography.

For the measurement, the subject is driving at a speed of 100-120 km/h in normal condition on highway and in the city street at 40-60 km/h. Results from the measurement can be seen in the Figure 5.10. In the figure, CCECG results while driving on highway, city street (good condition) and uneven street in city are shown in top, middle and bottom of the figure respectively.

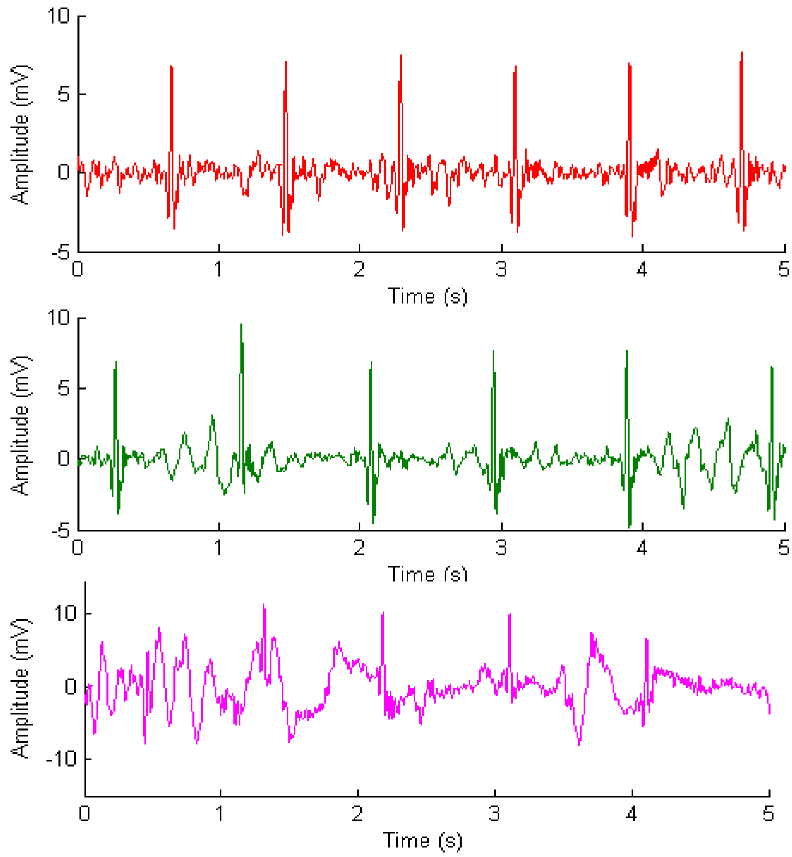

Figure 5.10 The CCECG result on highway (top), city street in good condition (middle), uneven street in city (bottom).

5.1.2.2.2 Influence of various car functions

Any electronics system to integrate into a car has to be passed through Electromagnetic Compatibility (EMC) test. EMC requires to that systems/equipment be able to tolerate a specific degree of Electromagnetic interference (EMI) and not generate more than a specified amount of the interference [20]. Daimler Ag uses its own standard (MBN-10284) for the EMC test [21]. This engineering standard defines the EMC performance requirements for electrical and electronic components and systems in vehicle. It describes the test methods and specifies the test levels and limits. In this measurement, Interferences from the car functionalities on the CCECG system are examined to step towards the EMC test.

In this study, an immunity test has been performed with several car functions. The test examines immunity of the system (CCECG) against radiated disturbances from electronics, electronics components and systems in vehicle. This test is near to a standard test called “E-06 Superimposed alternative voltage” from general requirement of electric, electronic components in passenger car [22]. Within the test, influence of various car functions like seat heating, seat movement, seat ventilation, GPS, hand free telephony etc. on the CCECG system have been evaluated.

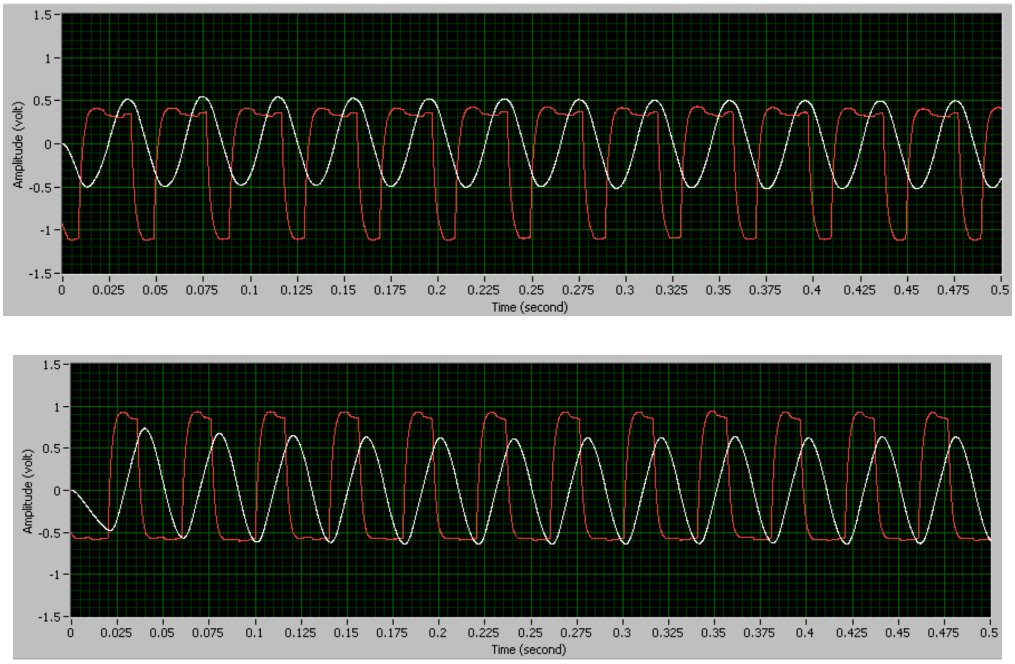

Figure 5.11 EMI from the seat heating level 1 (top) and 2 (bottom)

To observe the Electromagnetic Interferences, it is crucial to analyze the measurement with the PCB CCECG system, which has bandwidth of 0.3 Hz to 75 Hz. The CCECG sensors were placed on the seat without doing any ECG measurement (no person around the seat). By enabling the functions, we activate the device to observe its influence on the system. This way, we try to get only signal from the system one by one and avoid any mixing of the interference signal. In each result, signal with red color depicts original signal and signal with white represents filtered signal, which is filtered with standard filter used throughout the measurements.

Figure 5.11 shows the interference from the seat heating level 1 and 2. In this case, the signal can be seen even after the filtering (white color signal). The original signal is modulated pulse as seen in the figure and has frequency of 24 Hz. Seat heating level 1 and 2, both have similar impact on the measurement result and are inside the ECG bandwidth.

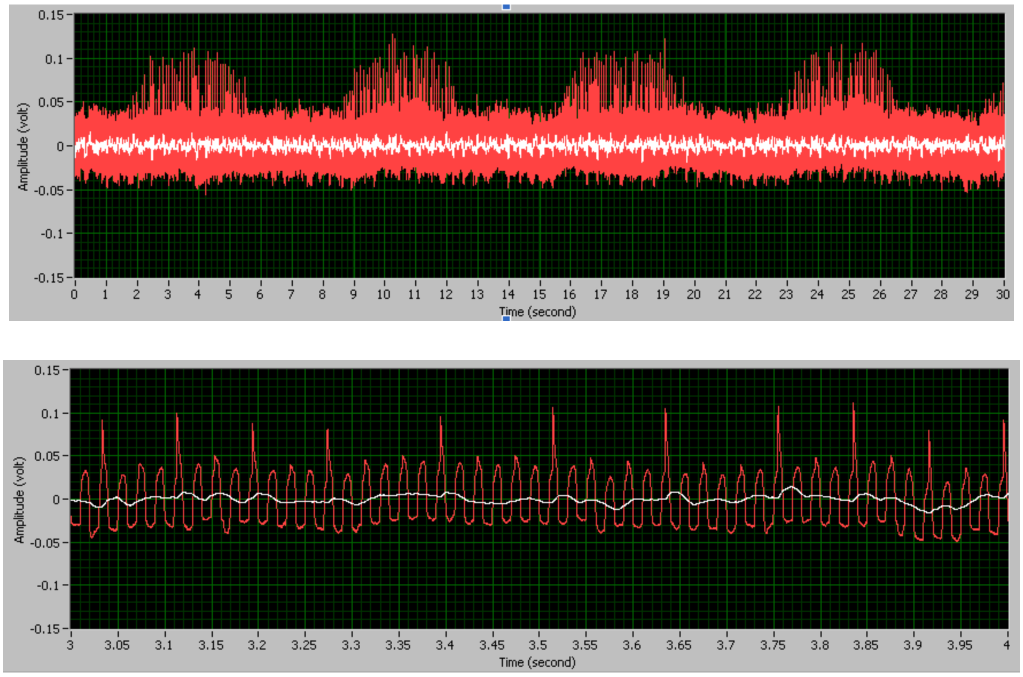

Figure 5.12 The seat heating level 3 (top) and zoomed version (bottom)

Severe interference effect on the system from the seat heating level 3 can be seen in the Figure 5.12 (top). Zoomed version of the signal is presented at the bottom of the Figure 5.12. Here too, the disturbance signal is pulse modulated and has signal frequency of 50 Hz. Hence this signal is filtered using the digital filtering (LabVIEW) and has no influence on the measurement results, what can be observed as white signals in the both figures.

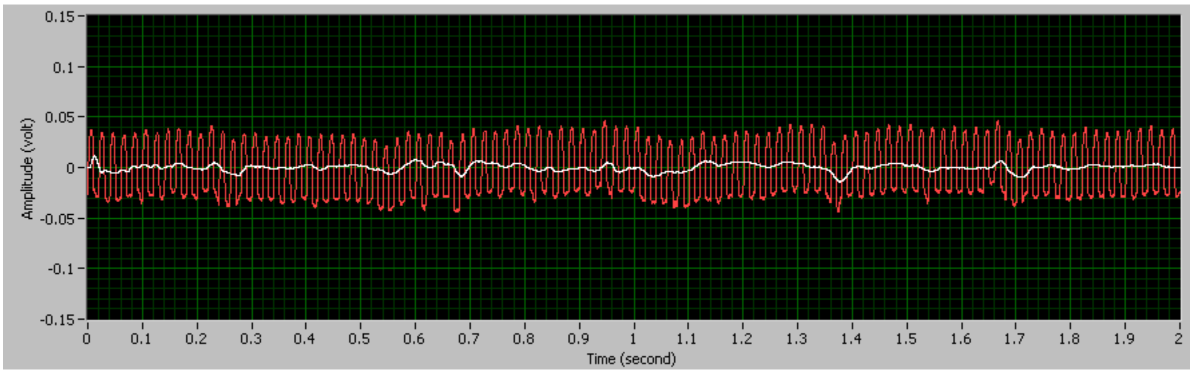

Figure 5.13 The seat cushion up and down movements.

Interference from the other functions didn't show any significant disturbance on the measurement results. For example, effects of up and down movement of the seat cushion are shown in the Figure 5.13. The movement function is driven by a DC motor, which in turn uses 50 Hz pulse to operate. This original pulse signal can be seen in the figure in red color, but it is filtered out (white signal) with the LabVIEW digital filters as it is 50 Hz signal (one of the main frequency interference e.g. power line noises).

Source	**Interference**	**Influence**
Heater level 1 & 2	PWM Signal with 1.5 V, 24 Hz	Significant
Heater level 3	PWM Signal with 0.15 V and 50 Hz	Filterable
Ventilator level 1,2 & 3	Pulse 0.075 V, 50 Hz	Filterable
Seat backrest forth and back	Pulse 0.075 V, 50 Hz	Filterable
Seat / cushion up & down	Pulse 0.075 V, 50 Hz	Filterable
GPS	None	
Hand free telephony	None	

Table 5.1 Interference and influence of the car finctions

Influence of the interferences while measuring CCECG signal is presented in the Figure 5.14 with the CCECG signal. The figure shows the low influence of telephone usage (top), automatic seat adjustment by DC motors (middle), and electrical seat heating (bottom). It is observed that only seat heating level 1 and 2 have significant influence on the capacitive ECG signal. All the other function either didn't have any impact on the CCECG signal or the interference from the respective function is filtered in the signal processing. Table 5.1 shows interference of various sources and its influence on the CCECG measurement results.

Functions of various seat movements, all level of the seat ventilations are performed by DC motors. It was observed that all of the DC motors are driven by 50 Hz pulses as example shown in the Figure 5.13. Hence all these functions have similar interference and impact on the measurement, which is filterable. While the seat heating level 1 & 2 are in the bandwidth of the ECG signal.

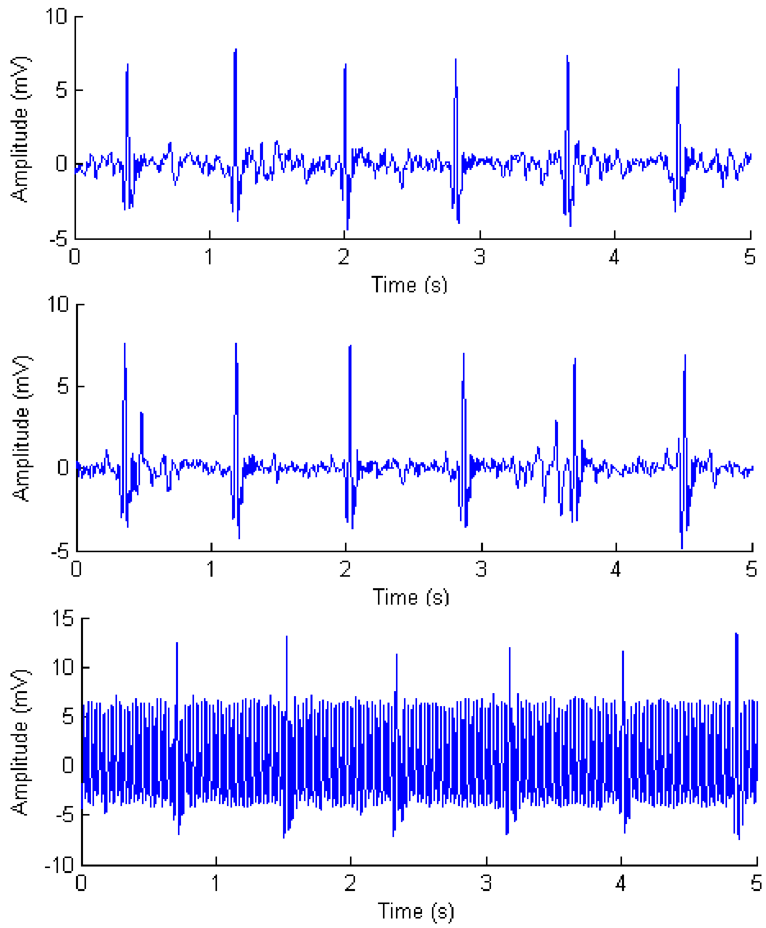

Figure 5.14 CCECG results from different driving activities: hands-free telephoning (top), adjusting the driver's seat (middle), with seat heating level 1 & 2 enabled (bottom).

5.1.2.2.3 Effect of Various dielectric (clothes)

In normal daily life, people prefer to wear different types of clothes because of various needs and reasons. Being a capacitive measurement, different kind of clothing changes dielectric of the capacitive coupling. This variation in the coupling can affect the result in various ways e.g. change in frequency response of the CCECG system [4]. Hence measurement with various climatic clothes like rain jacket, winter jacket and sport coat are carried out on the same subject to find out their influence on the signal.

Figure 5.15 shows a clear and strong effect of the drivers clothing on the signal quality, since this will strongly influence the capacitive coupling and thus the monitoring result. The clothes consisted of a winter jacket made up of 85% polyester and 15% polyamide with 0.35 mm thickness, a rain jacket made up of 100% nylon lined with 0.44 mm PU and a sport coat made up of 55% linen and 45% viscose with 0.85 mm thickness. It is noted here that it was possible to get the ECG signal through all the clothing.

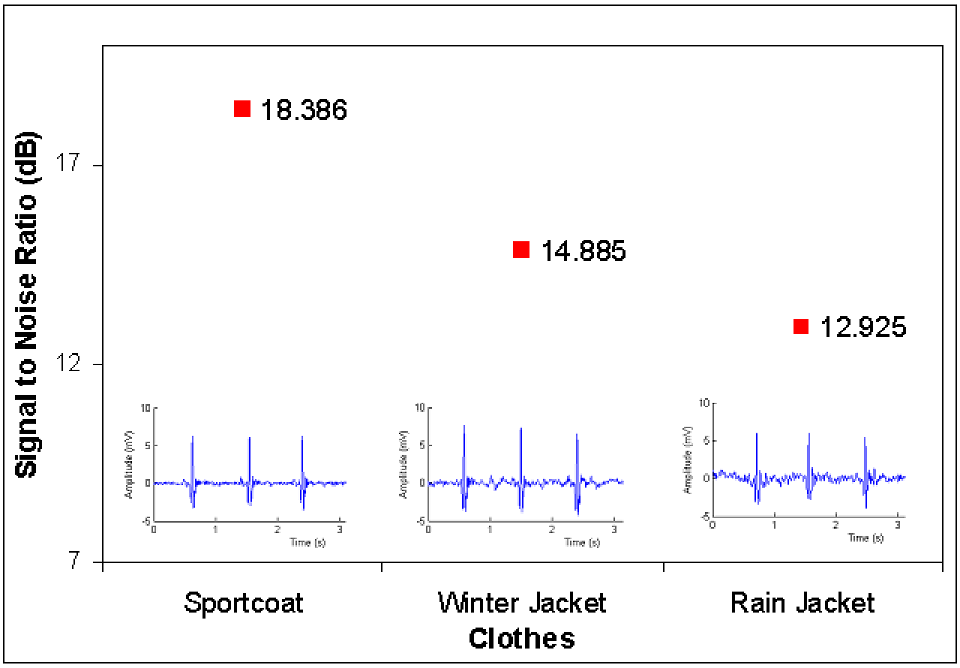

Figure 5.15 Signal to noise ration of the CCECG signal with various clothes and respective CCECG Signals.

5.2 Hospital Environment

Similarly to the CCECG integration in to automotive environment, an incorporation of the CCECG system into hospital can make life of patient with continuous monitoring easy. A possibility to measure ECG without any galvanic contact can provide more mobility and freedom to the patients as there is no wire attachment with the ECG electrode needed. The capacitive coupled Electrocardiography as first recorded by Richardson [24] is electrically insulated and can remain stable for long-term monitoring.

5.2.1 Clinical Bed

An unintrusive Electrocardiography integrated into a bed in ordinary bedroom environment with conductive textile was conducted by Ishijima in 1993 [25]. He selected some of exposed part of a normal sleeping subject to have galvanic contact with the ECG electrodes. Two kinds of textile electrodes were implemented, one type was composed of carbon fibers and another was metal platted fibers. The textile electrodes were placed on the pillow (head, negative pole) and the lower part of the bed sheet (legs, positive pole) where the feet are positioned.

In 2007, Y.G. Lim et al presented a study on non-contact ECG measurement on a bed during sleep [26]. They implemented an array of 8 copper clad capacitive PCB electrodes (4X4 cm^2) with embedded electronics and a large conductive textile electrode that was used as ground plane. To measure heart rate, R-peak was detected from one of the 8 channels, sorting by its sufficient quality.

In the same year, Ueno et al demonstrated influence of various factor like cloth thickness, electrode area and coupling pressure on the result of the Capacitive ECG [27]. During the measurement in the bed, all the factors had minor to major influence on the ECG signal, in that electrode area had greater impact than cloth thickness and the pressure. It was also showed here that input capacitance of the preamplifier plays dominant role in the signal coupling and should be reduced as much as possible to achieve better signal quality.

Next year, Wu & Zhang designed capacitive electrodes with stretch conductive fabrics that was integrated beneath a bed sheet [28]. The long electrodes (belt type) were placed under the shoulder and the lumber region of an adult, while reference electrode was placed under hip and thighs. A conducting tail in each of the electrode was tailored beneath the bed sheet to convey the ECG signal to the pre-amp module. The measurement took place inside a RF-shielded room with constant temperature of 22^o C. Cotton was used as main dielectric material for subject clothing and bed sheet as well.

An interim study of capacitive ECG measurement in a clinical practice was conducted by Eilebrecht et al at Aachen university clinic in 2009 [29]. They integrated stiff capacitive electrodes into a pillow to use it in a clinical bed or a chair with active driven reference electrode, analogous to “Driven right leg circuit”. In the following we propose a textile electrode based, non-contact ECG monitoring system integrated in hospital items like a stretcher and a standard hospital bed.

5.2.1.1 1st Generation Textile CCECG system

First version of the sys textile capacitive electrocardiography was designed and implemented as described in section 4.2. This design was in resemblance to the stiff CCECG system; hence two layer capacitive electrodes were realized with preamplifier and differential amplifier electronic circuit fastened to the back of the electrode.

5.2.1.1.1 Experimental setup

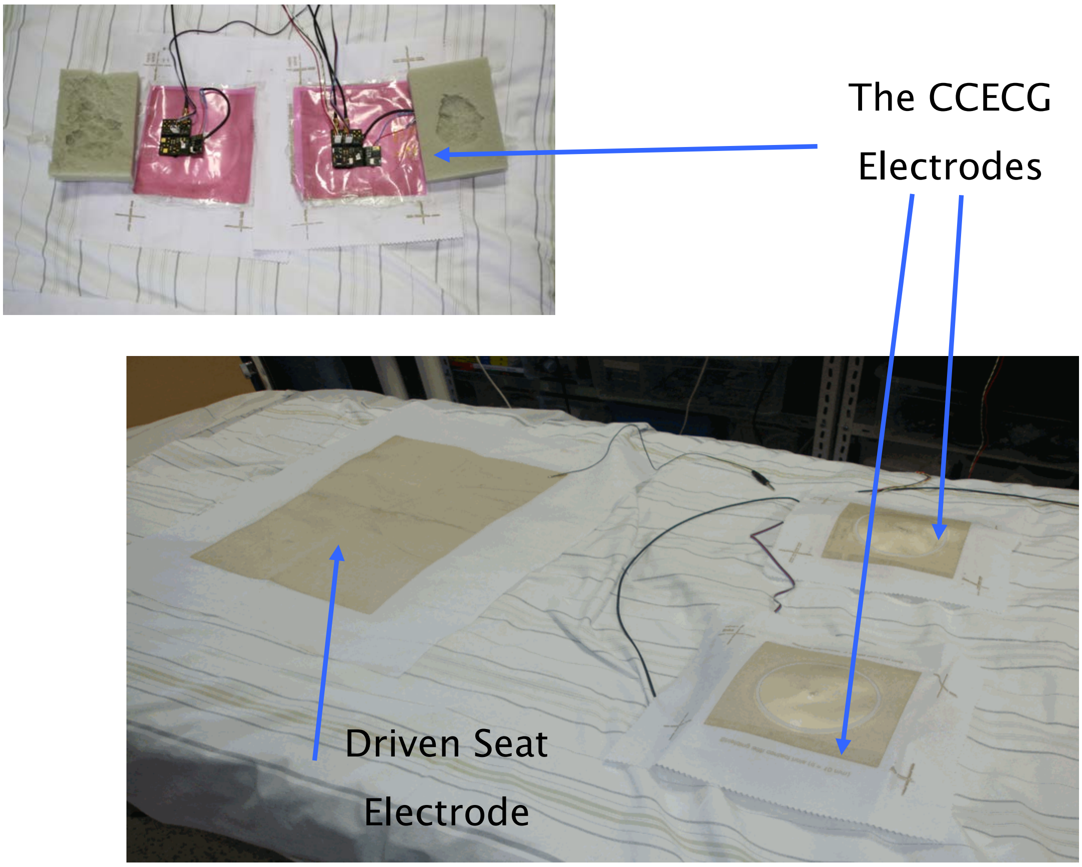

Figure 5.16 Configuration of the 1st generation CCECG measurement in a clinical bed.

After realizing the 1st version of the Capacitive ECG electrodes, a laboratory test with a clinical bed from University clinic hospital was conducted. The placement of the electrodes on the clinical bed can be seen in bottom of the Figure 5.16.

The CCECG electrodes were arranged in a way that posterior of the subject's heart lie down on them and Driven seat electrode was positioned to make contact with the subject's buttocks. The electronics of the textile electrodes were supported with a sponge, placed beneath the electrodes as shown in top of the Figure 5.16.

Exact position of the subject while taking measurements is presented in Figure 5.17. As exhibited in the picture, continuously monitoring of the CCECG signal is configured in the laptop with help of the LabVIEW program. Differential signal of the Signals from each electrode is fed to a digital acquisition card (NI USB 9162) to convert the analog signal into digital for LabVIEW utilization.

Figure 5.17 The measurement setup while subject lying down on it.

To minimize various noises in the CCECG signal, digital signal processing is carried out in the LabVIEW program. The differential CCECG signal after anti-aliasing filter in the module is filtered with a 2nd order Butterworth notch filter (45-55 Hz), 2nd order Butterworth band-pass filter (5-20), wavelet detrend and wavelet denoise in a chronological sequence as depicted in Figure 5.18. An algorithm to detect the ECG peaks was also implemented in the program after the filtering.

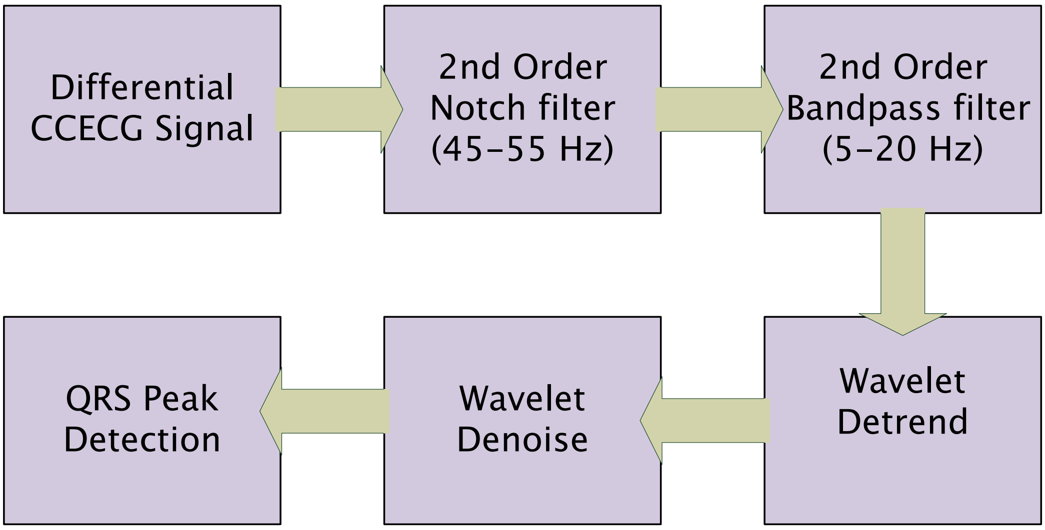

Figure 5.18 Sequence of the signal processing stages of the CCECG system

5.2.1.1.2 Results

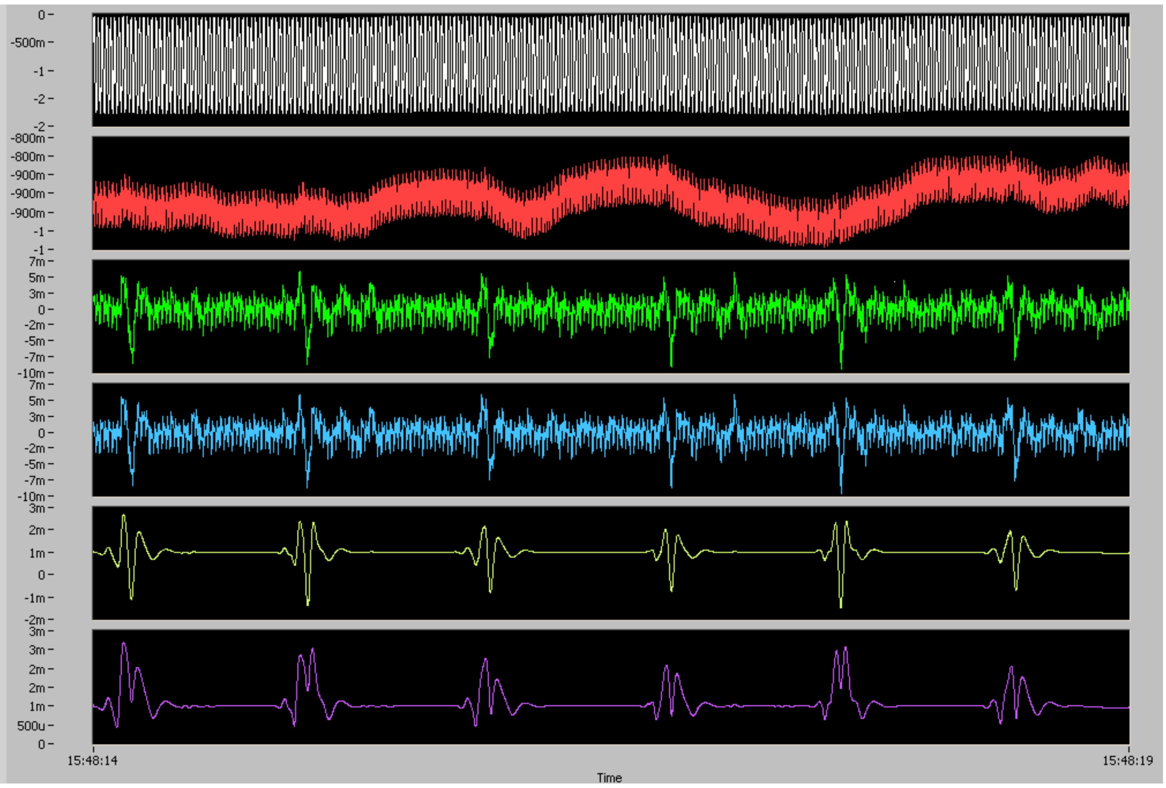

Figure 5.19 Various filtering stages of the CCECG signal.

With the above measurement setup, various subjects are examined for the capacitive ECG measurement. The subjects were asked to lie down in supine position as supposed while placing the electrodes. The capacitive ECG result from a 25 year old subject (weighed 73 kg and 187 cm tall) is shown in the Figure 5.19.

The subject wore a cotton sweater (1.75 mm thick), t-shirt (0.75 mm thick) and a jeans pant. Figure 5.19 shows the resultant signal after each step of the filtering described in Figure 5.18. The first graph of the figure shows differential CCECG signal (raw signal) from the CCCECG module, subsequently notch filtering, band-pass filtering, wavelet detrend, wavelet denoise and QRS peak detection.

Additionally he was asked to touch the driven seat electrode to compare both of the signals. Figure 5.20 demonstrators the capacitive ECG signals while subject's hands place on the driven seat electrode.

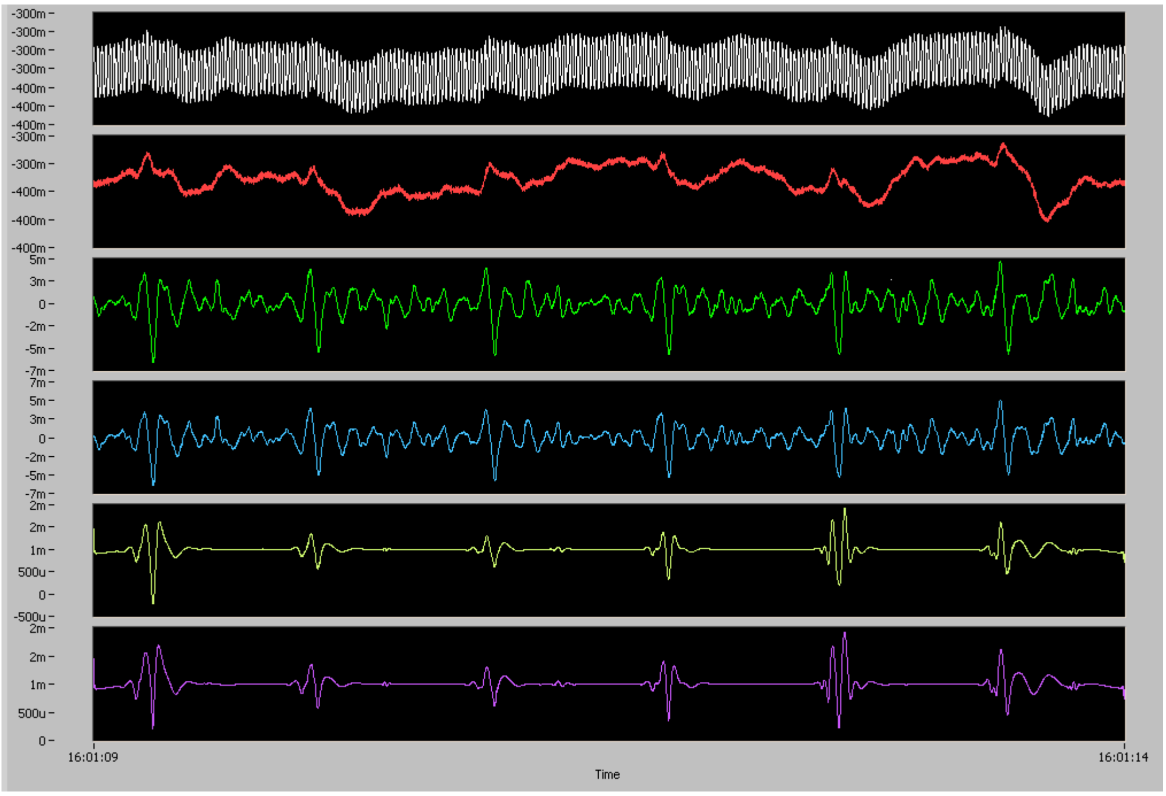

Figure 5.20 Various filtering stages of the CCECG signal while subject touching the DSC.

5.2.1.2 2nd Generation of the CCECG System

After the trial with the 2 layer CCECG electrodes, it was learnt that the signal quality was not up to the mark. So in the process to improve the existing design, three layer CCEGC electrodes were design and realized as described in section 4.3. An Experiment of these electrodes is carried out by incorporating them into a clinical bed. This experiment is elaborated here in the section in detail with its results.

5.2.1.2.1 Experimental Setup

After the patient is admitted to the hospital, he commonly spends major portion of his hospitalized time in a clinical bed. Figure 5.21 (L) shows the locations of two CCECG electrodes on the bed-sheet. The contact ECG electrodes are also placed on two sides of the bed-sheet such as they are easily accessible by the volunteers' hands as indicated in Figure 5.21 (R).

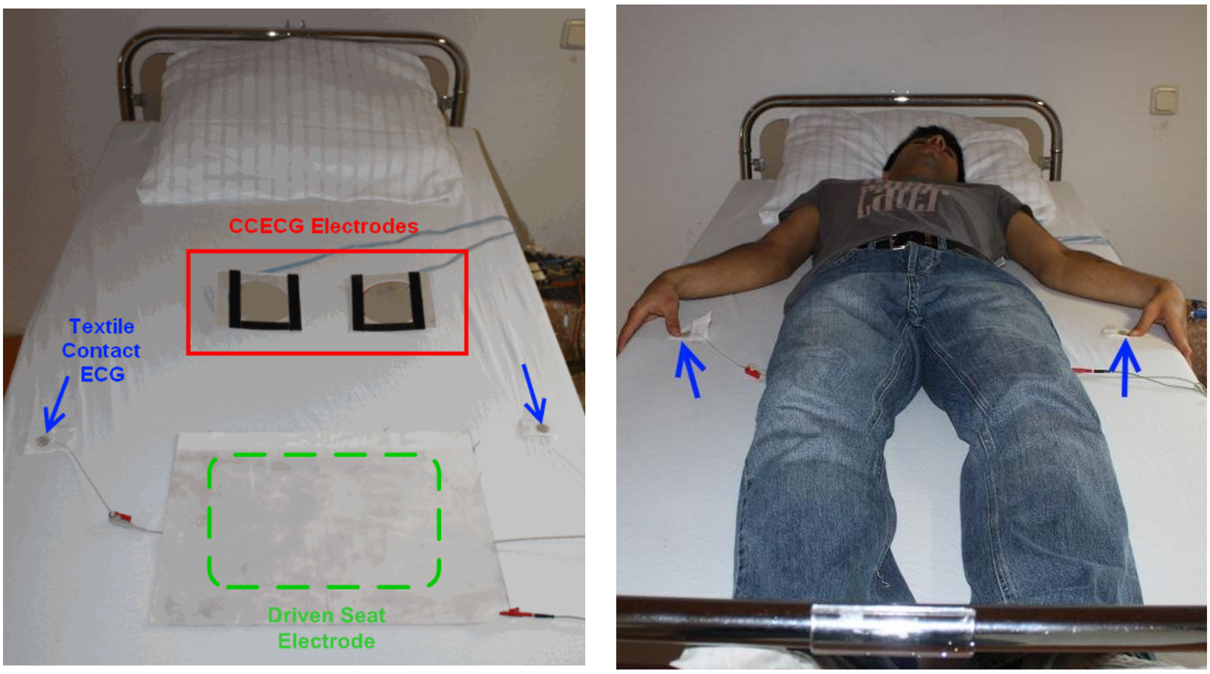

Figure 5.21 The measurement setup (L) electrode arrangement, (R) with subject

A capacitive ECG system is highly prone to noise due to its ultra-high and sometimes fluctuating input impedance. In this case, signal processing plays a very important role to remove noises.

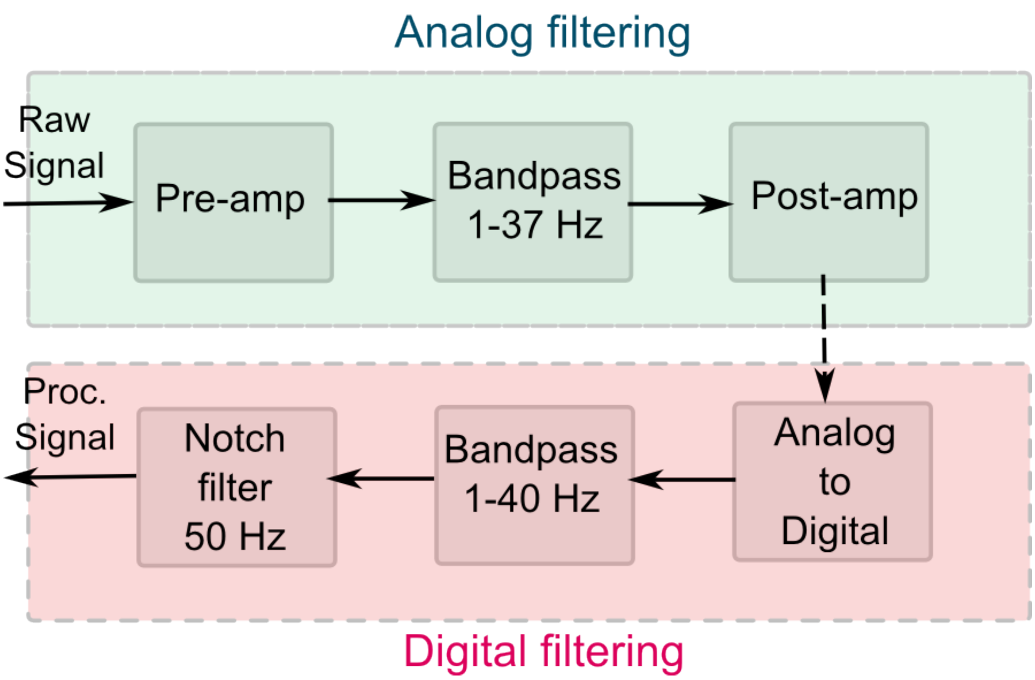

Figure 5.22 Block diagram of the signal processing.

Capacitively coupled signal from each of the CCECG electrodes is fed to a differential filter in the analog signal processing toolbox (90IPB, Frequency devices) [30]. The differential signal from the two CCECG electrodes is filtered with a window of 1- 37 Hz by an 8th order elliptical (1.56) band-pass filter. The signal was amplified before and after the filtering by gain of 10 and 20 respectively.

The filtered signal is acquired by a LabVIEW program for further processing after digitizing it with a DAQ card (NI USB-9162 with NI 9215) [31][32]. Here the signal is digitally filtered by a 4th order Butterworth band-pass filter with a bandwidth of 1-40 Hz and a 4th order Butterworth notch filter with 50 Hz. The resulting signal is displayed by the LabVIEW application.

5.2.1.2.2 Results

Here, volunteers lied down in supine position emulating a patient on clinical bed as presented in Figure 5.21 (R). Placement of the CCECG electrodes was little separated and right behind heart of the subject. The softness and sponginess of the clinical bed-mattresses is an advantage in maintaining an adequate contact pressure between the subject's back and the mattress surface. The exemplary subject (subject 1) was a 28 year old male, weighed 65 kg and was 172 cm tall. The test subject wore a t-shirt (cotton, 0.4mm thick) with a sweater (cotton, 1.23 mm thick) on top and corduroy trousers (cotton, 1.6 mm).

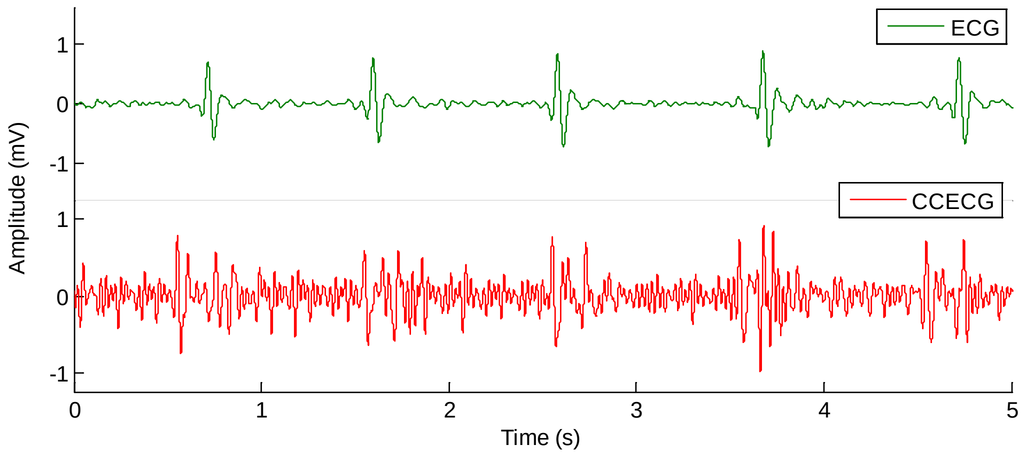

Figure 5.23 ECG Measurement for Subject 1 for 5s

Even though the soft bed-mattress is supposed to provide better contact between the textile electrodes and the body, the CCECG signal showed a higher noise level than ECG signal from subject 2 (Figure 5.25). We hypothesized that the elastic mattress distorts the textile electrodes in an unforeseen way and hence makes the system more prone to environmental noise.

An ECG signal from this setup shows interferences as depicted in the Figure 5.23. The signal displays a noisy baseline and hence a worse signal to noise ratio. Baseline noises as well as some other artifacts including movement artifacts are visible in a minute long signal (Figure 5.24). This clearly needs to be addressed by appropriate signal processing.

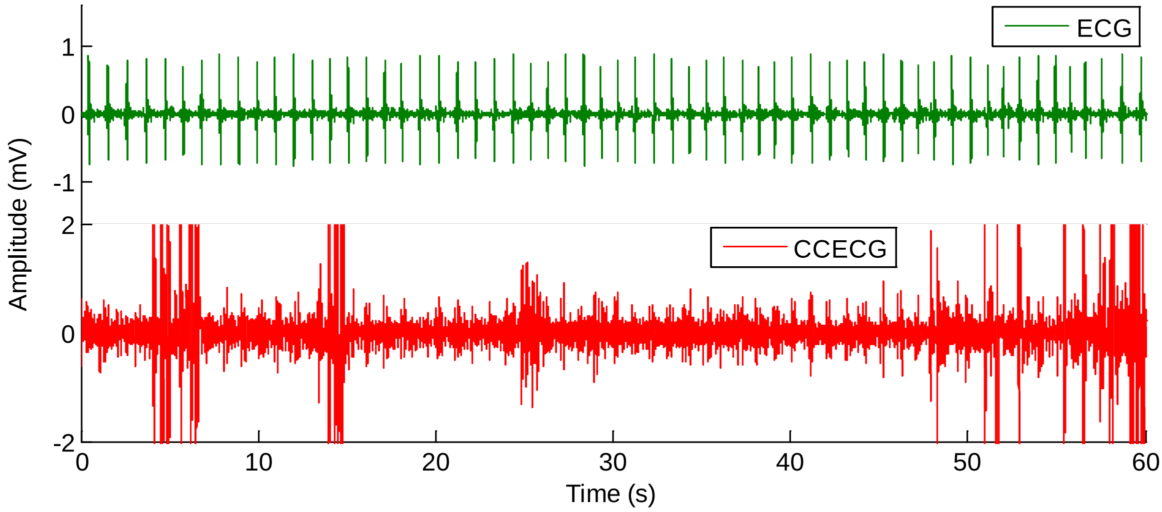

Figure 5.24 ECG Measurement for Subject 1 for 60s

Additional experiments were conducted with another subject in the same experimental position as subject 1. The subject was a 28 year old male, weighed 68 kg and was 178 cm tall. The subject wore a t-shirt (cotton, 0.35mm thick) and jeans trousers (cotton, 0.87 mm).

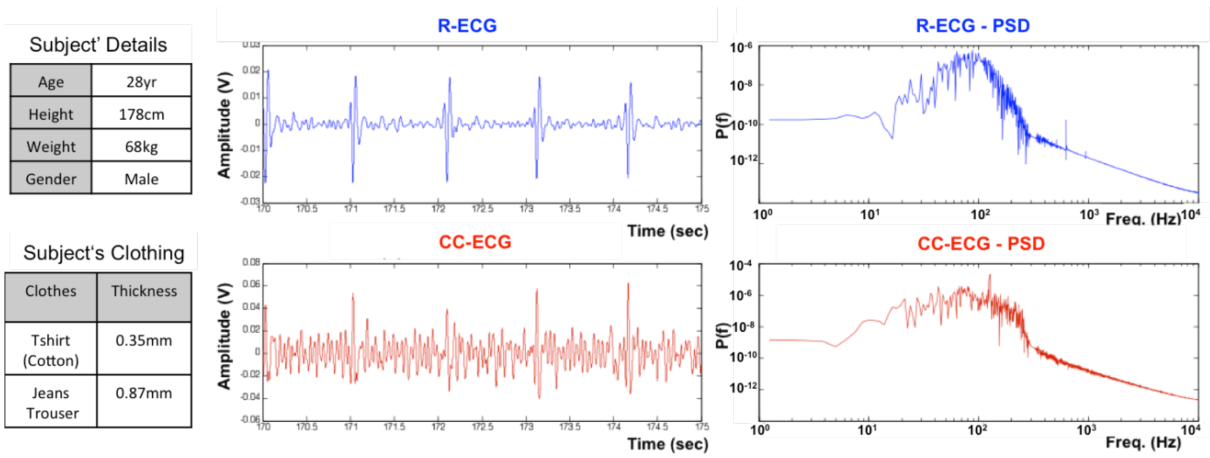

Figure 5.25 ECG Measurement for Subject 2 for 5s

A CCECG and an ECG signal from subject 2 are shown in Figure 5.25 with power spectral density (PSD) of both signals in frequency bands up to 100 Hz. QRS detection from 1 minute ECG and CCECG signals of the subject are shown in Figure 5.26. QRS complexes from the recording have been detected with time of occurrences leading to the heart-rate, RR-interval timings and heart-rate sequences.

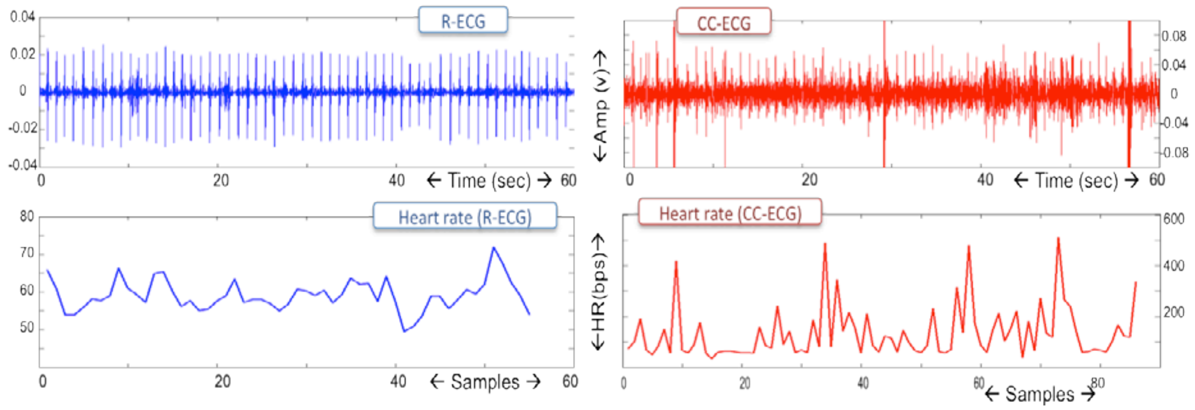

Figure 5.26 ECG Measurement for Subject 2 for 60s

Heart rate variability (HRV) analysis of the one minute signal is graphed in Figure 5.27. Various parameters of the analysis are described in the figure. The analysis is done through Fast Fourier Transform (FFT) in frequency domain as seen in the graph. Each parameter of the time domain analysis is explained in Table 5.1.

Time Domain Parameters

Variable (unit)	R-ECG	CC-ECG
Mean HR (bps)	59.10	88.72
SDNN (ms)	70	310.4
NN50 (count)	24	60
pNN50 (%)	44.4	85.7

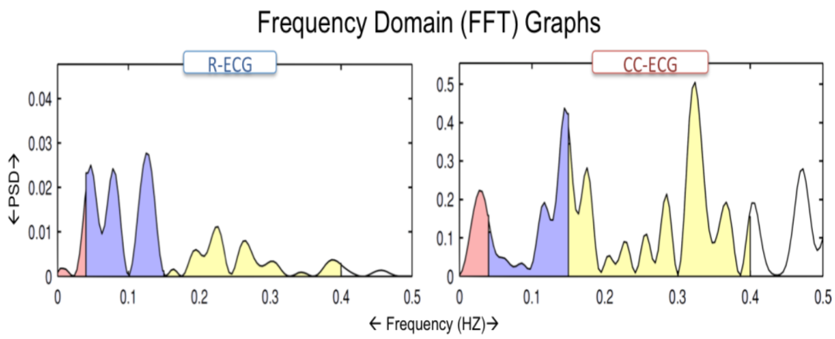

Figure 5.27 HRV analysis of the 1-min ECG measurement during the clinical bed experiment.

Parameter	Description
Mean HR (bps)	Mean Heart rate in beats per minute
SDNN (ms)	Standard deviation of NN intervals (beat to beat)
NN50 (count)	The number of pairs of successive NNs (interval) that differ by more than 50 msec
pNN50%	NN50 count divided by the total number of all NN intervals

Figure 5.28 Time domain parameters of the HRV analysis [33][34].

5.2.2 Stretcher

A stretcher is often a patient's first-point of contact with the clinical environment. This provides a good platform to capture contactless ECG in ambulatory conditions as the patient's back surface is in good contact with the stretcher.

5.2.2.1 Experimental Setup

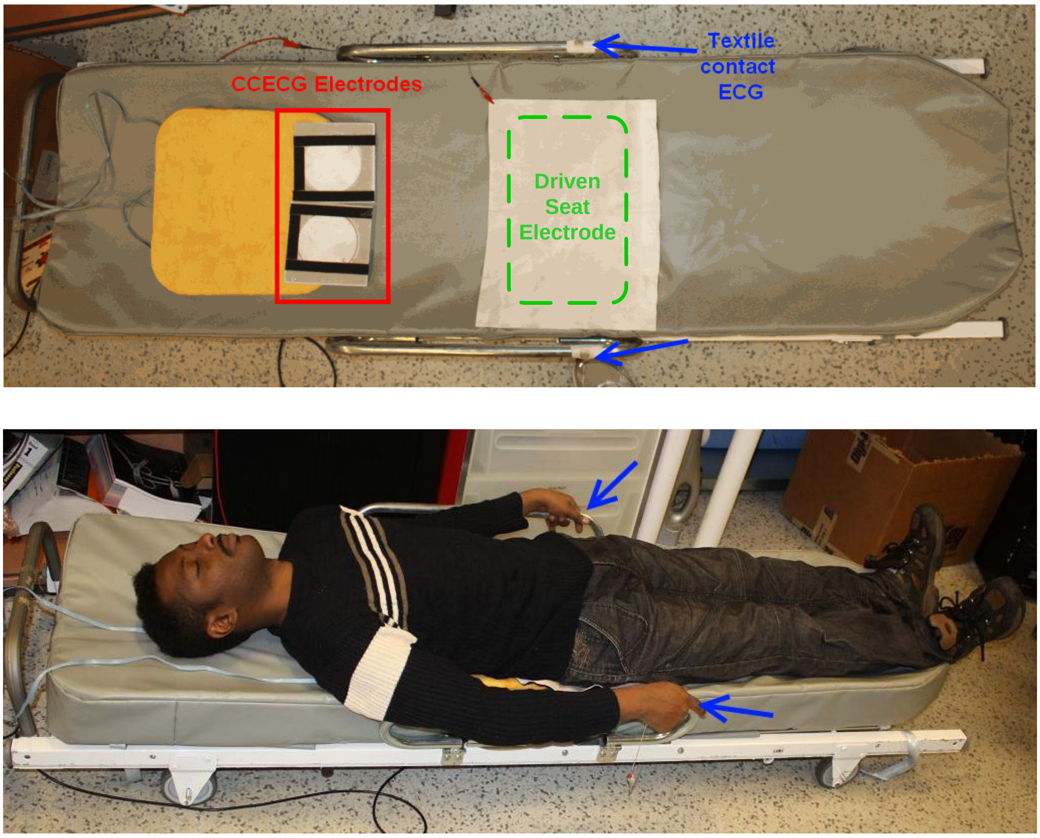

Figure 5.29 The measurement setup on a stretcher (Top) arrangement of the electrodes (Bottom) with subject on it.

As shown in Figure 5.29 (Top), CCECG electrodes are simply placed in the thoracic section of the stretcher and are facing towards the back of the patient. No gelled electrodes have to be fixed on the patient. A square driven electrode is placed at the lumbar section of the stretcher. For validation purposes, contact ECG electrodes made of conductive textile are attached on the stretcher's hand rest and are easily reachable by a volunteer's hands as can be seen in the figure.

Placement of the subject on the stretcher is shown in the Figure 5.29 (B), where he is asked to hold the textile contact ECG electrodes for comparison purpose. The signals from the CCECG modules are processed in similar fashion as described in Figure 5.22 of the section 6.1.2.1.

5.2.2.2 Results

Volunteers were asked to take the conventional supine position on the stretcher, as illustrated earlier in Figure 5.29 (B). In this position electrodes were located posterior of the subject's heart. A 25 year old subject (subject 1), weighing 70 kg and 175 cm tall was tested for the experiment in the position described above. He had put on a cotton t-shirt (0.43 mm thick) on top and a cotton trouser (0.55 mm thick).

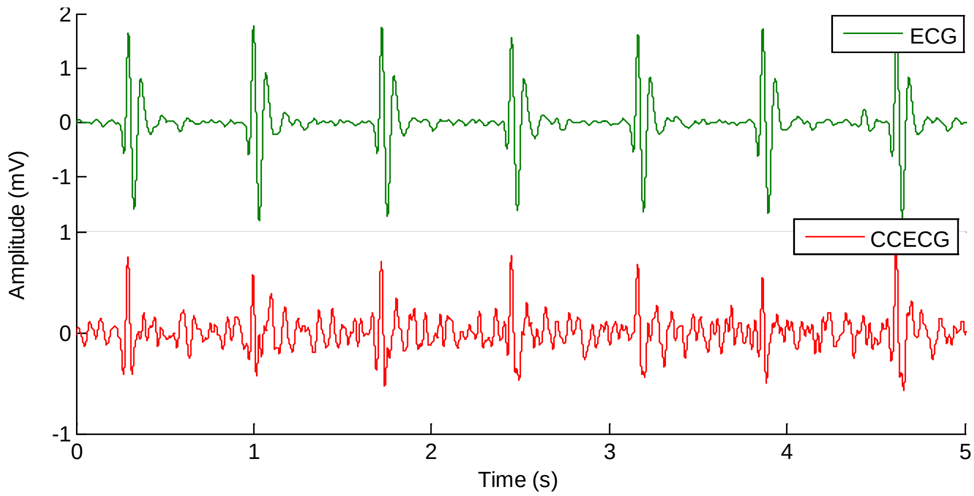

Figure 5.30 ECG Measurement on Stretcher for subject 1 for 5s

Figure 5.32 depicts exemplary capacitive ECG recordings together with the contact ECG. Resemblance of the capacitive ECG is evident when compared to the contact ECG. A minute long signal is shown in Figure 5.33 for consideration of heart rate (HR) and heart rate variability (HRV) analysis. Movement artifacts appear in this signal as larger spikes than the ECG signal itself.

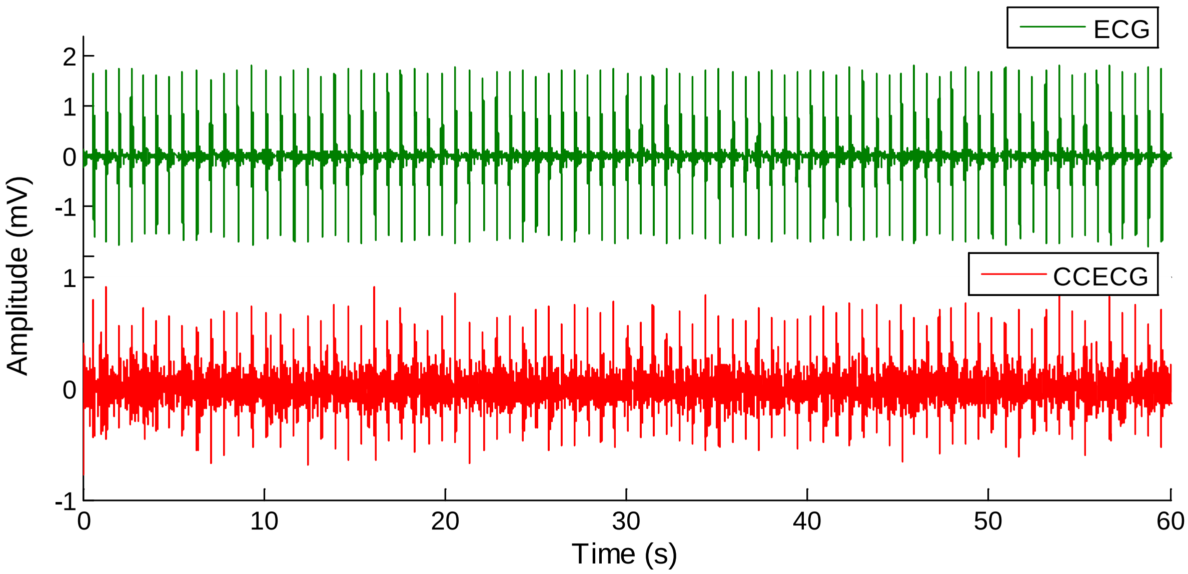

Figure 5.31 Measurement on Stretcher for subject 1 for a minute.

Additionally another subject (subject 2) wore a t-shirt (cotton, 0.4mm thick) with a sweater (cotton, 1.23 mm thick) on top and corduroy trousers (cotton, 1.6 mm). He was a 28 year old male, weighed 65 kg and was 172 cm tall.

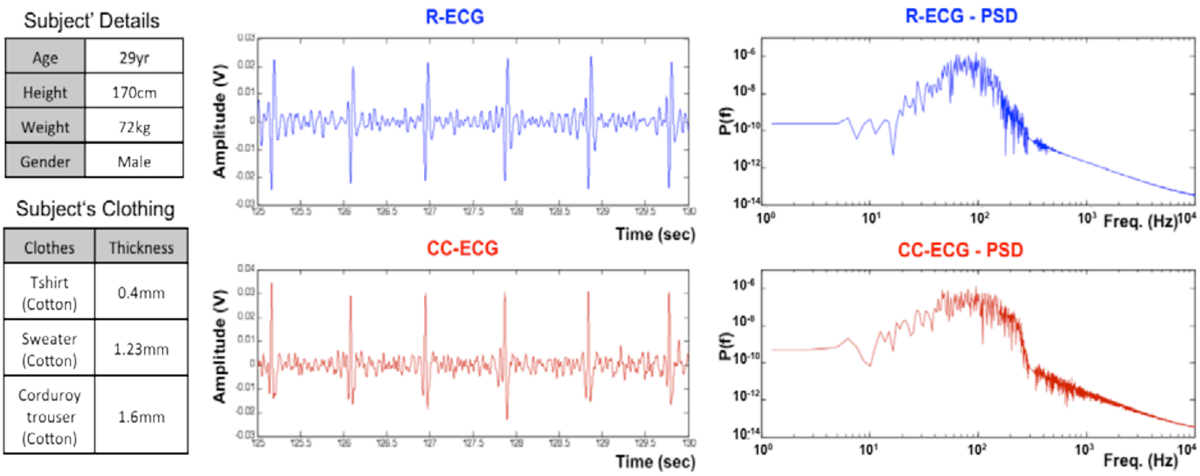

Figure 5.32 ECG Measurement on Stretcher for 5s

Contemporized capacitively coupled and conventional ECG measurements of this subject are presented here. A short capacitive ECG signal of 5 second is exhibited in the Figure 5.32 while comparing it with contact ECG.

Figure 5.33 visualizes results of the stretcher setup for a 1 min recording of both ECG and CCECG. The ECG plot displays no obvious artifacts, while the CCECG plot shows the presence of large spikes and unwanted small spikes between regular RR intervals. Extremely high heart-rate values, as detected by the CCECG (e.g. at 8 sec and 23 sec in the bottom right part of Figure 5.33), illustrate the false positive QRS counts.

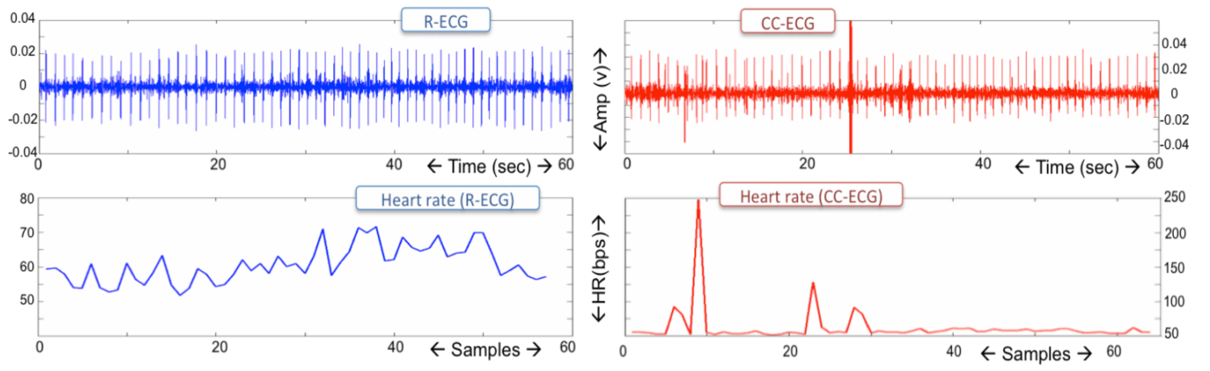

Figure 5.33 ECG Measurement on Stretcher for 60s.

A Fast Fourier Transform of the same signals for a HRV analysis is illustrated in Figure 5.34 with various parameters of the analysis. Mean HR value of the analysis shows slight deviation for CCECG signal compare to its ECG signal.

Time Domain Parameters

Variable (unit)	R-ECG	CC-ECG
Mean HR (bps)	60.61	64.81
SDNN (ms)	83.5	152.4
NN50 (count)	27	31
pNN50 (%)	48.2	53.4

Frequency Domain (FFT) Graphs

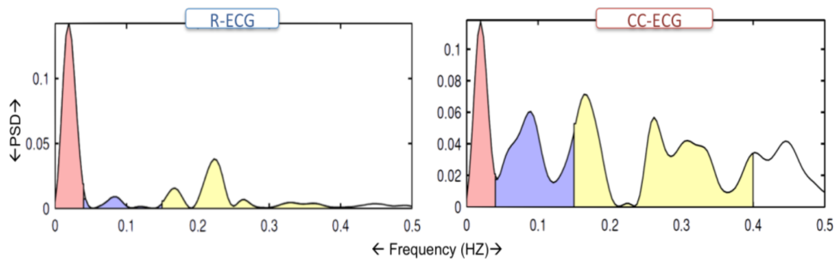

Figure 5.34 HRV analysis of the 1-min ECG measurement during the stretcher experiment.

5.3 Home environment

In 2005, Matthews et al from Quantum Applied Science and Research (QUASAR) presented their study on capacitive ECG measurement [35]. They used tiny capacitive sensors to measure biosignals and named it IBEs (Insulated BioElectrodes). The work was able to show ECG R-Peaks detection from a CCECG chair setup without describing much detail about the scenario.

ECG measurement on an office chair without conductive contact was presented by Lim et al in 2006 [4]. They employed capacitive Electrodes to measure ECG without any galvanic contact. It also included effect of different clothing material on the frequency response of the system. Addition to this work, same group also demonstrated in their work a way to reduce common mode signal with Driven Seat Circuit, similar to Driven Right Leg Circuit [5]. This circuit helps to improve signal to noise ration of the ECG signal and ultimately helps in improving resolution of the signal.

At university of Aachen, Aleksandrowicz and Leonhardt also developed a non-contact ECG measurement on an office chair in 2007 and named it “Aachen Smartchair” [23]. They measured Electrocardiogram of the occupant capacitively by capacitive electrodes. A wireless communication module was integrated to transmit the ECG signal to a PC or to an ICU patient monitor wirelessly.

A study to acquire heart rate and respiratory rate of a subject seating on a wheel chair and to transmit an event message to remote server under an emergency situation was performed by Han et al in 2008 [36]. Conventional Ag/AgCl electrodes and Cushion type sensors (EMFi sensor) were utilized to measure Electrocardiogram and Ballistocardiogram respectively.

5.3.1 Wheel Chair

5.3.1.1 Experiment Setup

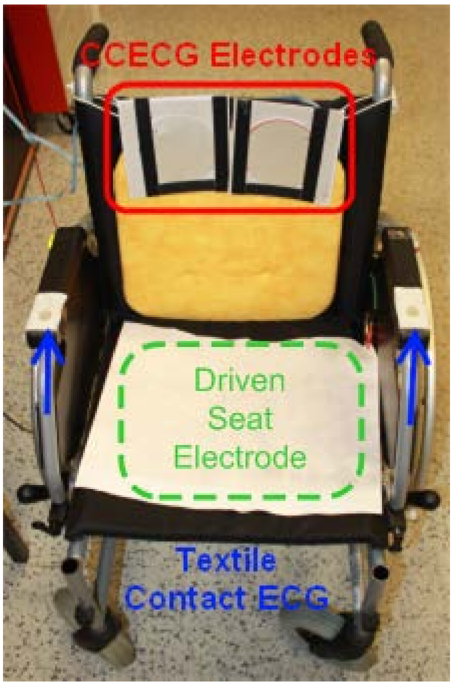

Figure 5.35 Arrangement of the electrodes in the experimental setup.

Many physically challenged people have mobility through electronic or manual wheel chairs. Even during several phases of their hospitalized recovery patients are allowed to mobilize themselves on wheelchairs. Wheelchairs also provide firm contacts between the patient's back and the wheelchair's back rest. On the other hand, a rigid contact of patient's bottom within the seat facilitates a good driven electrode. Our exemplary wheelchair was prepared for CCECG measurement by placing electrodes in the back-rest and the driven electrode on the seat as seen in the Figure 5.35. Comparison of the capacitive ECG is done by textile contact ECG electrodes, which are stuck onto both arm-rests (shown in figure by blue arrows).

The capacitive ECG signals from the CCECG electrodes are subtracted as a standard ECG procedure. The subtracted signal from the two CCECG electrodes is filtered with a window of 1- 37 Hz by an 8th order elliptical (1.56) band-pass filter in an analog signal processing toolbox (90IPB, Frequency devices) [16]. The signal was amplified before and after the filtering by gain of 10 and 20 respectively.

Subsequently the filtered signal is acquired by a LabVIEW program for further processing after digitizing it with a DAQ card (NI U-9162 with NI9215) [31][32]. Here the signal is digitally filtered by a 4th order Butterworth band-pass filter with a bandwidth of 1-40 Hz and a 4th order Butterworth notch filter with 50 Hz. The resulting signal is presented by the LabVIEW application on the Laptop as shown in the Figure 5.36. The whole signal processing sequences can be depicted in the Figure 5.22.

5.3.1.2 Results

Figure 5.36 Measurement setup on the wheelchair.

Actual measurement scenarios where the capacitive and the contact ECG are being measured from a subject with the setup can be seen in the Figure 5.36. Contact with the textile ECG electrodes is pointed out in the figure, where the subject is asked to hold the electrodes with proper contact to have a stable conventional Electrocardiography.

It can be observed that the final signals from the CCECG and the contact ECG are displayed on the laptop in LabVIEW platform. Various subjects are examined on the wheel chair to test performance of the system.

5.3.1.2.1 Subject 1

First subject was a 39 years old with weight of 85 kg and height of 178 cm. The subject was wearing a t-shirts with innerwear, both are 100% cotton and the thickness of both the apparels was 1.55 mm. On the bottom, he was wearing jeans trousers with thickness of 0.92 mm. The subject was asked to sit in the wheel chair comfortably and as relaxed as possible while holding the textile contacts for conventional ECG measurement.

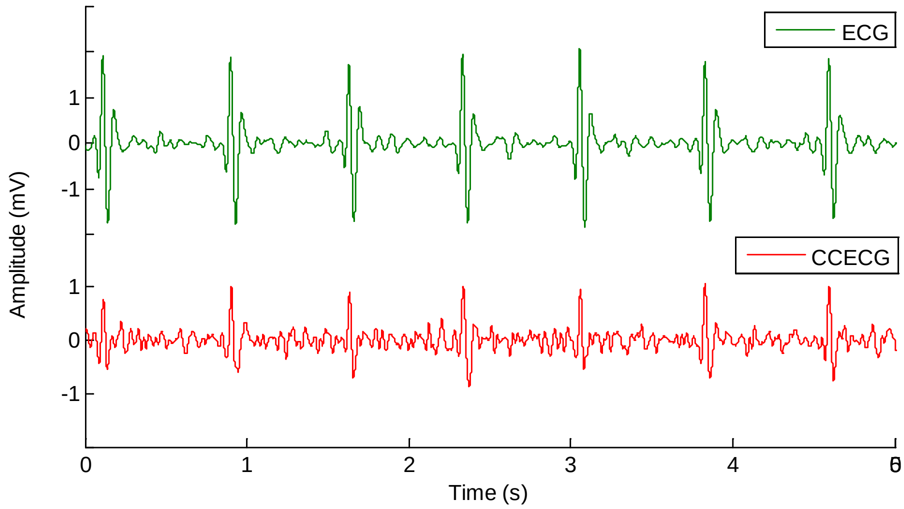

Figure 5.37 ECG measurement of the subject 1 on the wheel chair for 5 seconds.

A short and qualitative result of the subject from the measurement is graphed in the Figure 5.37. Top and bottom of the figure shows conventional ECG signal and capacitively coupled ECG signal respectively. Long term (1-minute) and quantitative measurement from the subject in this setup is presented in the Figure 5.38, which can be helpful for HR and HRV analysis. The results in these recordings exhibits better signal to noise ratio than clinical bed setup.

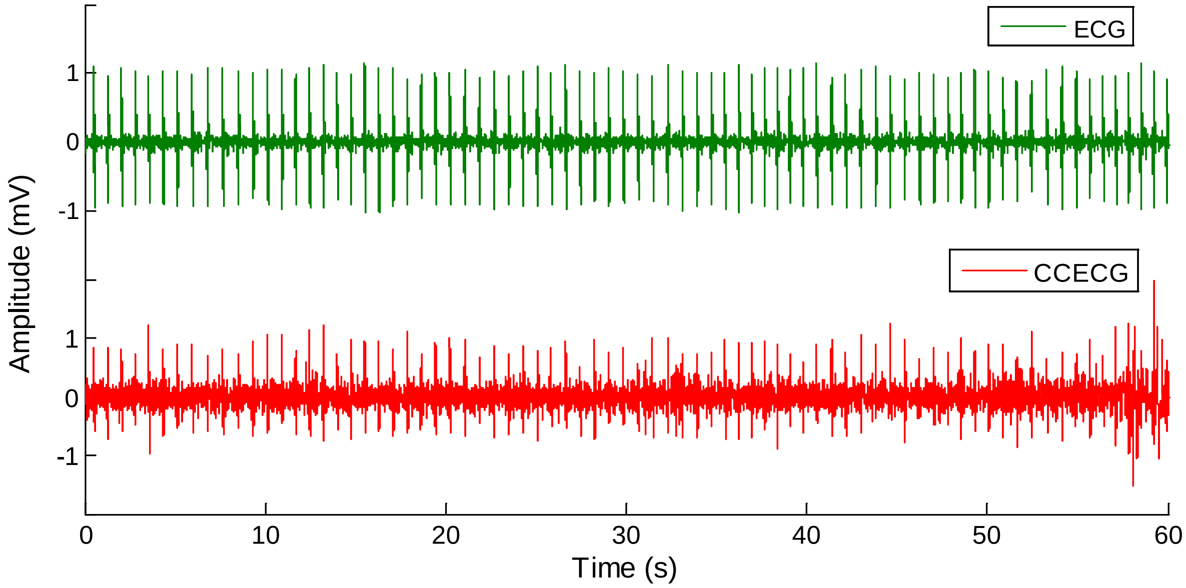

Figure 5.38 Measurement of the subject 1 on the wheel chair for a minute.

5.3.1.2.2 Subject 2

Another measurement was exercised on a 28 old year subject, who weighed 78 kg with 175 cm height. He was also requested to take the similar comfortable position as exhibited in the Figure 5.36. During the entire measurement, he wore a cotton t-shirt (0.61 mm thick) and a cotton pant with thickness of 0.86 mm.

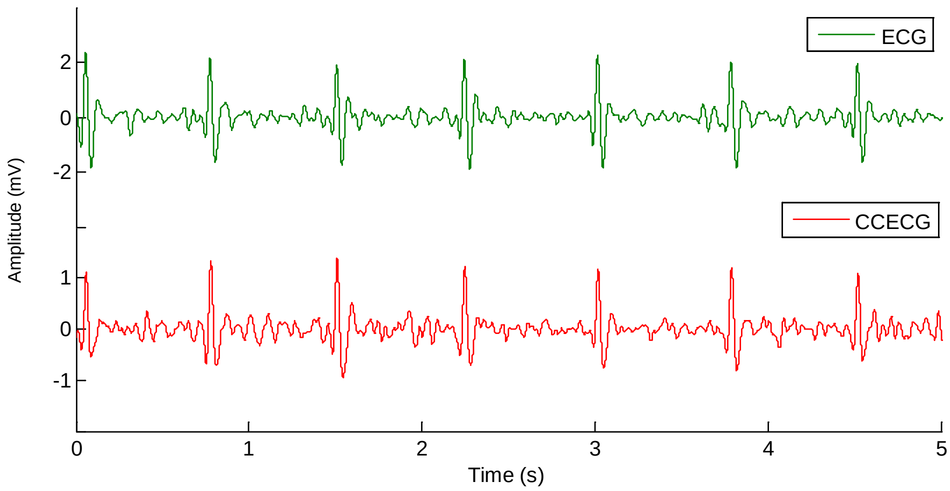

Figure 5.39 ECG measurement of the subject 2 on the wheel chair for 5 seconds.

A shorter version of the capacitive Electrocardiogram can be seen in the Figure 5.39, where the comparison and qualitative assessment of the signal can be observed. It indicates that the Heart Rate of the person is approximately 84 beats/min.

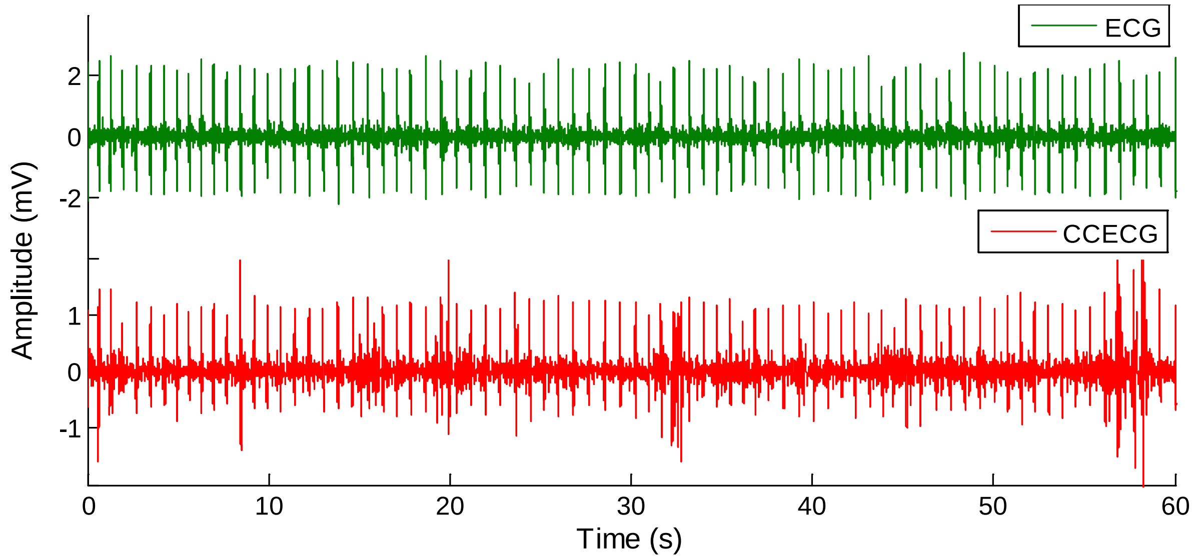

Figure 5.40 measurement of the subject 2 on the wheel chair for a minute.

Longer capacitive Electrocardiograms of the subject, with comparison of contact Electrocardiogram, are presented in the Figure 5.40. The effect of motion artifacts can be observed in the end of the signal in the Figure 5.40. The long term result shows artifacts in form of spikes in addition to the standard ECG peaks in the capacitive signal.

5.3.1.2.3 Subject 3

Measurements were also taken for subject 3 who was 34 year old female, weighing 67 kg at 167 cm height. The subject wore a t-shirt (viscous, 0.34 mm thick) and trousers (polyamide & cotton, 0.96 mm).

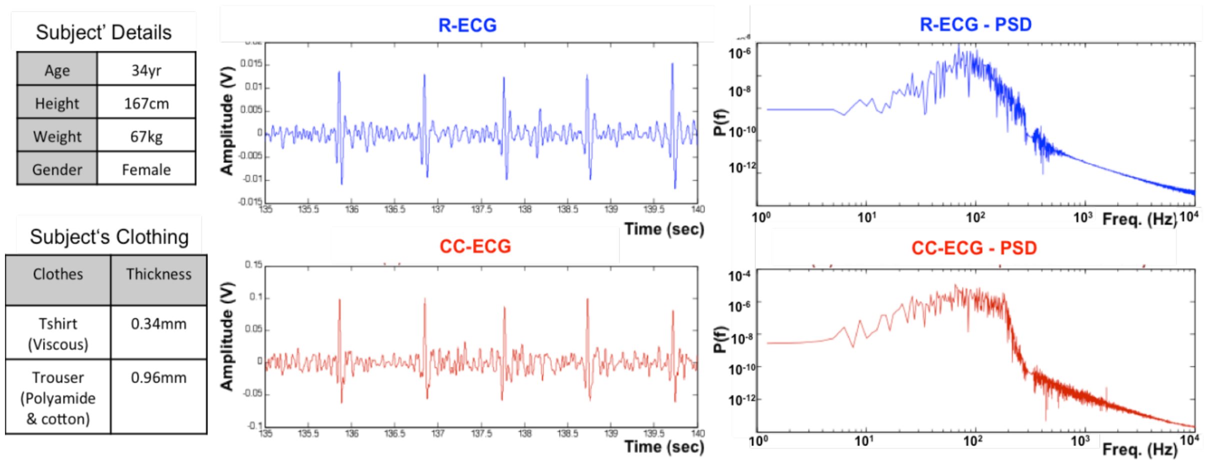

Figure 5.41 ECG measurement of the subject 3 on the wheel chair for 5 seconds.

Shorter and longer capacitive and contact Electrocardiogram can be seen in the Figure 5.41 and the Figure 5.42 respectively. In addition to the short version of the signal, subtle difference of the PSD can be observed in the CCECG compared to the convention ECG in Figure 5.41, except at higher frequency (near 1 kHz).

Signals that are a minute longer (Figure 5.42) have good stability in this case except few ripples. The figure shows QRS complexes of the measurement achieved from the heart-rate, RR-interval timings and heart-rate sequences. Both of the signals indicate a heart rate in the range of 60-70 beats per minute over a one minute signal recording except for a few false detections.

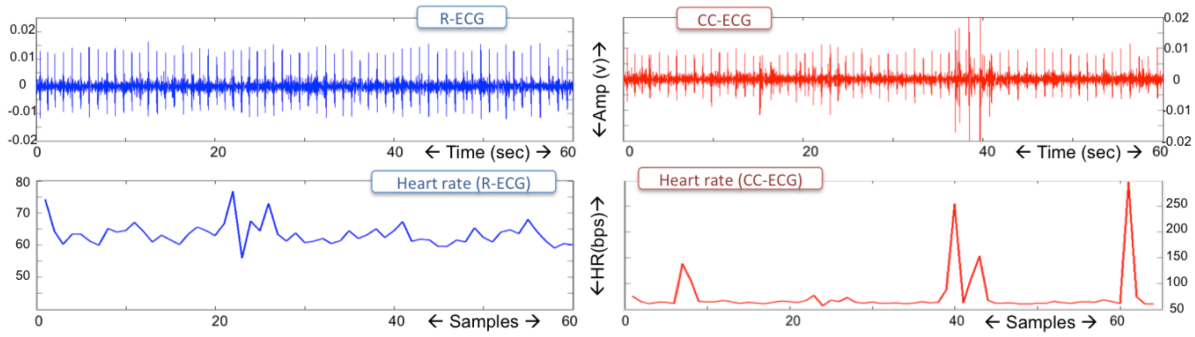

Figure 5.42 ECG measurement of the subject 3 on the wheel chair for a minute.

Time domain and frequency domain HRV analyses of the 1-minute signal are depicted Figure 5.43. Various time domain parameters are provided in the table of Figure 5.43. and the PSD of the low frequency component is graphed on the right side of Figure 5.43.

Time Domain Parameters

Variable (unit)	R-ECG	CC-ECG
Mean HR (bps)	63.25	67.72
SDNN (ms)	48.9	135.3
NN50 (count)	15	22
pNN50 (%)	25.9	36.7

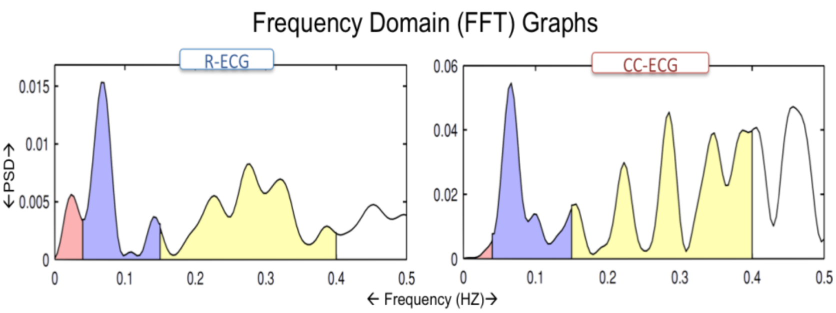

Figure 5.43 HRV analysis of the 1-min ECG measurement during the wheelchair experiment.

Reference

[1] L. D'Angelo, J. Parlow, W. Spiessl, S. Hoch and T. Lüth, "A system for unobtrusive In-Car Vital Parameter Acquisition and processing," 4th International Conference on Pervasive Computing Technologies for Healthcar, Garching, Germany 22-25 march 2010.

[2] H. Lee, J. Kim, Y. Kim, H. Baek, M. Ryu, K. Park, “The relationship between HRV parameter and stressful driving situation in the real road,” 6th International Special Topic Conference on ITAB. Tokyo, Japan 2007.

[3] Project, “INSITEX : Aktive InsassenSicherheit durch Intelligente Technische Textilien,“ BMBF (German ministry for Education and Research) funded research project, 2007-2010.

[4] Y.G. Lim, K.K. Kim, and K.S. Park, “ECG measurement on a chair without conductive contact,” IEEE transactions on bio-medical engineering, vol. 53, pp. 956-9, May 2006.

[5] K. Kim, Y. Lim, and K. S. Park, “Common mode noise cancellation for electrically non-contact ECG measurement system on a chair,” Proc. 2005 IEEE Engg in Med. & Bio. 27th annual conference, Shanghai, China, September 2005.

[6] S. Leonhardt and A. Aleksandrowicz, “Non-Contact ECG monitoring for Automotive application,” Proc. of 5th Internt. Workshop on wearable and implantable body sensor networks, HKSAR, china, 1-3 June 2008.

[7] T. Wartzek et al. “ECG on the road : Robust and Unobtrusive estimation of Heart rate,” IEEE Transaction on Biomedical Engg., Vol. 58 (11), November 2011, pp. 3112-3120.

[8] T. Matsuda and M. Makikawa, “ECG monitoring of a car drive using capacitively-coupled electrodes,” 30th Annual International IEEE EMBS Conference, Vancouver, Canada, pp. 1315-1318, 20-24 August 2008.

[9] B. Eilebrecht, T. Wartzek, J. LEM, R. Vogt and S. Leonhardt, “Capacitive Electrocardiogram measurement system in the driver seat,“ ATZ worldwide eMagazine Edition vol.113, pp. 50-55, march 2011.

[10] TITV (Institut für Spezialtextilien und flexible Material), Greiz. Website : www.titv-greiz.de

[11] Burr-Brown corporation, “INA 116, an ultra low input bias current instrumentation amplifier,” Datasheet, pp. 1-9, September 2010.

[12] K.M. Lee, S.M. Lee, K.S. Sim, K.K. Kim, and K.S. Park, “Noise Reduction for Non-Contact Electrocardiogram Measurement in Daily Life,” Computers in Cardiology, vol. 36, pp. 493-496, 2009.

[13] B.B. Winter and J.G. Webster, “Reduction of interference due to common mode voltage in biopotential amplifiers,” IEEE transactions on bio-medical engineering, vol. 30, Jan. 1983, pp. 58-62.

[14] A. Rich, “Shielding and Guarding, how to exclude interference-type noise, what to do and why to do - A rationale approach,” Analog Dialogue 17-1, pp. 124-129, 1983.

[15] R. Pallas-Areny and J. G. Webster, Analog Signal Processing. New York: Wiley-Interscience Publication 1999, pp. 482-484.

[16] Frequency Devices, “90IPB: External battery powered Instrumentation platform,” datasheet, August 2010.

[17] B. Chamadiya, S. Heuer, M. Wagner and U. Hofmann, “Textile Capacitive Electrocardiography for an automotive environment,” International conference on Biomedical electronics and devices 2011 (BIODEVICES), Rome, Italy, 26-29 January 2011.

[18] W. Zimmermann GmbH & Co. KG “Novonic E-Blocker,” 2010. Wabpage : http://www.novonic.de/web/NovNeu_FDI.nsf/id/pa_novonic_e_blocker_e.html

[19] S. Heuer, B. Chamadiya, A. Gharbi, C. Kunze and M. Wagner, „ Unobtrusive In-Vehicle Biosignal Instrumentation for advanced driver assistance and active safety,“ IEEE EMBS Conference on Biomedical Engg. And Sci. 2010 (IECBES), Kuala Lumpur, Malaysia, 30 November - 2 December 2010.

[20] J. Colotti, “EMC Design fundamentals,” Lecture notes from Telephonics - Command systems division, Staff Analog Design Engineer, may 2011.

[21] Daimer AG, “EMC Performance requirements – Vehicle testes and components tests,” Daimler Standard : MBN-10284, March 2008.

[22] Mercedes-Benz, “Electric and Electric components in Passenger cars up to 3.5t -General requirements, test conditions and tests, Part 1: Electrical requirement,” Standard : MBN LV 124-1, March 2011.

[23] A. Aleksandrowicz and S. Leonhardt, “Wireless and Non-contact ECG measurement system – the “Aachen Smartchair”,” Acta Polytechnica, vol. 47, No. 4-5, pp. 68-71, 2007.

[24] Richardson, P. C., “The Insulated Electrode,” In Proceedings of the 20th Annual Conference on Engineering in Medicine and Biology. Boston, MA (USA), p. 157, 1967.

[25] M. Ishijima, “Monitoring of Electrocardiograms in bed without utilizing body surface electrodes,” IEEE Trans. on Biomed. Engg., Vol. 40, No. 6, pp. 593-594, June 1993.

[26] Y. G. Lim, K. K. Kim and K. S. Park, “ECG recording on a Bed during Sleep without Direct Kin-Contact,” IEEE Tras. On Bio. Engg., vol. 54, no. 4, pp. 718-725, April 2007.

[27] A. Ueno et al, “Capacitive sensing of Electrocardiographic potential through cloth from the dorsal surface of the body in a supine position: A prelminary study,” IEEE Trans. on Biomed. Engg., Vol. 54, No.4, pp. 759-766, April 2007.

[28] K. Wu and Y. Zhang, “Contactless and Continuous Monitoring of Heart Electric Activities through Clothes on a Sleeping Bed,” Proc.of 5th Internt. Conf. on IT and Appl in Biomedicine, pp. 282- 285, 2005.

[29] B. Eilebrecht et al, “Implementation of a capacitive ECG measurment system in clinical practice: an interim report,” IFMBE Proc. 25, pp. 370-372, 2009.

[30] Frequency Devices, “90IPB: External battery powered Instrumentation platform,” datasheet, August 2010.

[31] National Instruments: NI USB-9162, “C series USB Single module Carrier,” Datasheet, 2010.

[32] National Instruments: NI 9215, “ Ni9215 with BNC 4 Channel ± 10V, 100kS/s per Channel, 16 bit, simultaneous sampling differential analog input,” Datasheet, 2010.

[33] Hear rate variability (HRV), Wikipedia. Source : http://en.wikipedia.org/w/index.php?title=Heart_rate_variability&oldid=480189253, last accessed on 14 March 2012.

[34] S. H Talib, P.Y. Mulay and A. N. Patil, “twenty-four hour ambulatory Holter monitoring and Heart rate variability in Healthy individuals,” Journal of Indian Academy of Clinical Medicine Vol. 6(2), April-June 2006, pp. 136-141.

[35] R. Matthews, N. J. McDonald, I. Fridman, P. hervieux and T. Nielsen, “The invisible electrode-zero prep time, ultra low capacitive sensing,” 11th International Conference on Human Computer Interaction (HCII), Las Vegas, pp. 22-27, July 2005.

[36] D. K. Han, J.M. Kim, J. H. Hong, E. J. Cha and T. S. Lee, “Performance evaluation of biosignal measurement at the wheelchair system,” 30th Annual International IEEE EMBS Conference, Vancouver, Canada, 20-24 August 2008.

6 Conclusion and outlook

Work of this doctoral thesis was a part of BMBF (German Ministry for Education and Research) funded project "INSITEX". The main topic of the work was to integrate non-contact Electrocardiography into a car seat, which was further extended to other applications like clinical and home setup.

Within this work frame, a pilot study was exercised to affirm the principle of capacitive coupled Electrocardiography with PCB (stiff) electrodes. Various Shapes and sizes of the capacitive electrodes were realized while keeping the same electronics circuit to study the influence of shape and size on the capacitive coupling and hence on the measurement. Setups like an open and closed seat cover configuration are considered during the measurements.

The aim of the "INSITEX" project was to develop technical textile solutions for various applications. Thus 1st generation of textile electrodes were developed for capacitive ECG measurement by taking into account the pilot study with stiff capacitive electrodes. Two layer textile electrodes were made up of printed textile technology. Starflex (semi flexible) PCBs were implemented for the electronics and the electrodes to have a flexible structure. Textile coaxial cable was developed to interconnect the electrode and the electronic circuit.

During the 1st generation of the textile capacitive ECG system, some problems were encountered regarding structure, design, performance and practicality. Therefore an improved version of the textile system was designed and developed as a 2nd generation system. This version contained a three layer textile structure (sensor, guarding and shielding), in which the 2nd and 3rd layers were to protect the sensitive sensor area. A compact PCB design for the electronics was realized. Each module contained only a preamplifier module, enabling more variation in the later stage of signal processing. Interconnection between the two components was accomplished using three conducting snap fasteners for each of the layers.

Various circuit techniques like movement compensation, a series capacitor at the input to compensate body movement, guarding to avoid any parasitic effects on the input and a so called driven seat circuit to suppress common mode noise have been utilized. To improve resolution of the capacitive ECG signal and to extract useful information several analog and digital signal processing method were employed in the system.

6.1 Conclusion

The pilot study showed very positive results from the capacitively coupled Electrocardiography. In the comparison to all the electrode combinations, it was observed that round electrode combinations work better in both open and closed cover configuration (section 5.1.2.1). Particularly the bigger size electrode, because of its coherent shape with BSPM (Body Surface Potential Mapping), performed best among the all electrodes.

It was learnt, during the usage, that the 1st generation of textile capacitive ECG systems were functional but had enough room for improvement in many aspects. The quality of the ECG signals and reproducibly of the system was not good enough to achieve stable Heart rate (HR). Performance of the system was unstable and was not delivering out at all in many occurrences. It was found that it is difficult to connect (by soldering) the textile coaxial cable with the electronics unit with conventional soldering equipments. It needed special soldering methods and equipment to accomplish the electrical connection. In addition, to confirm mechanical adherence with the electrode, flexibility of the Starflex PCB was not as flexible as intended.

Following generation of the textile ECG system overcame many shortcomings of the previous version as it was designed to optimize the former system. The new three layer structure of the electrode performed better stability in the signal acquisition than the previous one and hence enabling possibility to extract Heart Rate and Heart Rate Variability (HRV) from the signal. The improved guarding design in the electronic module and an additional (3rd) layer to provide passive shielding enhanced the performance and efficiency of the system. Metal snap fasteners delivered firm mechanical and electrical interconnection between the two counterparts.

Fluctuation and wide amplitude variation between ECG signal artefacts caused by different movements can be compensated up to certain extend with the movement compensation by adding series capacitor of appropriate value (section 3.4.1 and 5.1.2.2). The technique is useful in amplitude compensation caused by various movement artefacts. Different guarding of the input rings (2 Dimensional in the case of 1st generation and 3 Dimensional in 2nd generation) improved stability of the system by minimizing parasitic effects. Driven Seat Circuit (DSC) helps to reduce common mode signal to a good extent. Still it varies case to case as the feedback signal can also cause noise if not in adequate proportion.

6.1.1 Driving Environment

Experiment with 1st generation textile CCECG system was conducted on demonstrator (experimental car seat in lab). It showed promising results to integrate a CCECG system into the car seat. The results demonstrate the possibility of determining the Heart Rate from the measured signals. However, being a first attempt with textile electrodes only, the quality of the signal needed to be improved. The 2nd generation of the system was considered after investigating it with the demonstrator to integrate into a real car seat and to have the ECG measurement while driving in real life scenarios.

A practical approach to integrate a textile CCECG system has been implemented in our experiments. Measurements during common driving situations could be demonstrated. It can be observed that only driving on bad and bumpy roads (hence strong car and body movement) did interfere with the monitoring by causing rapid base line drifting. Some of the seat functions also have, from mild to intense, influences on the signal as depicted in Figure 5.14. Interference from automatic seat adjustment while driving was minor as the function is enabled by DC motors driven with 50Hz pulses (Figure 5.12) and the body maintained a stable contact with the electrodes in the seat. Low frequency base line drift and 50Hz hum noise from the DC motors were filtered by the monitoring system (Figure 5.13).

Seat heating with level 1 and 2 showed major effects on the monitoring results as they had a PWM signal of 24 Hz. However, we speculate that interfacing our monitoring setup with the car‘s own controls and sensors could alleviate the severity of these distortions. Clothes in general did have an impact in the signal-to-noise ratio (Figure 5.15), but did not prohibit heart rate monitoring and require further investigation.

Summing up, this work demonstrates promising non-contact monitoring results with a textile CCECG system in real world driving situations. The system shows a strong potential to be incorporated in a car for long term ECG measurement for safety and healthcare.

6.1.2 Hospital Environment

In today's ageing society, the demand for unobtrusive health monitoring is growing, not the least due to a growing number of persons living in nursing homes or serviced apartments. Together with the presumed advantages of continuous ECG monitoring in the clinical environment, a need for contactless, non-obtrusive ECG recordings arises.

With this study, we showed the feasibility of contactless ECG measurements with a prototype capacitive-coupled ECG system. Our system uses conductive textiles, actively shielded by a driven seat circuit. Flexible textile electrodes were placed in two very common clinical settings. Here, the prototype was able to successfully record ECG signals from volunteers without the need to glue conductive electrodes on the subject‘s skin. Signals displayed in all two settings are of good visual quality and thus later are used for further standard ECG analysis like QRS complex detection and HRV analysis. The data presented strengthens the case for noise-reducing guarding layers to be used in CCECG. Our experiments demonstrated that the CCECG signals are prone to interference and movement artifacts, due to their delicate recording physics. This will become an obstacle in detecting QRS complexes and HRV analysis from the signals later. In order to utilize contactless ECG measurements in locations of high nursing, further steps to improve stability, signal quality, and long-term acceptance have to be taken.

Even though the primary objective of our experiments was not to compare the subject's clothing and its effect on quality of ECG detection, we observed that ECG detection using the CCECG was hardly affected by the subject's clothing. In other words, thickness and material of the clothes worn by the subject didn't change quality of detected ECG signals. At one instance, the clothes, not unexpectedly, became a point of hindrance to the signal quality when a subject was wearing a fur coat exceeding the minimal distance between skin and electrode. Based on these observations, we conclude that the ECG detection quality of our system remains unaffected, when a subject is dressed for room temperature. Subsequently, as the layers of the garment increase, ECG detection quality deteriorates. However a rigorous experiment on the influence of clothing on the CCECG acquisition is beyond the scope of this and subject to a follow up study.

6.1.3 Home Environment

Similarly to the clinical environment, a lab demonstrator with a standard wheel chair was used to perform contactless Electrocardiography. The measurement was performed successfully achieving signals with a quality to extract QRS complexes and Heart Rate Variability parameters with various subjects (male and female). Measurement setup of the wheel chair exhibited better signal resolution than the clinical setup overall including same subjects. The “electrode-subject” contact is better (for capacitive coupling) in the clinical setup, where the person lies down on the setup.

Some of the analysis and observation of the clinical setup are also noticed for home environment experiment as the same electronic setup in laboratory was used. Therefore similar problems as described in clinical setup, which leads to a need of improvement in signal quality, signal stability, and reproducibility of the system for this setup too.

6.2 Outlook

During the development of the CCECG system, various technical challenges were encountered. Some of the issue related to design and performance of the CCECG system are still persistent and need to be solved. Here in this section some of the suggestions or visions for the future are expressed for future improvement.

It was learnt that the printed textile technology has some limitation regarding life cycle of the conducting textile, in other words its conductivity deteriorates over the time (in few years) albeit being costly (silver printing) and less flexible with more layers (six). So it is necessary to try out more variants of conducting textile to yield robust and cost effective textiles. It is also crucial to have more variants in interconnection technology e.g. snap fasteners with electrical isolation from outside to have overall robust structure and to prevent environment effects like moisture. Textile integrated electronics can be a good possibility to improve the integration and to simplify the design. There is still possibility to improve circuit techniques and parameters of the preamplifier like input impedance.

One of the significant problems in the CCECG measurement is signal processing and useful data extraction. An adequate analogue signal processing is required to improve signal resolution, so that the later stage of digital signal processing can have more experimental approaches. Similarly appropriate digital signal processing with a sophisticated algorithm for each case can refine the signal further to extract ECG features like HR and HRV. Movement artifacts, being a major problem in the non-contact measurement, need to address comprehensively.

6.2.1 Driving Environment

Within this doctoral work, various aspect of CCECG integration into an automobile are covered. ECG measurements in the study show very promising results. In addition to the above mentioned suggestions, practical integration of the CCECG system into the car seat is very important. The integration shall include aspect from automobile perspective like mechanical and electrical coherence with the other devices, software to extract useful information for healthcare and safety applications etc. Reproducibility and robustness have to be verified in order to use the system flawlessly.

Joining the CCECG system of an automobile to the telemedicine or telemetry can be very interesting as it can make health monitoring very convenient (for some people as heart diseases are wide spread) and mobile. Adding more physiological parameter may help to estimate psychophysiological condition of the driver and ultimately various healthcare and safety applications.

The Current Driver Assistance System available in various automobiles often give false alarms for driver’s tiredness. Availability of physiological parameters like ECG, combined with a system that can lead to better assessment of the driver’s condition and may improve the accuracy of the tiredness alarm with different degrees.

6.2.2 Hospital Environment

In the clinical ambience, there are many electronics devices nearby. So considering all the interferences, a dedicated signal processing is needed to design and develop to remove the noise.

Telemetry with the CCECG integrated stretcher can help learn about the patient’s health condition beforehand. Knowing the condition beforehand and being prepared for it can help to avoid fatal consequences. Hence we interpret our results as motivating enough to envision the potential future care facility featuring a personal, non-obtrusive and yet permanent health monitoring system providing reassuring baseline data and fast response times against serious health problems.

All in all, we interpreted our results as sufficiently promising to envision the potential future care facility featuring a personal, non-obtrusive and yet permanent health monitoring system providing reassuring baseline vital signs and fast response times against serious health problems.

6.2.3 Home Environment

Home setup is a favorite place (and cozy) for people to monitor the heart activity among the other cases. So there is a need to conduct some experiments to integrate and to customize the CCECG system into different furniture like table chair, TV chair, sofa, couch etc. Heart monitoring in daily life can enhance people’s health as heart diseases are wide spread and leading cause of death around the world.

It also can be interesting here to customize software to display simplified and readable health related information from the ECG signal like body composition analyzer (Bio-impedance analyzer). These kinds of gadgets and information can improve awareness regarding heart diseases (like weight from weigh machine), that can lead to health improvement to greater extend. It is also possible to incorporate other physiological sensors (non-contact) without hindering daily chores to estimate health conditions (Personal healthcare).

Publications

1) B. Chamadiya, K. Mankodiya, M. Wagner and U. G. Hofmann, "Textile based, contactless ECG monitoring for non-ICU clinical settings", Journal of Ambient Intelligence & Humanized Computing, Springer-Verlag, Berlin / Heidelberg, July 2012, DOI : 10.1007/s12652-012-0153-8.

2) B. Chamadiya, M. Wagner, H. Meinel, Keynote presentation on "Insassenschutz durch intelligente technische Textilien im Automobil" Textil und Sensorik 2011, Bayern Innovativ, October 2011, Regensburg, Germany.

3) B. Chamadiya, K. Mankodiya, M. Wagner, R. Nasressine and U. G. Hofmann ,"Non-contact, non-obtrusive electrocardiography in clinical environments", 5th International ICST Conference on Pervasive Computing Technologies for Healthcare 2011, May 2011, Dublin, Ireland.

4) B. Chamadiya, S. Heuer, M. Wagner, U. G. Hofmann, "Textile Capacitive Electrocardiography for an automotive environment" International conference on Biomedical electronics and devices 2011, January 2011, Rome, Italy.

5) S. Heuer, B. Chamadiya, B. Gharbi, C. Kunze, M Wagner, "Unobtrusive In-Vehicle Biosignal Instrumentation for Advanced Driver Assistance and Active Safety", IEEE EMBS conference on Biomedical Engineering and Science, Nov-Dec. 2010, Kuala Lumpur, Malaysia 2010.

6) M. Wagner, Bhavin Chamadiya, Holger Meinel, Keynote presentation on "Automotive applications of Smart textiles in car interior " Advanced textiles 2010, June 2010, Paris, France.

7) M. Wagner, B. Chamadiya, H. Meinel, Keynote presentation on "Automotive applications of smart textiles in car interior", Smart fabrics 2010, April 2010, Miami, USA.

8) B. Chamadiya, M. Wagner, W. Wondrak and U. G. Hofmann, "Active passenger safety by intelligent textile", 7th international conference on wearable micro and nano technologies for personalized health 2010, May 2010, Berlin, Germany.

9) K. Mankodiya, Y. Ali Hasan, O. Christ, B. Chamadiya and U. Hofmann, "Textile based ECG Collection with Portable Dual-core Embedded System", 7th international conference on wearable micro and nano technologies for personalized health 2010, May 2010, Berlin, Germany.

10) M. Wagner, B. Chamadiya, H. Meinel, Keynote presentation on "Automotive applications of Smart textile technology " Printed Electronics 2009, April 2009, Dresden, Germany.

11) B. Chamadiya, S. Heuer, M. Wagner, U. Hofmann, "Towards a capacitive coupled ECG integration into a car" European Congress for Medical and Biomedical Engineering 2008, November 2008, Antwerp, Belgium.

Patents :

- Textilelektrode zum Messen von Körperfunktionen und/oder Vitalparametern von Personen für Fahrzeuganwendungen. (DE102008049112A1)
- Elektrode zur kapazitiven Messung biologischer Signale eines Insassen. (DE102010023369A1)
- Sensorik Lenkrad mit leitfähigen textilen Kontakten zur Erfassung von Vitalparametern des Fahrers.

List of abbreviations

1. AC : Alternating current
2. Ag : Silver
3. AgCl : Silver cloride
4. AV node : Atrioventricular node
5. BMBF : Bundesministerium für Bildung und Forschung
6. BSPM: Body surface potential mapping
7. CAD : Computer-aided design
8. CAE : Computer-aided engineering
9. CCECG: Capacitively coupled Electrocardiography
10. CCNE : Capacitively coupled non-contact electrode
11. CMMR : Common mode rejection ration
12. DC : Direct current
13. DSC : Driven seat circuit
14. DWT : Discrete wavelet transform
15. FFT : Fast Fourier transform
16. FIR : Finite impulse response
17. ECG : Electrocardiogram
18. ECU : Electronic control unit
19. EDA : Electronic design automation
20. EEG : Electroencephalogram
21. EMC : Electromagnetic compatibility
22. EMFi sensor : Electromechanical film sensor
23. EMI : Electromagnetic interference
24. EMG : Electromyogram
25. EDA : Electrodermal activity
26. FFT : Fast Fourier transform
27. GND : Grounding
28. GND-GRD : measured between grounding and guarding layers
29. GmbH : German for LLC, limited liability company
30. GPS : Global positioning system
31. GRD : Guarding
32. GRD-IN : measured between guarding layer and input (sensing) layer
33. GSR : Galvani skin response
34. GUI : Graphical user interface
35. HR : Heart rate
36. HRV : Heart rate variability

37. IBE : Insulated BioElectrode
38. IIR : Infinite impulse ratio
39. INSITEX : Aktive **In**sassen**S**icherheit durch **I**ntelligente Technische **Tex**tilien
40. JFET : Junction gate field-effect transistor
41. LabVIEW : Laboratory Virtual Instrumentation Engineering Workbench
42. LCR : Inductance (L), Capacitance (R) and Resistance (R)
43. MOSFET : Metal–oxide–semiconductor field-effect transistor
44. NI : National Instruments
45. PCB : Printed circuit board
46. PR : Perfect reconstruction
47. PSD : Power spectral density
48. PTT : Pulse transit time
49. PU : polyurethane
50. PWM : Pulse width modulation
51. QUASAR : Quantum Applied Science and Research (San Diego)
52. R-R : R wave to R wave in QRS complex
53. SMD : Surface mount device
54. SPICE : Simulation Program for Integrated Circuits Emphasis
55. SpO2 : Saturation of peripheral oxygen
56. TE : Textile Electrode
57. TITV : Institut für Spezialtextilien und flexible Material (Greiz)
58. UN :United nations
59. USB : Universal serial bus

List of figures

Appendix

Appendix I : Textile electrodes

I.1 Various versions of the textile electrodes

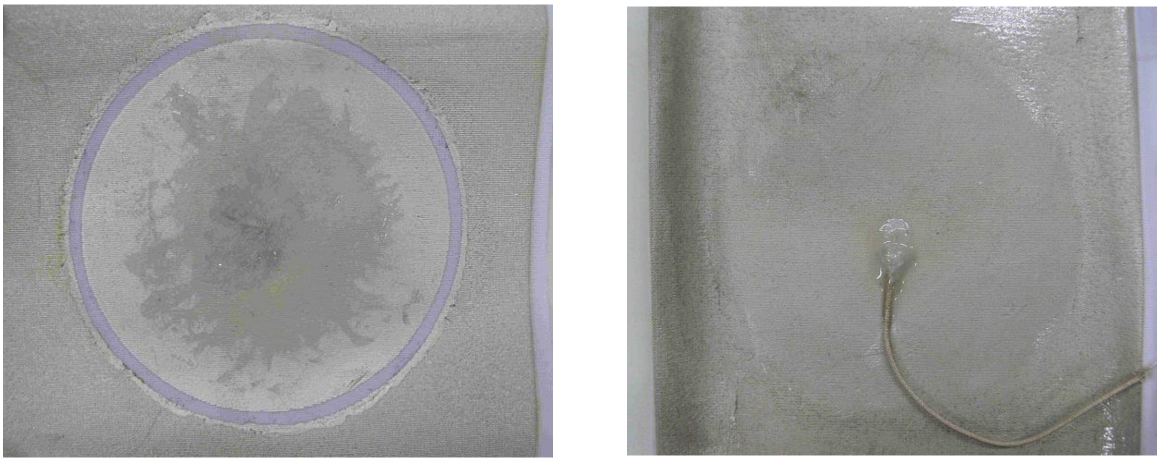

Figure A 1 1st Version of the textile electrodes with textile coaxial connection (uncovered).

Figure A 2 2nd Version of the textile electrodes (sensor area covered and uncovered) with textile coaxial connection.

Figure A 3 3rd Version of the textile electrodes with conventional coaxial cable.

Figure A 4 4th version of the textile electrodes covering the sensor area with big snap fasteners.

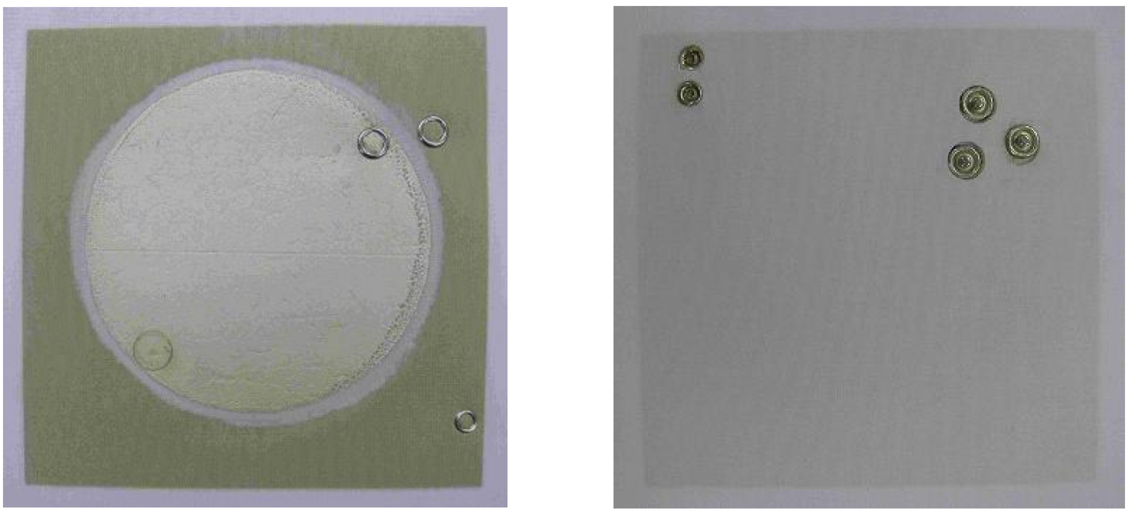

Figure A 5 5th Version of the textile electrodes with big snap fasteners.

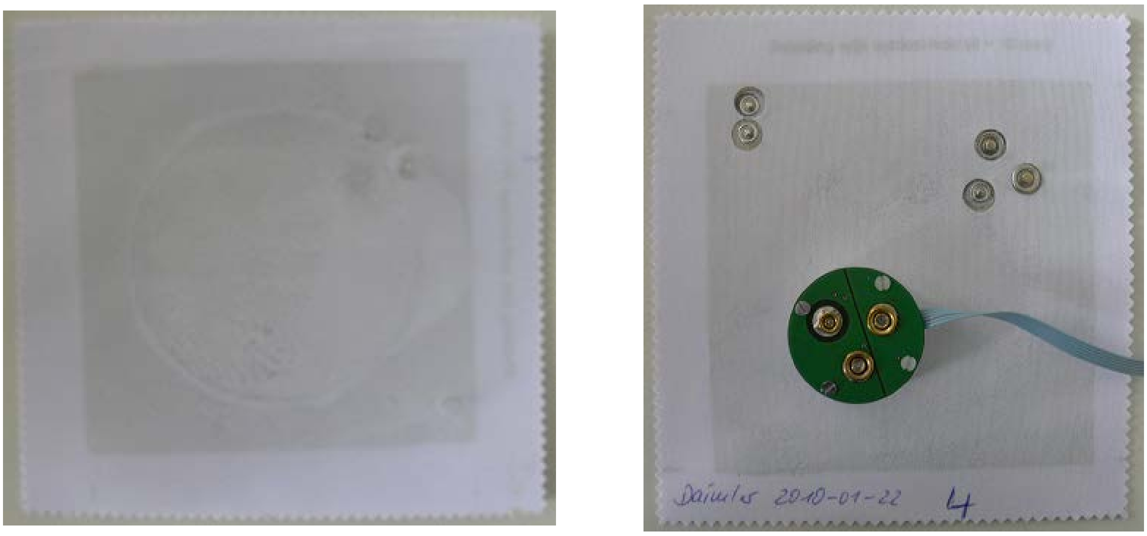

Figure A 6 6th Version of the textile electrode with cover in sensor area with combination of snap fasteners.

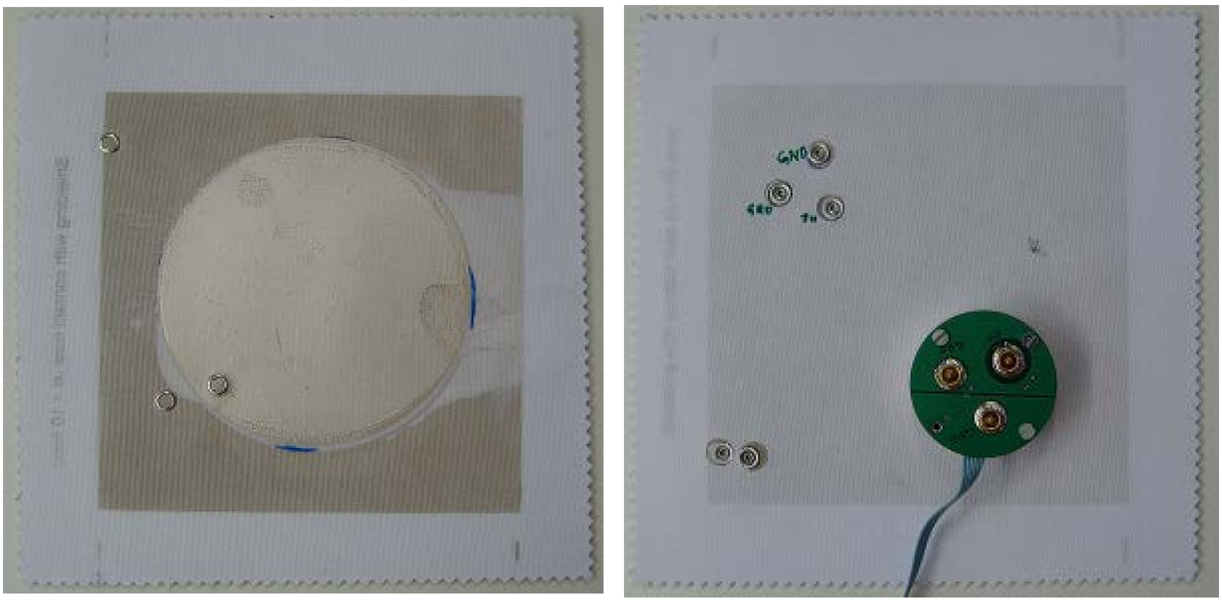

Figure A 7 7th version of the textile electrode with small snap fasteners for all the connection.

Appendix II : Components

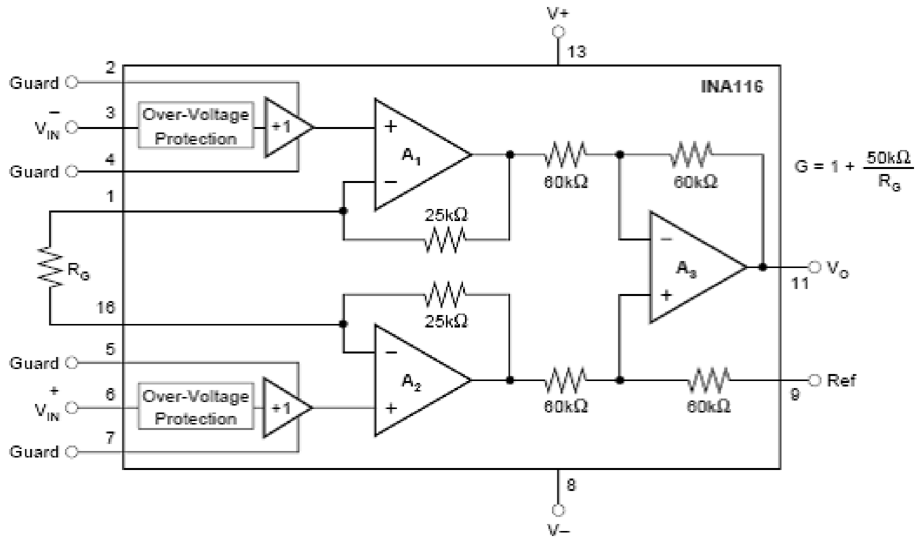

Figure A 8 Internal diagram of INA 116

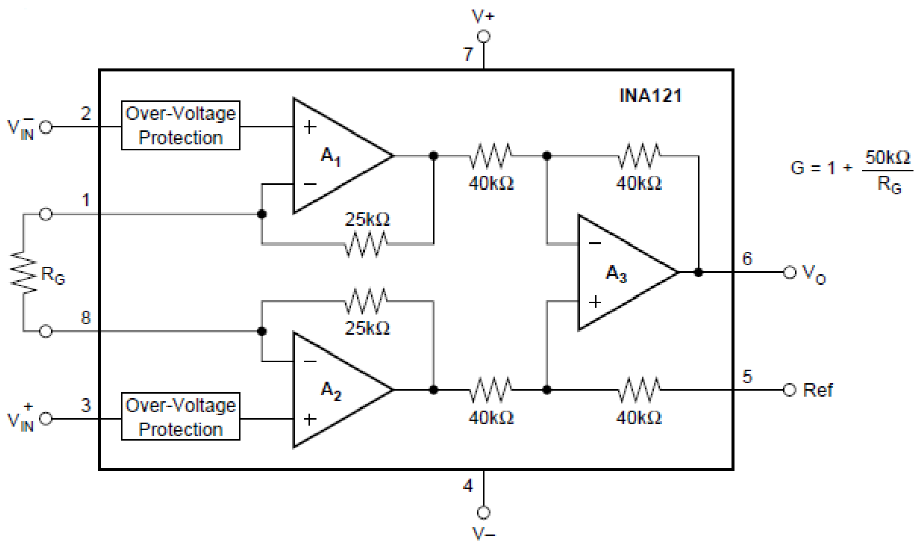

Figure A 9 Internal diagram of an INA121

Parameters	**INA121**	**INA116**
Input impedance	10^{12} Ω / 1 pF	10^{15} Ω / 0.2 pF
Input bias current	+/- 4 pA (typical)	+/- 3 fA (typical)
Input offset voltage	+/- 500 µV (max)	+/- 5 mV (max)
Input offset current	+/- 4 pA	+/- 100 fA

Table II.1 Some parameters of INA116 & INA121

Appendix III : Layouts and PCB Designs

III. 1 Electrode

III.1.1 Stiff PCB CCECG electrodes

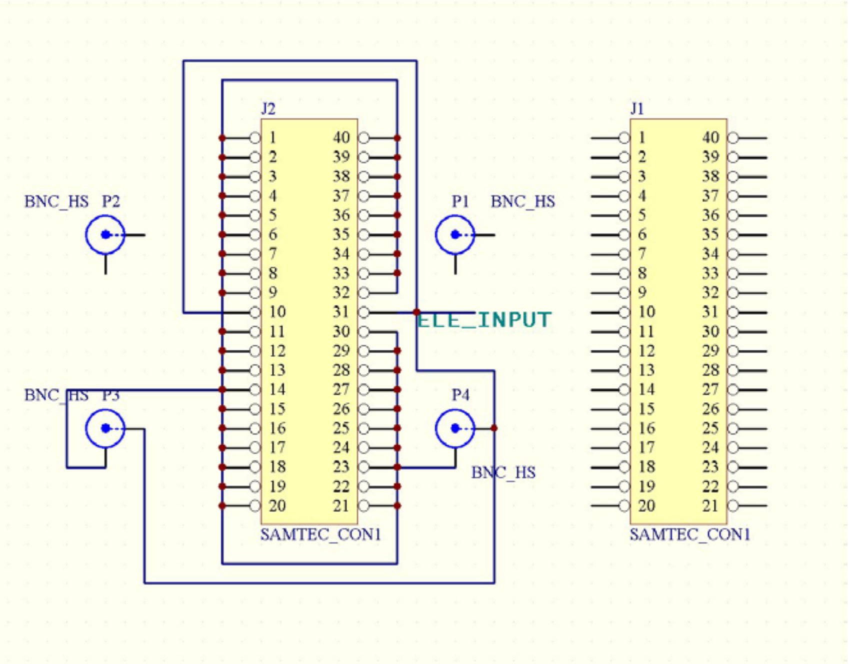

Figure A 10 Schematic of PCB CCECG electrode.

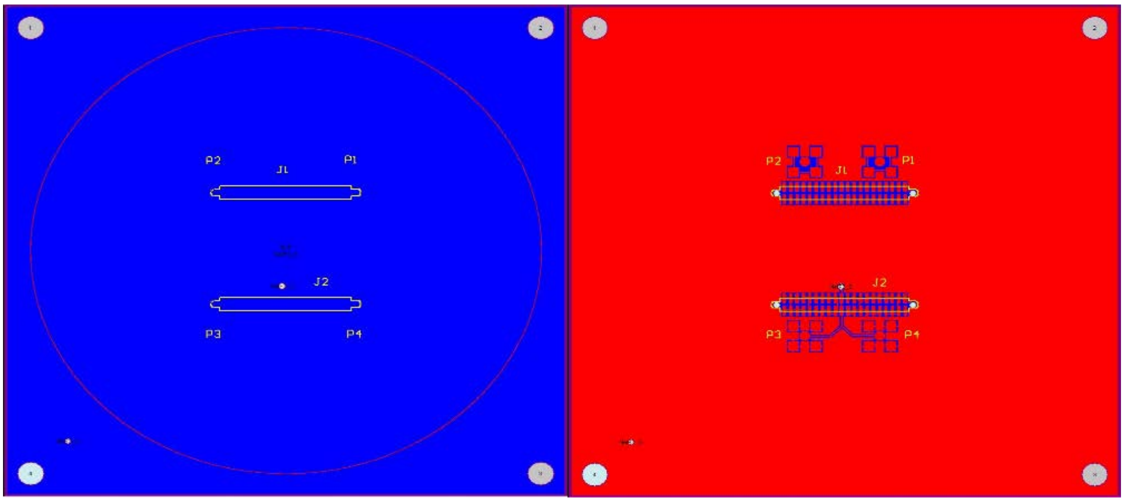

Figure A 11 PCB layout of PCB CCECG electrode.

III.2 Electronic circuit

III.2.1 Pilot Stiff electrodes PCB CCECG System

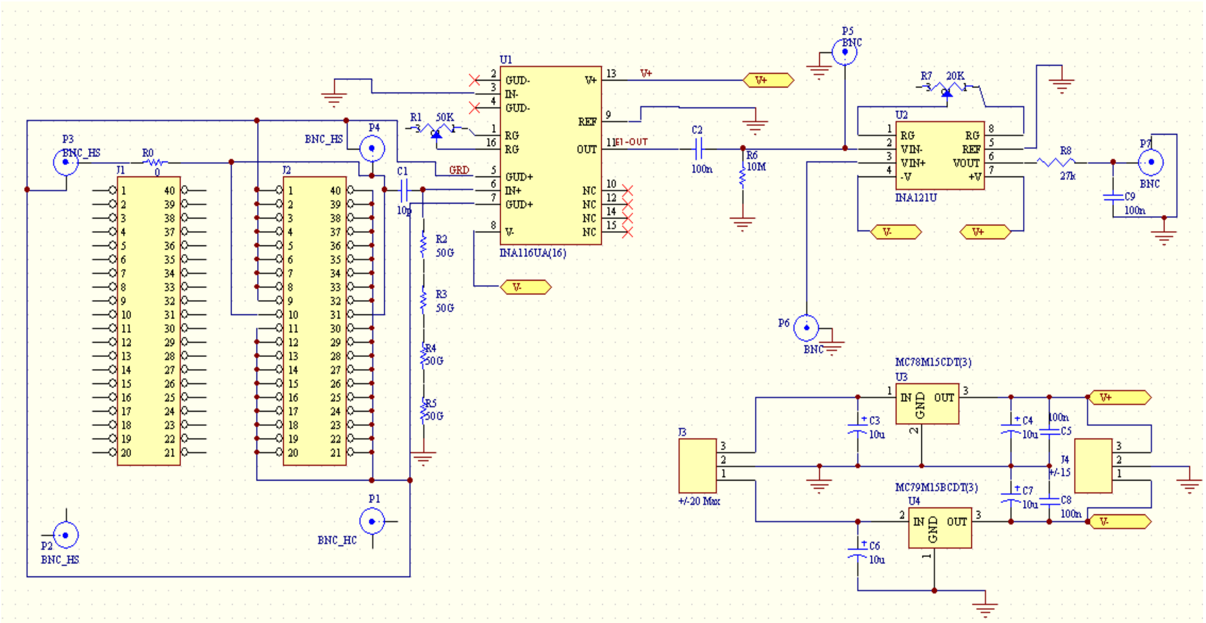

Figure A 12 Schematic of the CCECG electronic circuit.

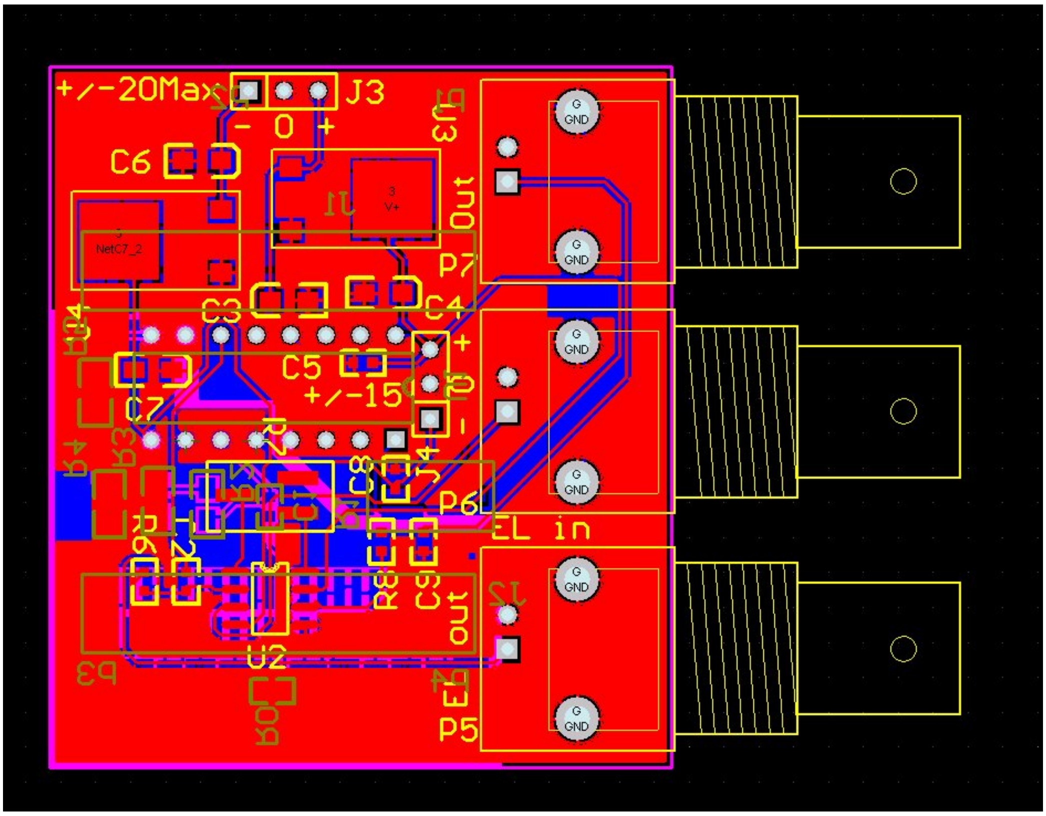

Figure A 13 PCB layout of the CCECG electronic circuit.

III.2.2 1st Generation of the textile CCECG System

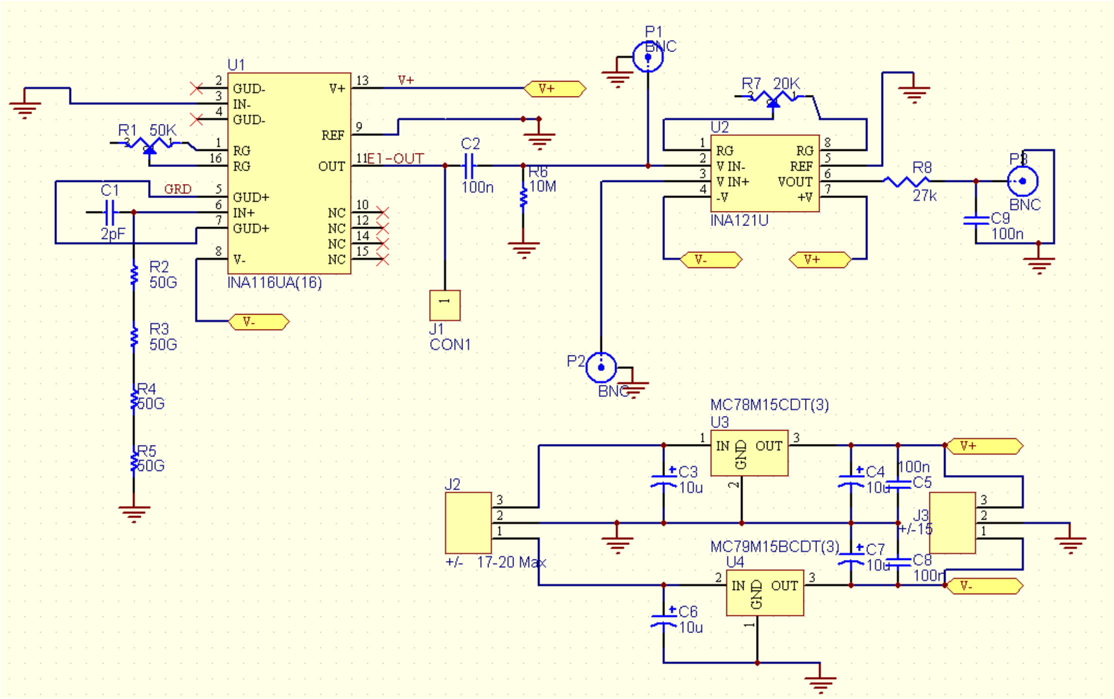

Figure A 14 Schematic of the Starflex CCECG electronics.

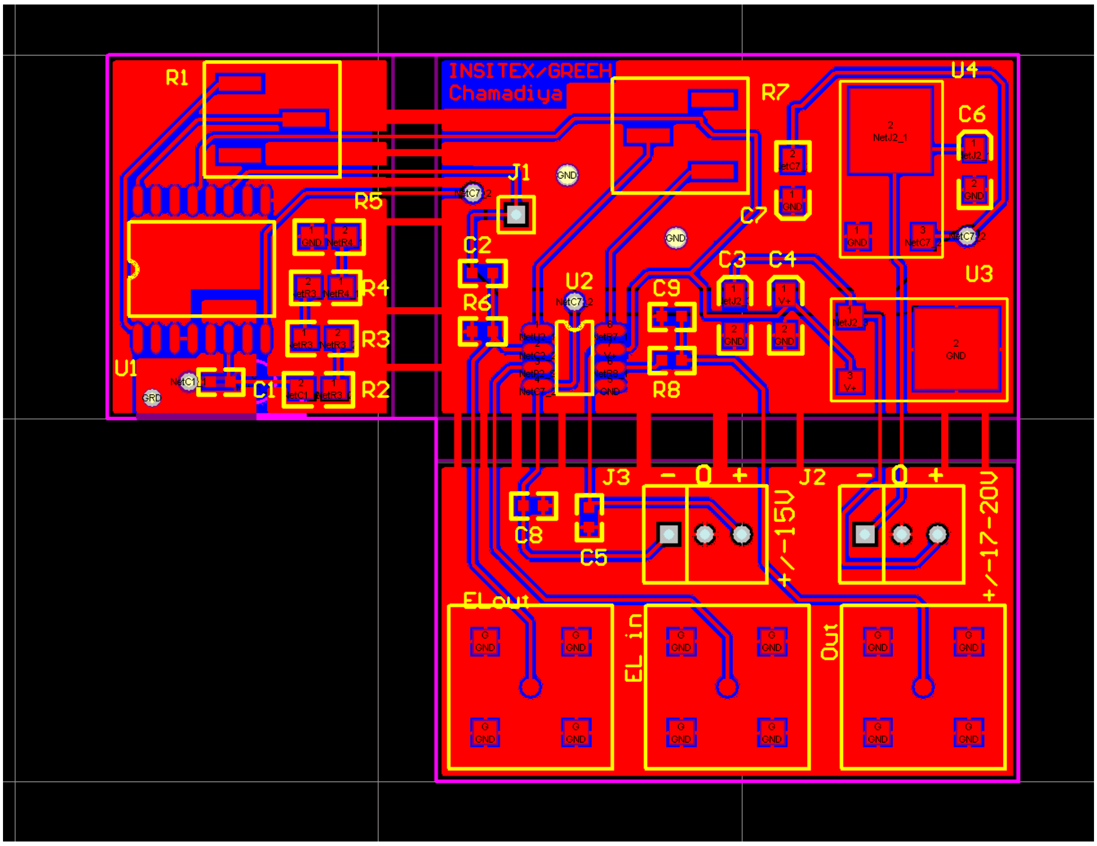

Figure A 15 layout of the Starflex CCECG electronic circuit.

III.2.2 2nd Generation of the textile CCECG System

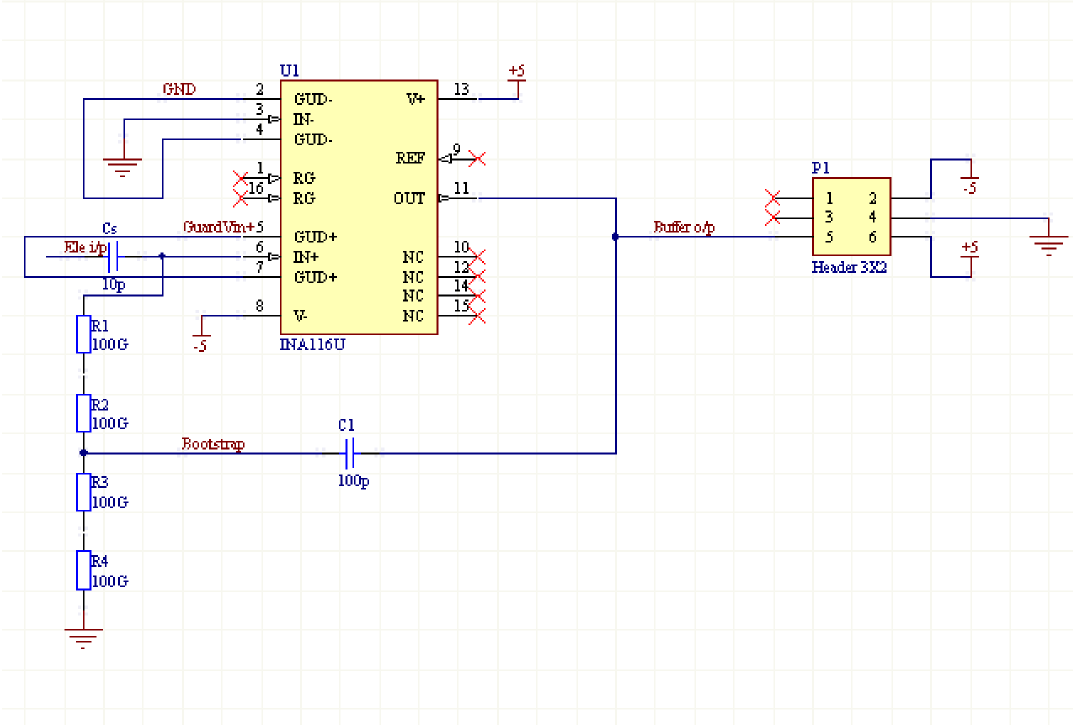

Figure A 16 Schematic of the input buffer (amplifier).

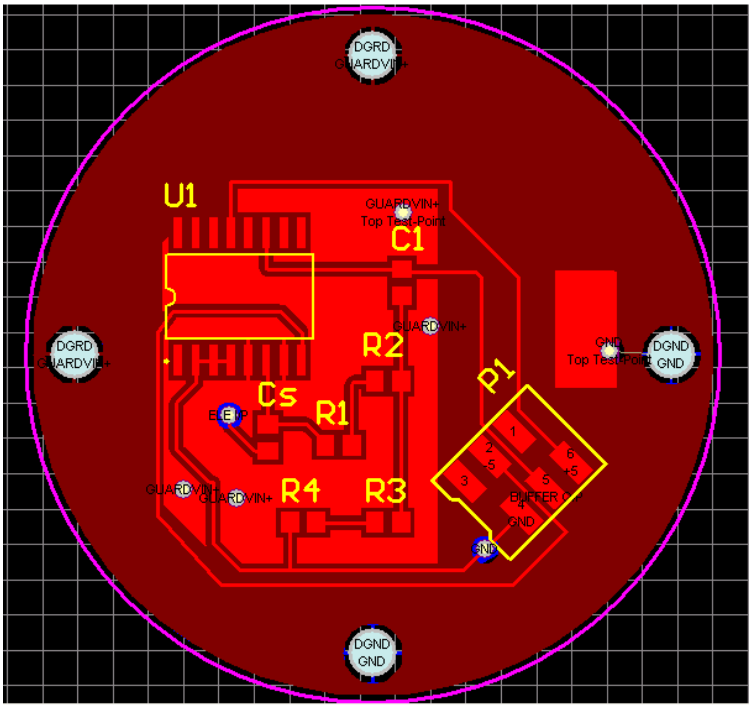

Figure A 17 PCB layout of the input buffer.

III.3 Seat driven circuit

III.3.1 Circuit Schematics

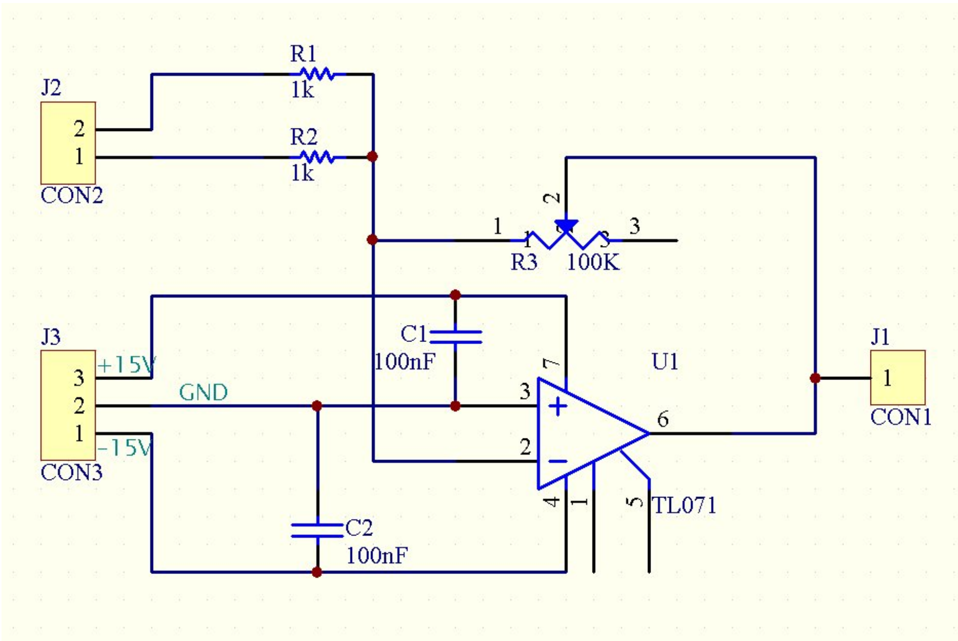

Figure A 18 Schematic of driven seat circuit.

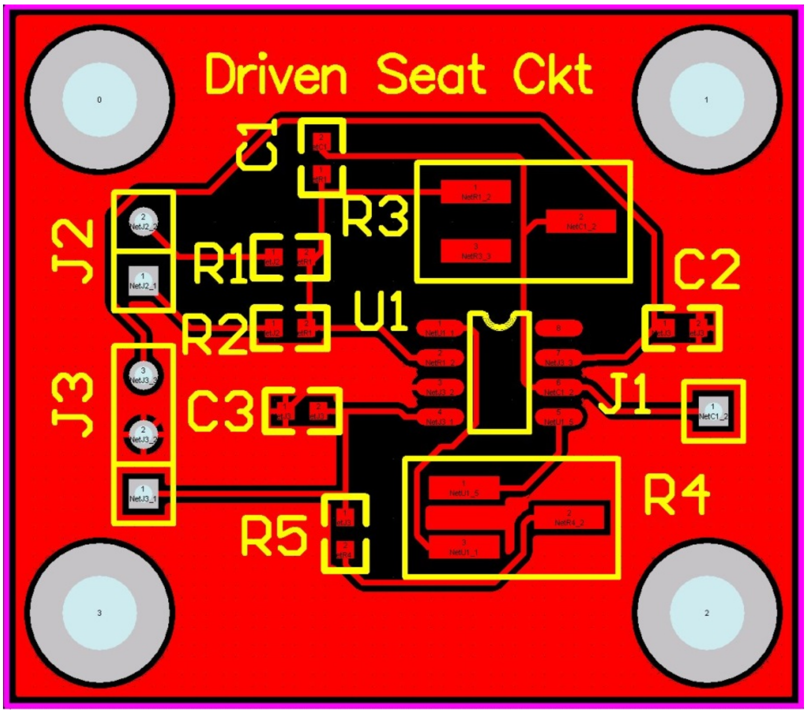

Figure A 19 PCB layout of the driven seat circuit.

Appendix IV : Simulations

IV.1 Simulink

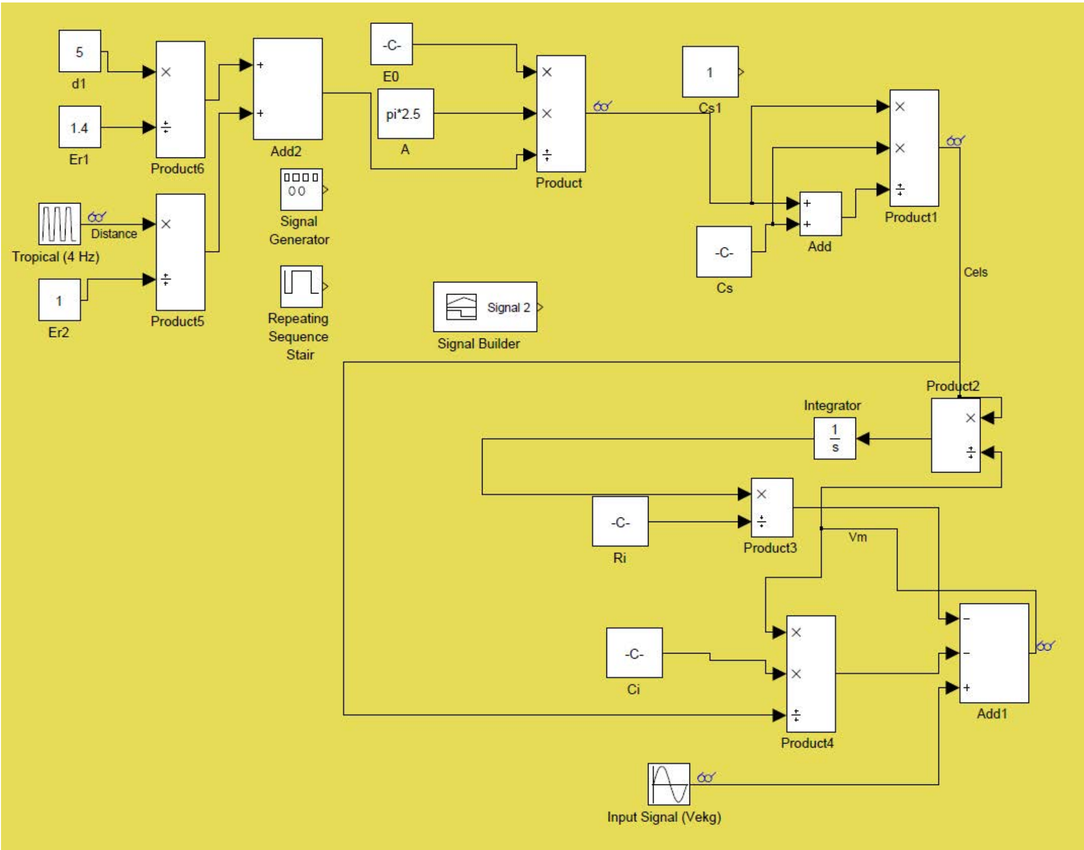

Figure A 20 Simulink model of the CCECG system.

IV.2 Pspice

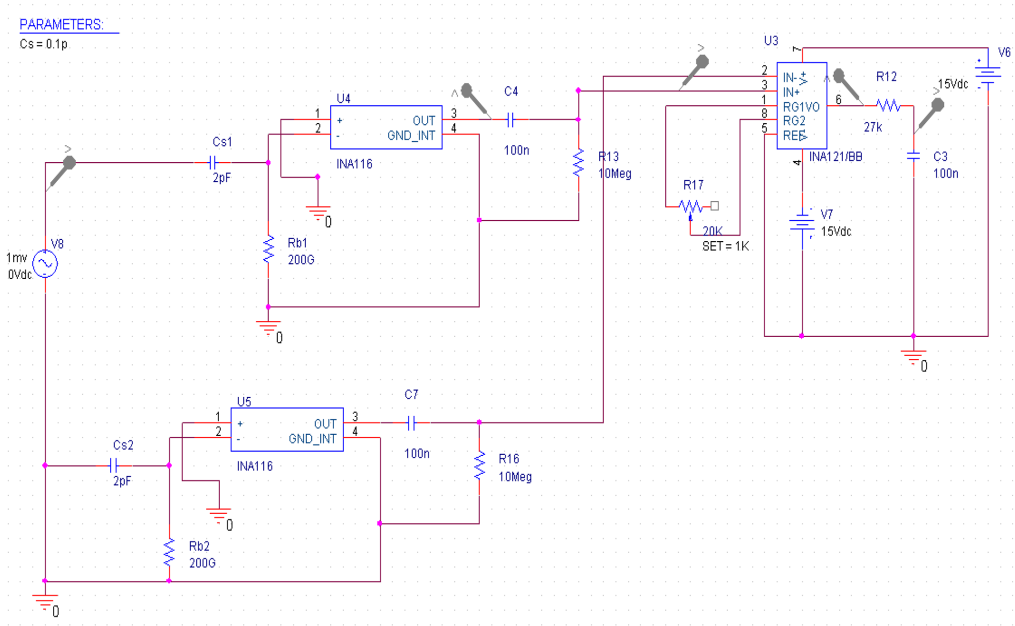

Figure A 21 Pspice model of the CCECG system.

Appendix V : LabVIEW programming

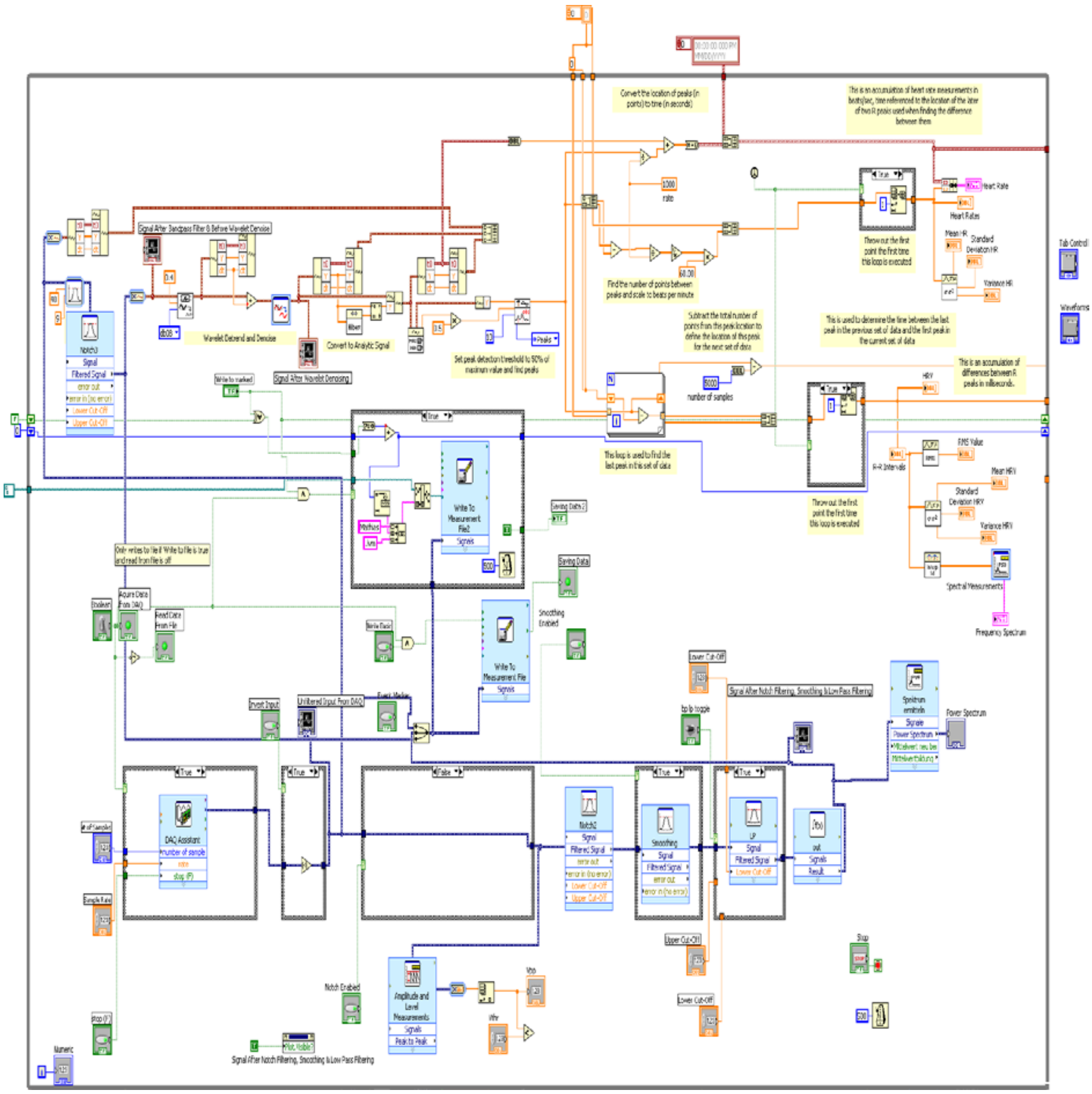

Figure A 22 LabVIEW program for Signal processing - 1.

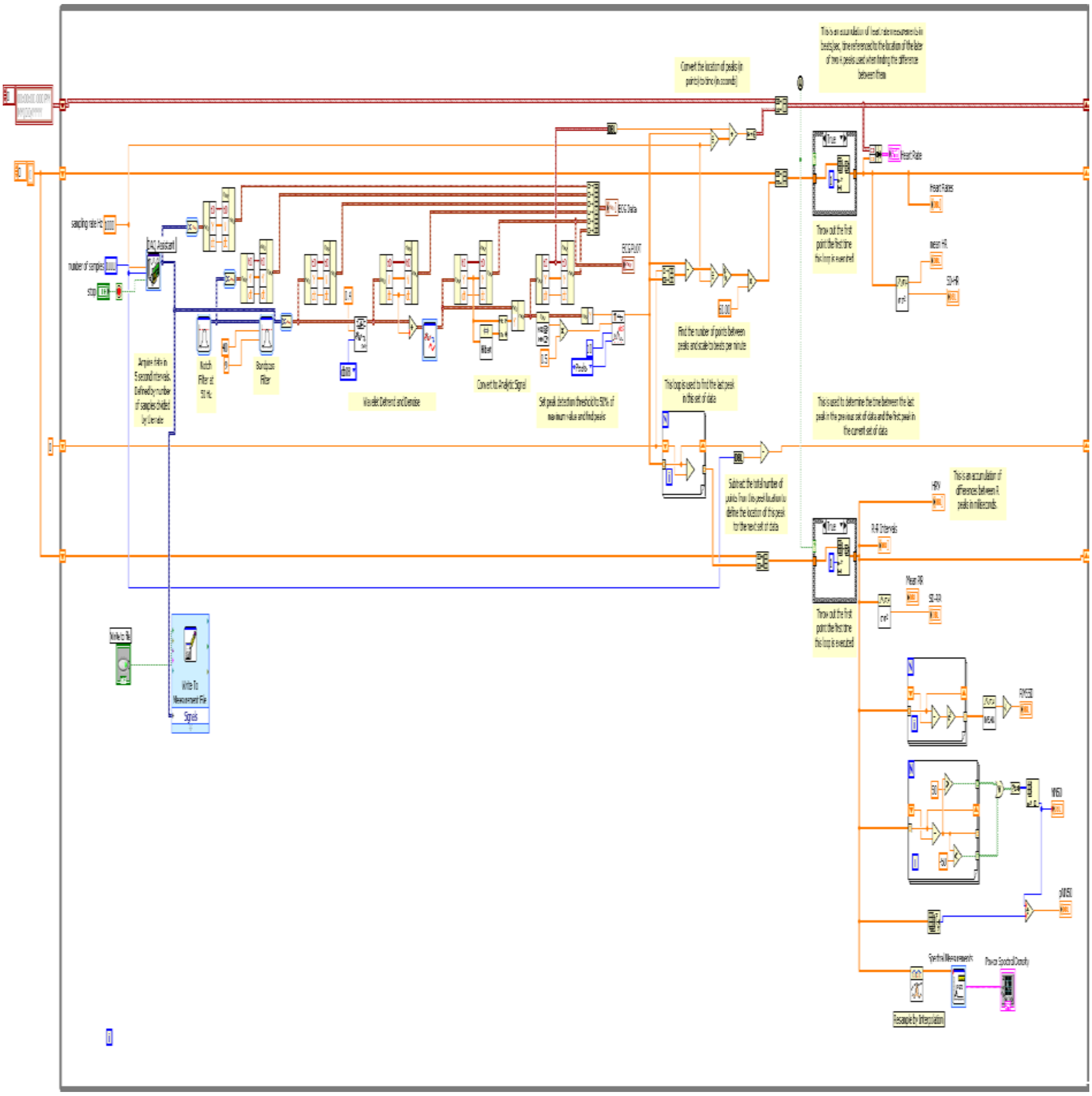

Figure A 23 LabVIEW program for Signal processing - 2.

Appendix VI : Biosensor Integrated Steering wheel

VI.1 Biosensor integrated Steering wheel

In the INISTEX project, there was also a task to have biosensors into an automotive steering wheel as conceptualized in the Introduction. Within this task, FZI (Forschungszentrum Informatik), Karlsruhe [1] developed the biosensors (ECG, EDA, SpO_2 and Skin temperature) with its central electronic unit including its software. After successfully testing of the system at FZI, it was our task at Daimler AG to integrate the developed system into a real automotive steering wheel (Mercedes Benz S Class, Series W221) [2]. The following sections detail the integration of the sensors into the steering wheel.

VI.1.1 Electrocardiography and Electro-dermal Activity

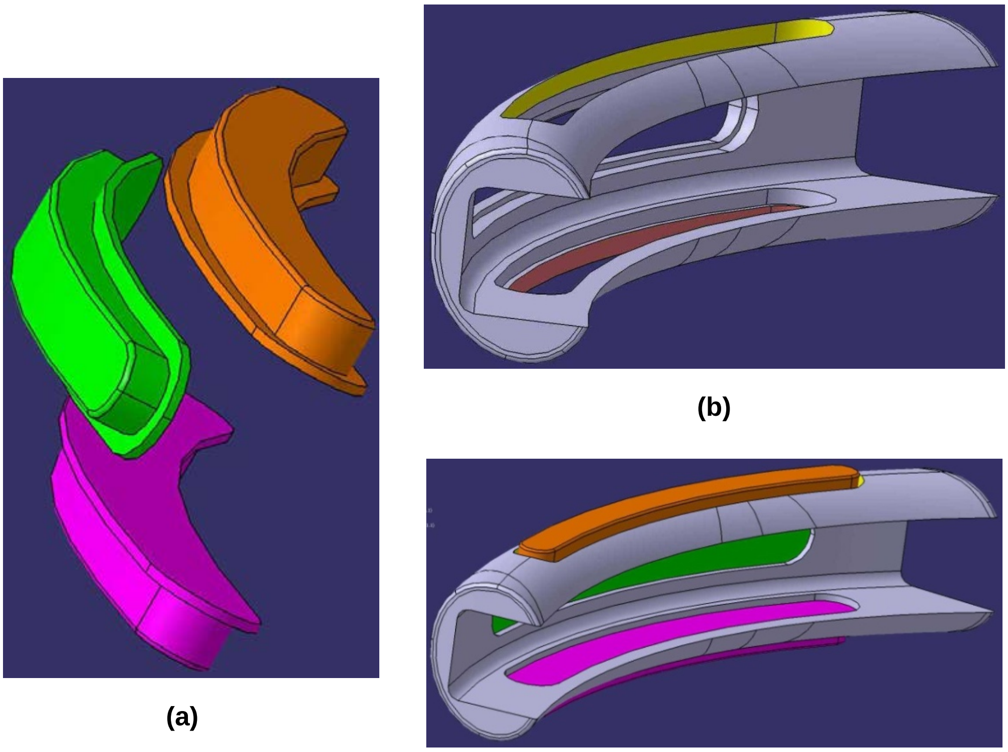

(a) (b) (c)

Figure A 24 The steering wheel electrode concept for ECG and EDA.

Electrocardiography is one of the most important physiological parameter. Electro-dermal activity helps to estimate mental activity of the subject. To conduct Electrocardiography and Electro-dermal activity (EDA) from the steering wheel, it should have electrically conductive surface. Along with this, shape of the electrodes should also be compatible to the shape of steering wheel and they should have good conductive surface.

After these considerations, brass electrodes shown in the Figure A 24(a) are conceptualized and implemented. To hold such electrodes, plastic holders are designed as depicted in the Figure A 24(b).

The electrodes can be fixed into the holder (refer Figure A 24(c)), which makes it possible to imbed the whole assembly onto the skeleton of the steering wheel. This imbedding as well as image of the actual electrodes and the holder can be seen in Figure A 25.

Figure A 25 Embedding the electrode holder to the steering wheel.

Two pieces of the holder were realized as part of the ECG and the EDA measurements, one with 3 electrodes (left side) and another with 2 electrodes (right side). Concept of the 3 electrodes can be seen in Figure A 24(c), where the electrodes are placed on front, lateral and rear side. Here the front electrode is utilized as an ECG electrode, while other two electrodes are utilized to measure EDA. Right side holder contains two ECG electrodes on front and rear side.

It must be noted here that the EDA measurement is executed by applying constant current on the EDA electrodes and measuring potential across these electrodes [3].

VI.1..2 Pulse oximetry

Pulse oximetry is a noninvasive method that enables rapid measurement of the oxygen saturation of hemoglobin in arterial blood (SpO2) [4]. It also measures pulse rate (bpm) of the subject. A ready-made pulse oximetry sensor, OEM III [5] with reflective sensor (8000 R) [6] from Nonin® Medical Inc., USA is integrated into the steering wheel. The signal from the sensor is fed to the central electronic unit for further processing and evaluation. The pulse oxymeter and its integration into the steering wheel are presented in Figure A 26.

It can be observed in the figure that the rubber surface of the steering wheel is engraved by considering shape and size of the sensor. Sensor surface of the pulse oxymeter is placed little high and out in order to level it with the steering wheel surface after its leathering. A hole is also drilled nearby to pass through the cable of the sensor.

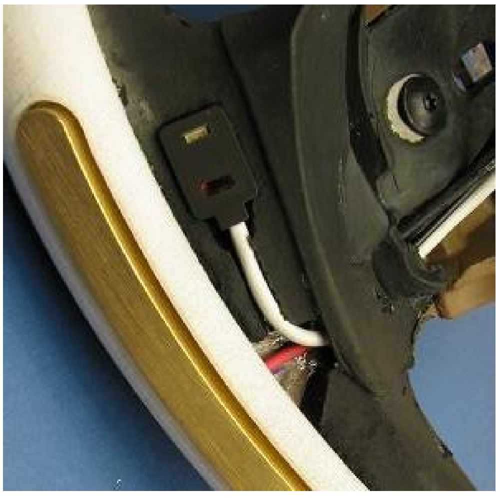

Figure A 26 Integration of the pulse oxymeter into the steering wheel.

VI.1.3 Skin temperature

Peripheral temperature measurement is carried out using an infrared temperature sensor. A thermometer (infrared), MLX90615 from Melexis [7] was utilized for the non-contact measurement. The sensor contains a low noise amplifier, a 16-bit ADC and a powerful DSP unit [7] which digitizes the obtained temperature value by itself.

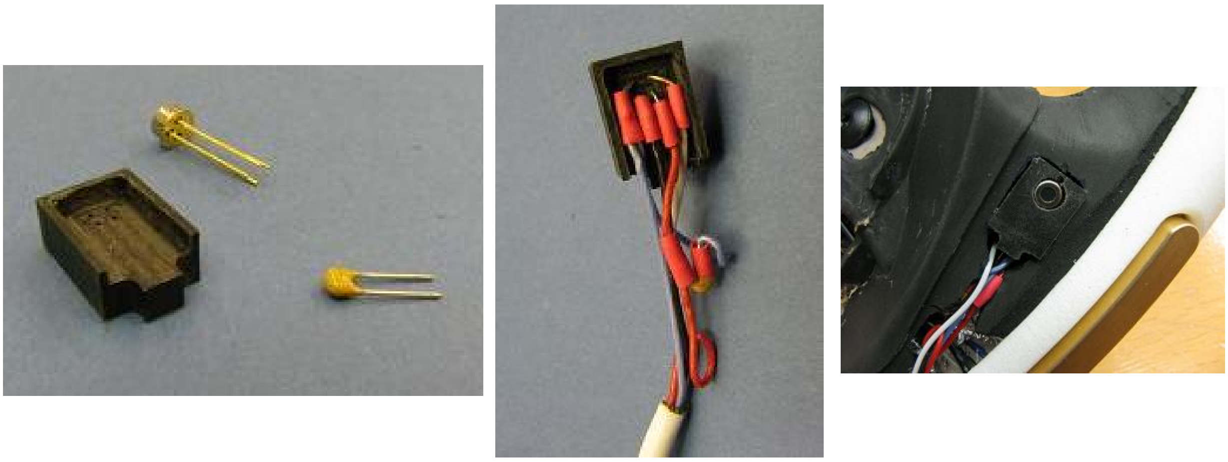

Figure A 27 L) the temperature sensor, capacitor and its case (M) Installing the sensor and capacitor into to case, (R) Embedding the temperature sensor into the steering wheel.

The sensor and a capacitor were installed into rubber housing for further integration into the steering wheel. The components and the rubber housing can be seen in Figure A 27(L), while its fixing with the housing and cabling is presented in Figure A 27(M). Installing of the temperature sensor into the steering wheel was similar to the pulse oxymeter as seen in Figure A 27(R). The sensor was engraved into the rubber chassis of the steering wheel before imbedding it. It was also place little high and up to maintain level with the leather surface.

VI.1.4 Sensor integrated Steering wheel

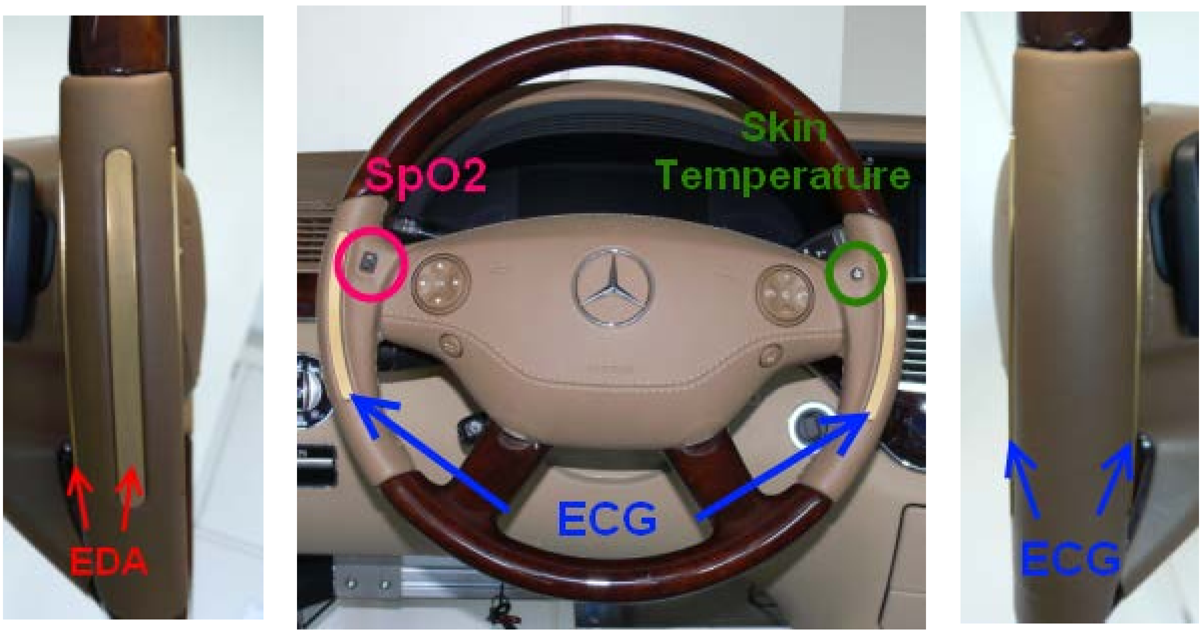

Figure A 28 (L) left side view, (M) The sensors integrated Steering wheel, (R) Right side view.

After integrating all the sensors, leathering was employed on the steering wheel. This is a standard process of leathering for the steering wheel of the Mercedes Benz series W221.

Final steering wheel after all the process can be seen in Figure A 28(M). Exact placement of the Biosensors is depicted in the figure. Left side view (L) and right side view (R) in the Figure A 28 indicate placement of the EDA and ECG electrodes respectively.

VI.2 Steering Wheel

Evaluation of the drive’s physiological state can be bettered with more vital parameters. Hence the concept of sensors integrated in the steering wheel was developed and implemented as described in earlier section. The central electronics system was equipped with a Bluetooth transceiver to couple the system with outer system wirelessly. The unit was paired with a laptop via Bluetooth technology, consequently using the signals from the steering wheel sensors in LabVIEW program. In the LabVIEW program, these signals were digitally processed and evaluated for final display purpose.

Figure A 29 The steering wheel demonstrator.

For the purpose of demonstrating, the steering wheel was equipped into an original cockpit of Mercedes Benz S class (W221). The Bluetooth wireless connection of the central electronic unit with the laptop eliminates a need of wirings, which makes it easy to fit the steering wheel into the cockpit with rotating configuration. Displaying the vital signals into the central display of the original cockpit configuration was very complex as it requires CAN bus interface with the display programming. A small VGA display monitor (7 inch) [8] was replaced to the standard display of the cockpit to make the demonstrator more realistic. This display was connected to the laptop as a second monitor via VGA cable.

The demonstrator was accommodated onto a roller stand to maintain a proper height for subjects while holding the steering wheel and to observe the biosignals. The fully furnished steering wheel demonstrator can be seen in Figure A 29. Zoomed screen of the display is shown in the insert image of the figure with graph of ECG signal. Description of the each sensor/parameter in the demonstrator is depicted in the graph of Figure A 29.

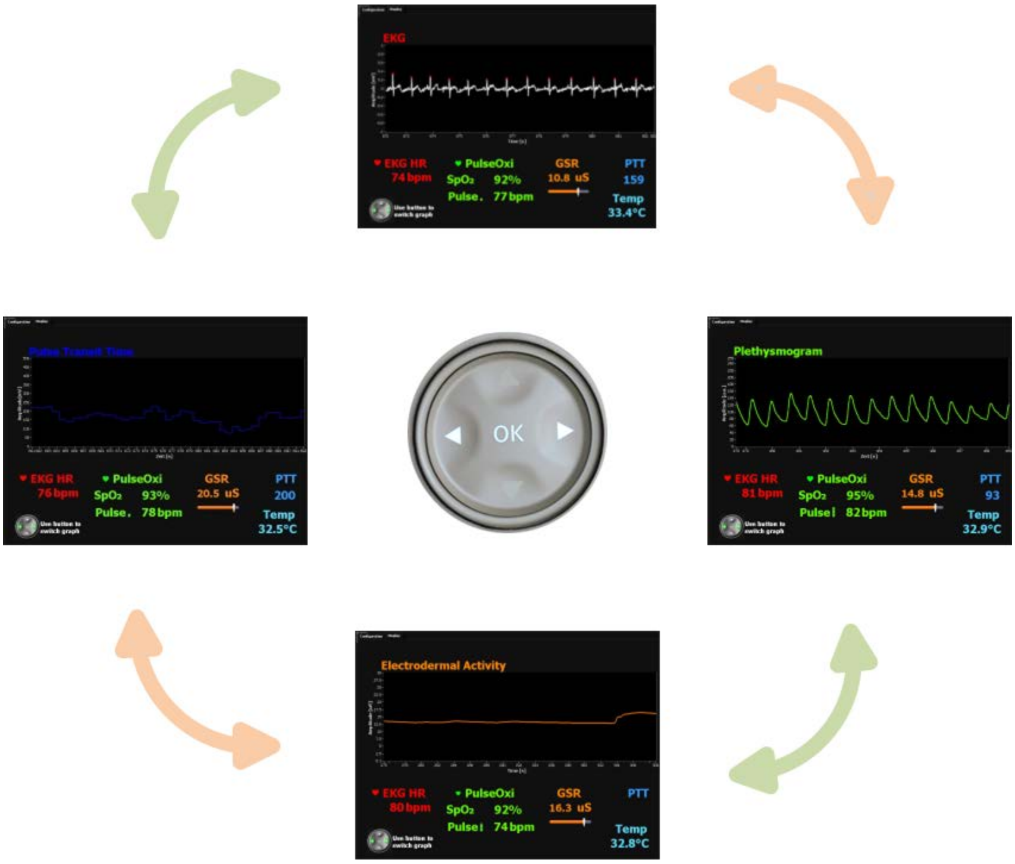

Figure A 30 Switching of the signal graph from the switch.

The screen of the monitor shows values of all the vital parameters (below the signal graph) and the signal graph for one of the selected parameter at one time. The values of the biosignal stay still over the course of measurement. Graphs for various parameters in the display screen can be selected for display using the left switch on the steering wheel. The flipping of the signal graphs is demonstrated in Figure A 30, where switching of the signal is depicted in repetitive circular fashion.

Readable screen shot of the display, representing all the values including a plethysmogram is shown in Figure A 31. In the figure, Heart rate extracted from the ECG signal is displayed 1st from the left side in red color. Value of pulse and oxygen saturation in hemoglobin (SpO_2) from the plethysmogram is displayed in 2nd of the left side in green color. Galvanic skin response (GSR) from the skin impedance measurement is shown 3rd from the left side in the figure in orange color.

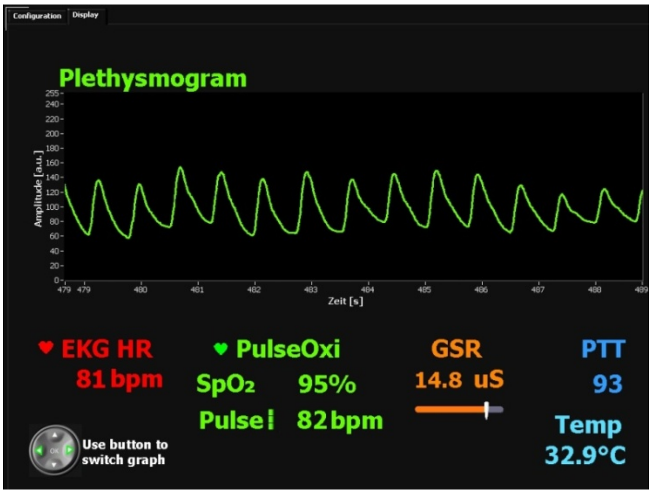

Figure A 31 Screen shot of the display.

Pulse transit time (PTT) refers to the time it takes a pulse wave to travel between two arterial sites and the speed at which this arterial pressure wave travels is directly proportional to blood pressure [9]. More specifically, PTT (Figure A 32) is the time delay between the R-wave of the ECG and the onset of the pulsation at a selected peripheral site detected by a sensor as seen in the figure [10]. This value is presented by blue color in the 4th from the left side in Figure A 31.

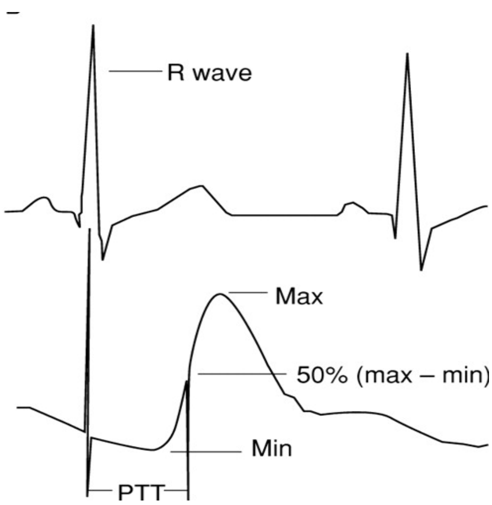

Figure A 32 Graphical description of the Pulse transit time (PTT) [9].

VI.2.1 Reference study

Meanwhile, to support the measurement of the vital parameters on the steering wheel, a study to evaluate psychophysiological status of a subject from various vital parameters was carried out with cooperation of FZI, Karlsruhe. Within this work, biosignals like conventional ECG, SpO2, EDA, Plethysmogram, pulse, thorax respiration and abdominal respiration were measured using a polysomnographic instrument called Somnoscreen plus (SOMNOmedics GmbH, Germany) [11]. Electroencephalography was measured as reference parameter to evaluate significance of the vital parameters for micro sleep or sleep detection as shown in Figure A 33.

Figure A 33 The similar reference EEG measurement [12].

During the measurement, drivers were asked to drive through an empty monotonous road to have more possibility of micro sleep or sleep. The route for the measurement was a dedicated track for various automotive measurements. The subjects were asked to drive on the route for four hours before the lunch time and another four hours after the lunch time. This process of gathering the data lasted around a month with collection of data from many subjects. A subject prepared with the measurement equipment (Somnoscreep plus) can be seen in Figure A 34, the preparation was followed by preparation for EEG measurement.

The measurements were performed for truck drivers as they normally drive for longer route and are highly prone to micro sleep or sleep. Another truck with similarly prepared subject was deployed behind the first truck. It provides another scenario where subject feels sleepy by seeing and driving behind same object continuously.

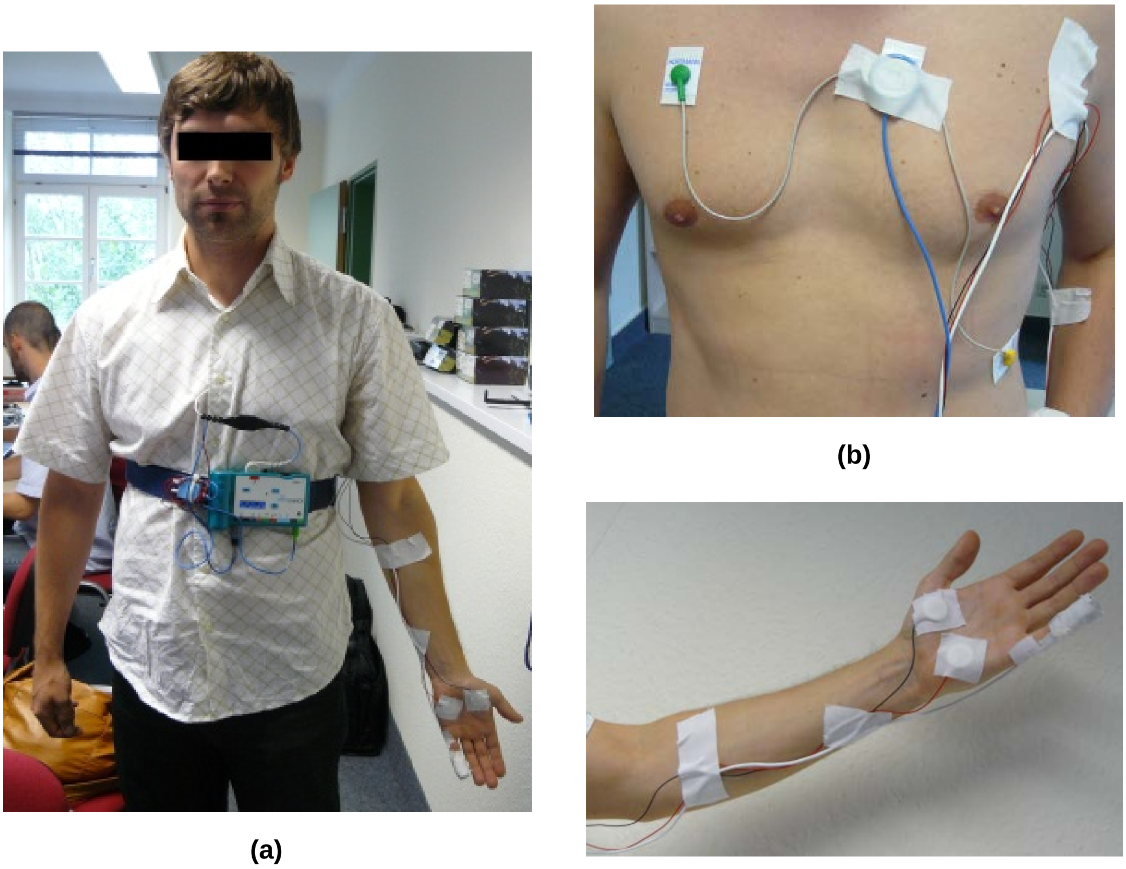

(a) (b) (c)

Figure A 34 (a) Subject preparation for the measurement, (b) ECG electrode on the chest, (c) EDA and SpO2 sensor on the hand.

Evaluation of the biosignal data is done by taking EEG as reference signal. Various events like micro sleep, sleep etc are analyzed on the EEG signals by the experts at Daimler AG with additional help of video camera used in front of the driver [12]. Variations in the combined behaviors of the measured parameter were analyzed taking the above mentioned EEG events as reference.

Analysis and evaluation of the vital parameters with reference to the events from the EEG signal was inconclusive.

Reference

[1] FZI (Forschungszentrum Informatik), Karlsruhe. Website : www.fzi.de

[2] S. Heuer, B. Chamadiya, A. Gharbi, C. Kunze and M. Wagner, „ Unobtrusive In-Vehicle Biosignal Instrumentation for advanced driver assistance and active safety,“ IEEE EMBS Conference on Biomedical Engg. And Sci. 2010 (IECBES), Kuala Lumpur, Malaysia, 30 November - 2 December 2010.

[3] B. Niedetzk, “Entwicklung einer Embedded-Plattform zur Vitaldatenerfassung im Lenkrad,” Diplomarbeit, FZI, 2010.

[4] MR. Neuman, “Pulse oximetry: physical principles, technical realization and present limitations,” Adv Exp Med Biol 220, 1987, pp.135-44.

[5] Nonin® Medical Inc., “OEM III Module Specification and Technical Information,” Datasheet, pp. 1-18, February 2010 .

[6] Nonin® Medical Inc., “8000 R, PureLight Reflective Sensor,”. Webpage, May 2011 : www.nonin.com/PureLight

[7] Melexis ,” MLX90615 : Infrared thermometer,” Datasheet, pp. 1-30, February 2010.

[8] Faytech, “7 inch VGA TFT LCD monitor,” Datasheet.

[9] R. P. Smith, J. Argod, JL. Pepin and P. A. Levy, “Pulse transit time: an appraisal of potential clinical applications,” Thorax 54,pp. 452-457,1999.

[10] S. Radhakrishna, “Commercialization of contact-free blood pressure monitoring technology,” Master thesis, Dept. of Biology, Case Western Reserve University, May 2010.

[11] SOMNOmedics GmbH “Polysomnographic device: Somnoscreen plus”, 2008, http://www.somnomedics.eu/products/polysomnography-18-33-channels.html.

[12] W. E. Kincses, S. Hahn, M. Schrauf and E. A. Schmitdt, “Measuring Driver’s mental workload using EEG,” ATZ worldwide eMagazine Edition vol.10, pp. 12-17, March 2008.